



**HAL**  
open science

# On Electric Grid Power Quality Monitoring using Parametric Signal Processing Techniques

Zakarya Oubrahim

► **To cite this version:**

Zakarya Oubrahim. On Electric Grid Power Quality Monitoring using Parametric Signal Processing Techniques. Electric power. Université de Bretagne Occidentale (UBO), 2017. English. NNT: . tel-01720952v1

**HAL Id: tel-01720952**

**<https://theses.hal.science/tel-01720952v1>**

Submitted on 1 Mar 2018 (v1), last revised 26 Mar 2018 (v2)

**HAL** is a multi-disciplinary open access archive for the deposit and dissemination of scientific research documents, whether they are published or not. The documents may come from teaching and research institutions in France or abroad, or from public or private research centers.

L'archive ouverte pluridisciplinaire **HAL**, est destinée au dépôt et à la diffusion de documents scientifiques de niveau recherche, publiés ou non, émanant des établissements d'enseignement et de recherche français ou étrangers, des laboratoires publics ou privés.



université de bretagne  
occidentale

UNIVERSITE  
BRETAGNE  
LOIRE

THÈSE / UNIVERSITÉ DE BRETAGNE  
OCCIDENTALE

*sous le sceau de l'Université Bretagne Loire*

pour obtenir le titre de

DOCTEUR DE L'UNIVERSITÉ DE BRETAGNE  
OCCIDENTALE

*Mention : Génie Electrique*

École Doctorale des Sciences pour l'Ingénieur

présentée par

Zakarya OUBRAHIM

Préparée au sein de la FRE CNRS 3744 IRDL

*Institut de Recherche Dupuy de Lôme*

On electric grid power  
quality monitoring using  
parametric signal  
processing techniques

**Thèse soutenue le 21 Novembre 2017**

devant le jury composé de :

**Marie CHABERT**

Professeur, INP – ENSEEIHT Toulouse / *rapporteur*

**Demba DIALLO**

Professeur, Université Paris-Sud / *président*

**Pierre GRANJON**

Maître de Conférences, Grenoble INP / *examineur*

**Marc PETIT**

Professeur adjoint, CentraleSupélec / *rapporteur*

**Tianzhen WANG**

Professor, Shanghai Maritime University, Chine / *examineur*

**Yassine AMIRAT**

Enseignant-Chercheur, ISEN Yncréa Ouest, Brest / *co-encadrant*

**Vincent CHOQUEUSE**

Maître de Conférences, Université de Bretagne Occidentale / *co-encadrant*

**Mohamed BENBOUZID**

Professeur, Université de Bretagne Occidentale / *directeur de thèse*

This project has received financial support from Brest Metropole and ISEN Brest



*"This thesis is dedicated to God, my teacher,  
Beloved parents, my inspiration and sisters,  
brothers and all my family, who are  
everything that a person  
could want."*

# Abstract

This thesis deals with electric grid monitoring of power quality (PQ) disturbances using parametric signal processing techniques. The first contribution is devoted to the parametric spectral estimation approach for signal parameter extraction. The proposed approach exploits the multidimensional nature of the electrical signals. For spectral estimation, it uses an optimization algorithm to minimize the likelihood function. In particular, this algorithm allows to improve the estimation accuracy and has lower computational complexity than classical algorithms. An in-depth analysis of the proposed estimator has been performed. Specifically, the estimator performances are evaluated under noisy, harmonic, interharmonic, and off-nominal frequency environment. These performances are also compared with the requirements of the IEEE Standard C37.118.2011. The achieved results have shown that the proposed approach is an attractive choice for PQ measurement devices such as phasor measurement units (PMUs).

The second contribution deals with the classification of power quality disturbances in three-phase power systems. Specifically, this approach focuses on voltage sag and swell signatures. The proposed classification approach is based on two main steps: 1) the signal pre-classification into one of 4 pre-classes and 2) the signature type classification using the estimate of the symmetrical components. The classifier performances have been evaluated for different data length, signal to noise ratio, interharmonic, and total harmonic distortion.

The proposed estimator and classifier are validated using real power system data obtained from the DOE/EPRI National Database of Power System Events. The achieved simulations and experimental results clearly illustrate the effectiveness of the proposed techniques for PQ monitoring purpose.



# Acknowledgements

The present work has been carried out at the Institut de Recherche Dupuy de Lôme, FRE CNRS 3744 IRDL, at the University of Brest. It has been financially supported by Brest Metropole and ISEN Brest. This financial support is gratefully appreciated.

I would like to thank **Professor Mohamed BENBOUZID** for giving me this PhD thesis work opportunity. Thanks Mohamed for your encouragements, support, help, inspiration, and supervision during the progress of this work. I would also like to thank my assistant supervisors **Dr. Vincent CHOQEUSE** and **Dr. Yassine AMIRAT**, who have guided and supported me throughout the research work, for their contributions, encouragements, and valuable discussions.

I would also like to deeply thank the PhD thesis defense committee members: the pre-examiners, **Prof. Marie CHABERT** from the INP-ENSEEIH Toulouse and **Prof. Marc PETIT** from CentraleSupélec Paris, for their valuable comments and suggestions; **Prof. Demba DIALLO** from the University of Paris-Sud, **Prof. Tianzhen WANG** from the Shanghai Maritime University, China, and **Dr. Pierre GRANJON** from Grenoble INP, for the insightful questions.

In addition, I would like to greatly thank all the laboratory colleagues and friends for their support and for making a fantastic working environment.

Finally, I am deeply indebted to my parents as well as to my family for their patience, sacrifice, and untiring support throughout all the years.



# List of Publications

Main results of this PhD thesis have lead to the following publications:

## Publications

### International Journals

1. **Z. Oubrahim**, V. Choqueuse, Y. Amirat and M.E.H. Benbouzid, “Maximum Likelihood Frequency and Phasor Estimations for Electric Power Grid Monitoring,” IEEE Transactions on Industrial Informatics, vol. 14, no. 1, pp. 167-177, January 2018.
2. **Z. Oubrahim**, V. Choqueuse, Y. Amirat and M.E.H. Benbouzid, “Disturbances Classification based on a Model Order Selection Method for Power Quality Monitoring,” IEEE Transactions on Industrial Electronics, vol. 64, no. 12, pp. 9421-9432, April 2017.

### International Conferences

1. Y. Amirat, **Z. Oubrahim**, G. Feld, and M.E.H. Benbouzid, “Phasor Estimation for Power Quality Monitoring: Least Square versus Kalman Filter,” in Proceedings of the 2017 IEEE IECON, Beijing (China), pp. 4339-4343, October-November 2017.
2. V. Choqueuse, E. Elbouchikhi, **Z. Oubrahim** and M.E.H. Benbouzid, “On the Use of Phase Diversity for Spectral Estimation in Current Signature Analysis,” in Proceedings of the 2017 IEEE IECON, Beijing (China), pp. 8093-8098, October-November 2017.
3. **Z. Oubrahim**, V. Choqueuse, Y. Amirat and M.E.H. Benbouzid, “Classification of Three-Phase Power Disturbances based on Model Order Selection in Smart Grid Applications,” in Proceedings of the 2016 IEEE IECON, Florence (Italy), pp. 5143-5148, October 2016.



- 
4. **Z. Oubrahim**, V. Choqueuse, Y. Amirat and M.E.H. Benbouzid, “An improved algorithm for power system fault type classification based on least square phasor estimation,” in Proceedings of the 2015 IEEE IECON, Yokohama (Japan), pp. 2735-2740, November 2015.
  5. Y. Amirat, **Z. Oubrahim** and M.E.H. Benbouzid, “On phasor estimation for voltage sags detection in a smart grid context,” in Proceedings of the 2015 IEEE ISIE, Buzios-Rio de Janeiro (Brazil), pp. 1351-1356, June 2015.

# Contents

<b>Abstract</b>	<b>i</b>
<b>Acknowledgements</b>	<b>iii</b>
<b>List of Publications</b>	<b>v</b>
<b>List of figures</b>	<b>xi</b>
<b>List of Tables</b>	<b>xiv</b>
<b>Glossary</b>	<b>xv</b>
<b>General Introduction</b>	<b>1</b>
<b>1 Power Quality Disturbances Characterization: State of the Art Review</b>	<b>7</b>
1.1 Introduction . . . . .	8
1.2 Power Quality and Signal Processing . . . . .	9
1.2.1 Definition . . . . .	9
1.2.2 Voltage and Current Quality . . . . .	10
1.2.3 Disturbances . . . . .	10
1.2.3.1 Voltage variations . . . . .	11
1.2.3.1.1 Frequency variations . . . . .	11
1.2.3.1.2 Voltage amplitude variations . . . . .	11
1.2.3.1.3 Waveform distortion: harmonic, inter-harmonic, and nonperiodic distortion . . . . .	12
1.2.3.2 Events . . . . .	13
1.2.3.2.1 Interruption . . . . .	13
1.2.3.2.2 Voltage sag and swell . . . . .	14
1.2.4 Monitoring . . . . .	15
1.2.5 Standards . . . . .	19
1.3 Phasor Measurement Units (PMUs) . . . . .	20
1.3.1 Definition . . . . .	20

1.3.2	Standards . . . . .	22
1.3.3	Estimation Performances Evaluation . . . . .	23
1.3.3.1	Frequency and ROCOF measurement evaluation . . . . .	23
1.3.3.2	Total vector error (TVE) evaluation . . . . .	25
1.4	Spectral Estimation Techniques for Power Quality Monitoring . . . . .	27
1.4.1	Non-Parametric Methods . . . . .	27
1.4.1.1	Zero-Crossing transform . . . . .	27
1.4.1.2	RMS and peak voltage techniques . . . . .	29
1.4.1.3	Fourier transform and its extensions . . . . .	29
1.4.2	Parametric Methods . . . . .	30
1.4.2.1	Discrete spectra . . . . .	31
1.4.2.2	Continuous spectra . . . . .	32
1.4.3	Discussion: parametric methods versus non-parametric methods . . . . .	32
1.5	Power Quality Disturbances Classification Techniques . . . . .	34
1.5.1	Classical Techniques . . . . .	34
1.5.1.1	ABC classifier . . . . .	34
1.5.1.2	Symmetrical component classifier . . . . .	34
1.5.2	Pattern Recognition Techniques . . . . .	35
1.5.2.1	Artificial neural network . . . . .	36
1.5.2.2	Support vector machine . . . . .	37
1.5.2.3	Fuzzy expert systems . . . . .	38
1.5.2.4	Genetic algorithm . . . . .	39
1.6	Conclusion . . . . .	40
<b>2</b>	<b>Phasor and Frequency Estimations</b>	<b>43</b>
2.1	Introduction . . . . .	44
2.2	Parameters Estimations . . . . .	46
2.2.1	Study hypotheses . . . . .	46
2.2.2	Signal model and phasor expression . . . . .	46
2.2.3	Least squares estimations . . . . .	48
2.2.3.1	Angular frequency estimation . . . . .	48
2.2.3.2	Phasor estimation . . . . .	51
2.2.4	Extension to non-stationary case . . . . .	52
2.3	Cost-Function Optimization Method . . . . .	54
2.3.1	Downhill Simplex Method . . . . .	55
2.3.2	Newton-Raphson Method . . . . .	57
2.3.2.1	Newton-Raphson iteration . . . . .	57
2.3.2.2	Derivatives of the exact cost-function . . . . .	58
2.3.2.3	Derivatives of the approximate cost-function . . . . .	60

---

2.4	Simulation and Experimental Results . . . . .	60
2.4.1	Monte Carlo Simulation Results . . . . .	61
2.4.1.1	Frequency error. Effect of the number of samples $N$ . . . . .	62
2.4.1.2	Frequency error. Effect of signal to noise ratio ( $SNR$ ) . . . . .	62
2.4.1.3	Total vector error. Effect of off-nominal frequency deviation . . . . .	63
2.4.1.4	Total vector error with frequency estimation. Effect of off-nominal frequency deviation . . . . .	64
2.4.1.5	Total vector error with frequency estimation. Effect of the number of samples $N$ . . . . .	65
2.4.1.6	Total vector error with frequency estimation. Effect of signal to noise ratio ( $SNR$ ) . . . . .	66
2.4.1.7	Total vector error with frequency estimation. Effect of harmonics and inter-harmonics . . . . .	66
2.4.1.8	Computation complexity . . . . .	68
2.4.1.9	Comparative study . . . . .	68
2.4.2	Experimental Results . . . . .	69
2.5	Conclusion . . . . .	70
<b>3</b>	<b>Power Quality Disturbances Classification based on Model Order Selection</b> . . . . .	<b>75</b>
3.1	Introduction . . . . .	76
3.2	Signal and Phasor Models . . . . .	77
3.2.1	Three-Phase Signals Model . . . . .	77
3.2.2	Phasor Model and 4-Classes . . . . .	78
3.2.3	General Vectorized Signal Model . . . . .	80
3.3	Proposed Classifier based on Information Theoretic Criteria . . . . .	82
3.3.1	Decision Tree . . . . .	82
3.3.2	Proposed Classifier Expression . . . . .	84
3.3.2.1	Expression of the log-likelihood function . . . . .	84
3.3.2.2	Expression of $\gamma_k$ . . . . .	85
3.4	Simulation and Experimental Results . . . . .	86
3.4.1	Monte Carlo Simulation Results . . . . .	87
3.4.1.1	Probability of correct classification versus number of samples . . . . .	87
3.4.1.2	Probability of correct classification versus noise variance . . . . .	88
3.4.1.3	Robustness of the proposed classifier . . . . .	90
3.4.1.4	Computation complexity . . . . .	91
3.4.1.5	Comparative study . . . . .	92
3.4.1.5.1	Symmetrical component algorithm (SCA) . . . . .	93
3.4.1.5.2	Three-phases three-angles algorithm (TP-TAA) . . . . .	94

---

3.4.1.5.3 Numerical examples . . . . .	95
3.4.2 Experimental Tests . . . . .	96
3.4.3 Discussion . . . . .	99
3.5 Conclusion . . . . .	102
<b>Conclusions and Perspectives</b>	<b>103</b>
<b>Appendices</b>	<b>109</b>
<b>Appendix A</b>	<b>109</b>
<b>Appendix B</b>	<b>111</b>
<b>Appendix C</b>	<b>113</b>
<b>References</b>	<b>115</b>

# List of figures

- 1.1 Power quality characterization diagram. . . . . 9
- 1.2 Electrical power system architecture. . . . . 10
- 1.3 Voltage/Current quality and distributed generation [1]. . . . . 11
- 1.4 Frequency variations measured in Sweden (top left), in Spain (top center),  
on the Chinese east coast (top right), in Singapore (bottom left), and in  
Great Britain (bottom right) [2]. . . . . 12
- 1.5 Overvoltage. . . . . 13
- 1.6 Interruption due to lightning (Event 2857) [3]. . . . . 14
- 1.7 Voltage sag (Event 0284) [3]. . . . . 15
- 1.8 Example of control strategy applied to power system based on phasor mea-  
surement units (PMUs). . . . . 16
- 1.9 Power quality measurements device: (1) signal input (voltage or current),  
(2) sampled and digitized signal, (3) quantity for further processing. . . . . 18
- 1.10 Example of threshold values triggering-based on rms voltage for event de-  
tection. . . . . 18
- 1.11 Synchrophasor representation of a sinusoid signal. . . . . 21
- 1.12 Phase angle change under off-nominal frequency conditions. . . . . 23
- 1.13 Complete PMU signal processing model. . . . . 24
- 1.14 Synchrophasor accuracy required by synchrophasor standard. . . . . 26
- 1.15 Zero-crossing approach illustration. . . . . 28
- 1.16 ABC classification: voltage sags types. . . . . 35
- 1.17 Six sub-types of three-phase unbalanced voltage sags among C and D types. 36
- 1.18 Network graph for a  $(L + 1)$ -layer perceptron. . . . . 37
- 1.19 Illustration of a rule-based expert system architecture. . . . . 38
- 1.20 Illustration of rule-based expert system for event classification of PQ dis-  
turbances. . . . . 39
  
- 2.1 Flowchart of the proposed algorithm. . . . . 45
- 2.2 Concept of sliding window under quasi-stationary conditions. . . . . 53
- 2.3 Grid search over the  $[a, b]$  interval. . . . . 55
- 2.4 Newton-Raphson method for finding a function zero. . . . . 59

2.5	Mean FE versus $N$ with noiseless signals ( $SNR = 150$ dB): comparison between LS and DTFT using NRA with LS using <i>fminsearch</i> estimations. . . . .	62
2.6	Mean FE versus $SNR$ for $N = 240$ samples: comparison between LS and DTFT using NRA with LS using <i>fminsearch</i> estimations. . . . .	63
2.7	TVE and Mean TVE versus frequency deviation for $N = 144$ samples and $SNR = 50$ dB: comparison between LS and DTFT estimations. . . . .	64
2.8	Mean TVE versus frequency deviation for $N = 144$ samples: comparison between LS and DTFT using NRA estimations. . . . .	65
2.9	Mean TVE versus $N$ with noiseless signals ( $SNR = 150$ dB): comparison between LS and DTFT using NRA with LS using <i>fminsearch</i> estimations. . . . .	66
2.10	Mean TVE versus $SNR$ for $N = 240$ samples: comparison between LS and DTFT using NRA with LS using <i>fminsearch</i> estimations. . . . .	67
2.11	Mean TVE versus harmonic level for $N = 76$ samples: comparison between LS and DTFT using NRA with LS using <i>fminsearch</i> estimations under harmonic environment. . . . .	69
2.12	Computation time versus $N$ for $SNR = 55$ dB: comparison between <i>Newton-Raphson</i> and <i>fminsearch</i> algorithms. . . . .	70
2.13	Mean FE versus $N$ for $SNR = 150$ dB: comparison between LS using NRA with zero-crossing estimations. . . . .	71
2.14	Three-Phase voltages and estimated frequency: comparison between LS and DTFT using NRA and <i>fminsearch</i> estimations. . . . .	72
2.15	Amplitude variation of phasors: comparison between LS and DTFT using NRA and <i>fminsearch</i> estimations. . . . .	73
2.16	Phases variation of phasors: comparison between LS and DTFT using NRA and <i>fminsearch</i> estimations. . . . .	74
3.1	Overview of the proposed power quality disturbance classifier. . . . .	77
3.2	Sags and swells signatures illustration [4]. . . . .	81
3.3	Flowchart of the proposed classification algorithm. . . . .	83
3.4	Average probability of correct classification versus samples number for $SNR = 15$ dB. . . . .	89
3.5	Average probability of correct classification versus $SNR$ for $N = 72$ and $N = 480$ . . . . .	90
3.6	Harmonic effect on the proposed classifier. Comparison between ML classifiers using BIC and AIC penalty terms. . . . .	93
3.7	Computation time versus $N$ : Comparison between ML and approximate classifiers. . . . .	94
3.8	Event 1 (2827): Voltage sag and swell classification. Comparison between ML classifiers using BIC and AIC penalty terms. . . . .	97

---

3.9	Event 2 (2825): Voltage sag and swell classification. Comparison between ML classifiers using BIC and AIC penalty terms. . . . .	98
3.10	Event 3 (2802): Voltage sag and swell classification. Comparison between ML classifiers using BIC and AIC penalty terms. . . . .	99
3.11	Event 4 (2786): Voltage sag and swell classification. Comparison between ML classifiers using BIC and AIC penalty terms. . . . .	100
3.12	Event 5 (2911): Voltage sag and swell classification. Comparison between ML classifiers using BIC and AIC penalty terms. . . . .	101
B.1	Flowchart of a phasor measurement unit. . . . .	112
B.2	Phasor measurement systems hierarchy and phasor data concentrators (PDC) levels. . . . .	112



# List of Tables

1.1	Power quality disturbances classification. . . . .	20
1.2	Interruption definitions in standard documents. . . . .	21
1.3	Steady-state frequency and ROCOF measurement requirements. . . . .	25
1.4	Frequency and ROCOF performance requirements under modulation tests. . . . .	25
1.5	Steady-state synchrophasor measurement requirements. . . . .	27
1.6	Synchrophasor measurement bandwidth requirements using modulated test signals. . . . .	28
2.1	Simulation parameters. . . . .	61
2.2	TVE versus inter-harmonic components for $N = 192$ samples and $SNR = 150$ db. . . . .	68
3.1	Expressions of $\mathbf{W}_k$ and $\mathbf{d}_k$ with respect to class $\mathcal{C}_k$ . . . . .	80
3.2	Link between the proposed technique and sag/swell signatures. . . . .	81
3.3	Penalty function with respect to class $\mathcal{C}_k$ . . . . .	86
3.4	4-Classes: Simulation parameters. . . . .	87
3.5	Signatures types: simulation parameters. . . . .	88
3.6	AIC criterion: ML pre-classifier confusion matrix. . . . .	89
3.7	BIC criterion: ML pre-classifier confusion matrix. . . . .	90
3.8	AIC criterion: ML classifier confusion matrix. . . . .	91
3.9	BIC criterion: ML classifier confusion matrix. . . . .	91
3.10	AIC criterion: approximate classifier confusion matrix. . . . .	92
3.11	BIC criterion: approximate classifier confusion matrix. . . . .	92
3.12	Voltage sags type C: comparison of the proposed classifier with SC and TP-TA algorithms. . . . .	95
3.13	Voltage sags type C: comparison of the proposed classifier with SC and TP-TA algorithms. . . . .	96
3.14	Voltage sags type D: comparison of the proposed classifier with SC and TP-TA algorithms. . . . .	96
3.15	Voltage sags type C and D: comparison of the proposed classifier with SC and TP-TA algorithms. . . . .	96
A.1	Classification of the power quality disturbances and their causes. . . . .	109

# Glossary

AI	Artificial intelligence
AIC	Akaike information criterion
ANN	Artificial neural networks
ARMA	Autoregressive moving average
BIC	Bayesian information criterion
CT	Clarke transform
CWT	Continuous wavelet transform
DWT	Discrete wavelet transform
DTFT	Discrete time Fourier transform
EMD	Empirical mode decomposition
ESPRIT	Estimation of signal parameters via rotational invariance techniques
FT	Fourier transform
FFT	Fast Fourier transform
HT	Hilbert transform
HHT	Hilbert-Huang transform
IA	Instantaneous amplitude
IF	Instantaneous frequency
IMF	Intrinsic mode function
GA	Genetic algorithm
MLE	Maximum likelihood estimation
MUSIC	Multiple signal classification
PMU	Phasor measurement unit
RMS	Root mean square
<i>SNR</i>	Signal to noise ratio
STFT	Short time Fourier transform
SVM	Support vector machine
SCA	Symmetrical component algorithm
<i>TVE</i>	Total vector error
<i>FE</i>	Frequency error
<i>ROCOF</i>	Rate of change of frequency

TP-TAA	Three-phases three-angles algorithm
$THD$	Total harmonic distortion
$\mathbf{A}$	Matrix
$\mathbf{a}$	Vector
$\mathbf{A}^T$	Transposed matrix of $\mathbf{A}$
$\mathbf{A}^{-1}$	Inverse of $\mathbf{A}$
$\mathbf{A}^\dagger$	Pseudoinverse of $\mathbf{A}$
$\mathbf{I}_m$	Identity matrix of size $m \times m$
$\triangleq$	Equal to by definition
$\approx$	Is approximately
$j$	Imaginary unit, $j^2 = -1$
$\text{Re}(a), \text{Im}(a)$	Real and imaginary part of variable $a$
$\text{vec}(\mathbf{A})$	Column-wise vectorization of matrix $\mathbf{A}$
$\text{Tr}(\mathbf{A})$	Trace of the matrix $\mathbf{A}$
$\mathbf{A} \otimes \mathbf{B}$	Kronecker product of matrices or vectors $\mathbf{A}$ and $\mathbf{B}$
$\hat{V}$	Estimate of variable $V$
$\mathbb{N}$	Set of natural numbers
$\ \mathbf{A}\ _F^2$	Frobenius norm of $\mathbf{A}$
$N$	Number of samples
$N_s$	Number of samples per window
$N_b$	Begin sample
$N_e$	End sample
$N_{mc}$	Monte Carlos trials
$f_n$	Nominal frequency
$f_0$	Fundamental frequency
$F_s$	Sampling frequency
$f_{ih}$	Inter-harmonic frequency component
$[\mathbf{v}]$	Voltage vector
$z$	Symmetrical component
$\sigma$	Noise variance
$\delta$	Kronecker delta
$\mathcal{P}_a$	Average probability of correct classification
$\omega$	Angular frequency
$\mathcal{J}(\omega)$	Exact cost function
$\mathcal{J}_a(\omega)$	Approximate cost function
$\nabla \mathcal{J}(\omega)$	The first-derivative of the cost-function
$\nabla^2 \mathcal{J}(\omega)$	The second-derivative of the cost-function

# General Introduction

Existing power systems are complex and are facing several challenges due to high penetration of renewable sources. In fact, the intermittent and discontinuous nature of renewable energy sources impact the power system and can lead to grid instability or even its failure. Moreover, power systems are lacking of monitoring, pervasive and effective communications, and fault diagnostics. To address these challenges, the concept of smart and self-healing electric power system has emerged.

The advent of smart grids have urged a radical reappraisal of power grid networks and power quality requirements, and effective use of the network are indexed as the most important keys for smart grid expansion and deployment. One of the most efficient ways of effective use of these grids would be to continuously monitor their conditions. This allows for early detection of power quality degeneration facilitating therefore a proactive response, prevent a fault ride-through the renewable power sources, minimizing downtime, and maximizing productivity. Within this context, power quality (PQ) has become essential to realize the envisioned smart grid. In fact, integration of renewable sources in a power system is considered as a major source of PQ disturbances. These disturbances could have a substantial influence on the customer load performance and efficiency. Moreover, they can cause million-dollar losses for industrial consumers. To overcome these problems, it becomes imperative to develop and integrate new advanced algorithms for PQ disturbances characterization. The characterization of disturbances can be decomposed into two main steps: 1) event detection that is concerned with determining the starting and ending times of the event. 2) event classification that is concerned with determining the type/cause of the disturbance.

Over the last decades, many studies have demonstrated the interest to use power quality monitoring based on voltage parameters. To that end, several studies have proposed to use signal processing techniques for feature extraction, and pattern recognition techniques are used to complete the classification process of PQ disturbances. In term of feature extraction stage, the main objective of signal analysis is to estimate relevant parameters from a signal, such as the frequency and the phasor. Fundamental frequency is the most important power system parameter for PQ monitoring since it allows to track the system operation state. Moreover, frequency is considered as the main step for the estimation of the voltage amplitude and phase angle. Under stationary conditions, the standard IEC 61000-4-30 proposes a conventional frequency estimator based on a zero-crossing technique. This is a simple and low-complexity estimator but it is sensitive to distorted signals and further processing must be considered to minimize the effect of DC components, harmonics, inter-harmonics, and other power quality disturbances. Furthermore, this conventional estimator is statistically suboptimal because it exploits only the information contained in a single-phase. To deal with these issues, several techniques based on the Clarke transform such as the widely linear least mean phase technique or the least mean squares differentiator have been proposed. Nevertheless, the main limitation of the

Clarke transform is that its use remains questionable in unbalanced three-phase systems. Once the fundamental frequency is estimated accurately, the voltage amplitude and phase angle can be easily estimated. For amplitude estimation, several basic techniques such as the Root Mean Square (RMS) and peak voltage have been proposed. These techniques are simple and well-proven, however they provide only the amplitude estimate without any information of the phase angle parameter. Moreover, these techniques are sensitive to noise or distortion. To overcome these issues, the discrete time Fourier transform (DTFT) is the basic technique for spectral analysis. DTFT suffers from leakage effect and from low-frequency resolution for finite number of samples. Under non-stationary conditions, more sophisticated techniques have been proposed. Regarding classical time-scale and time-frequency representations, these techniques also have several limitations (limited time-frequency resolution, artefacts such as cross terms, etc.). However, statistical performances of the aforementioned techniques are suboptimal since they do not fully exploit the three-phase nature of the electrical signals. Moreover, the performances of the previously published techniques critically degrade under off-nominal conditions.

In term of classification, the estimated parameters can be used as inputs of the classification techniques whose output is the disturbance type or cause. Several techniques have been presented, discussed, and applied to the classification of power quality disturbances. These techniques can be classified into two classes: 1) classical techniques and 2) pattern recognition techniques. Regarding classical techniques, most of previous works use two parameters to classify the power quality disturbance type. These two parameters are amplitude or residual voltage and duration of the event. These techniques are suited for single-phase measurements since they only exploit the rms voltage contained in a single-phase. However, these techniques are suboptimal since they do not fully use the phase angle and other parameters. Moreover, they are very sensitive to large variations in amplitude or phase angle, and a small error in frequency estimation may lead to an erroneous results. Pattern recognition has been applied in power systems for PQ disturbances classification, protection, and consumer profile identification. For pattern recognition techniques, several techniques for pattern recognition of the PQ disturbances have been proposed. These techniques include: artificial neural network (ANN), fuzzy expert system, genetic algorithm, and support vector machine (SVM). In fact, the main advantage of a pattern recognition machine is its capability of learning by examples and generalization. However, the performances of theses techniques critically depend on the learning stage and feature extraction process. Furthermore, the learning stage requires relatively high computational complexity effort.

In this context, this thesis work focuses on electric grid power quality monitoring using parametric signal processing techniques under non-stationary conditions. The main objective is the development of new PQ characterization algorithms allowing to ensure an efficient and reliable diagnosis of the power system state. To this purpose, suitable

feature extraction techniques are of extreme importance for reliable disturbance detection and classification. A parametric spectral estimation technique based on voltage parameters has been proposed. Compared to the existing estimation techniques, the proposed technique exploits the multidimensional nature of electrical signals that allows better estimation performances. Furthermore, an optimization algorithm based on the Newton-Raphson method has been proposed. This optimization algorithm has lower computational complexity than classical techniques. Moreover, the performances of the previously published techniques critically degrade under off-nominal conditions, while the proposed algorithm achieves good performances. On the other hand, a new classifier for power quality disturbances based on the analysis of the three-phase signal has been proposed. As opposed to published classification techniques, the proposed technique is able to provide a complete classification of voltage sag and swell. Moreover, this technique fully exploits three-phase information that allow better classification performances. Furthermore, it has a lower computation complexity and it does not require any training database and no parameter to be set.

The contributions of this thesis work could be summarized as follows:

- A new techniques for power quality monitoring have been proposed. The first technique deals with frequency and phasor estimations and the second one is for the disturbances classification.
- The proposed optimization algorithm and the downhill simplex algorithm are compared for frequency and phasor estimations. Moreover, the performances of the proposed estimation method are evaluated under various operating conditions, and are compared with the requirements of the IEEE Std. C37.118.2011. Finally, a comparison has been performed between the proposed estimation technique and others estimators, which are the least square and the discrete time Fourier transform (DTFT) estimators using `fminsearch` technique and DTFT using Newton-Raphson algorithm.
- The proposed classifier and two others techniques are compared for PQ disturbance classification.
- The benefits of the proposed algorithms are highlighted with simulated and real power system data obtained from the DOE/EPRI National Database of Power System Events.

The thesis manuscript is organized as follows:

- A Chapter I dealing with a critical state of the art of spectral estimation and classification techniques for power quality monitoring.

- A Chapter II dealing with a new synchrophasor and frequency estimations technique.
- A Chapter III dealing with a novel algorithm for power quality disturbances classification based on model order selection.





# Chapter 1

## Power Quality Disturbances

### Characterization: State of the Art Review

**T**HIS chapter presents a review of power quality (PQ) disturbances characterization, where a literature review of signal processing and pattern recognition-based techniques used for PQ disturbances monitoring is given with a focus on the estimation and classification issues. Several PQ disturbances and their origins and consequences are presented. These disturbances are characterized by international standards and can be extremely different in terms of characteristics and consequences. Furthermore, PQ measurement device called phasor measurement unit (PMU) is also presented.

## 1.1 Introduction

Power quality has become a major industrial topic as PQ disturbances could have a substantial influence on grid stability, efficiency, operation, and measurements performances [5–9]. The increased interest in power quality can also be explained by the following reasons [10]:

- Metering: PQ disturbances affect the power system measurements performances
- Protective relays: PQ disturbances could lead to the protection relays malfunction
- Equipments lifetime: PQ disturbances lead to equipment lifetime reduction and damage
- Electromagnetic compatibility: power quality disturbances are considered as a source of electromagnetic noise [11].

This thesis focuses on power quality issues, where the use of signal processing techniques is required [2, 12, 13] and leads to the use of advanced algorithms to characterize the power quality disturbances in order to enhance efficiency and reliability of the power systems. In this context, the characterization of the power quality disturbances is one of the most PQ monitoring issue. A power quality characterization diagram is shown in Fig. 1.1, it involves the following main stages [12].

- Parameters estimation stage: this deals with the estimation of signal parameters (i.e. frequency and phasor) from the recorded data.
- Parameters detection stage: this involves triggering i.e. determining the starting and ending points of the disturbance.
- Parameters classification stage: this allows to determine the type of disturbance.

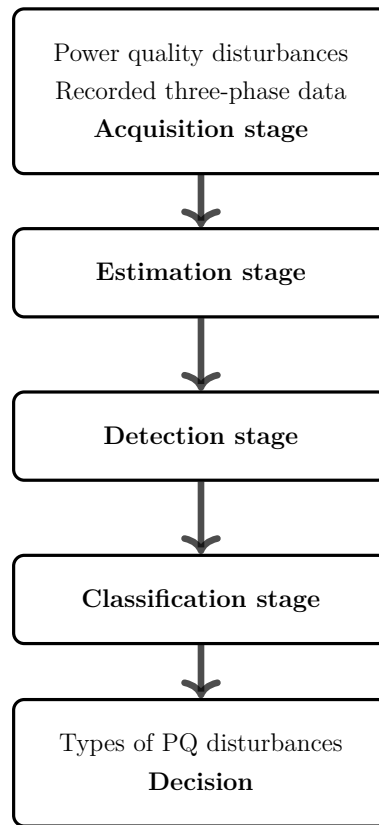


Figure 1.1: Power quality characterization diagram.

## 1.2 Power Quality and Signal Processing

### 1.2.1 Definition

Power quality is a general term that concerns the electrical interaction between the power system and customers [14]. PQ involves the voltage quality, which refers to the impact of supply voltage on the equipment and presents a voltage deviation from the nominal voltage. PQ involves also the current quality, which is a current deviation from the nominal value [14, 15]. Figure 1.2 presents an electric power system architecture, where the customers or end users can be consumers, producers, or both [1, 10, 16, 17]. Due to the integration of renewable energies (REs), the electric power system architecture becomes more complicated [18–21]. In fact, intermittent and discontinuous nature of renewable resources may impact power quality and make the balance between energy production and consumption difficult to maintain [22]. This could have a substantial influence on grid stability by affecting voltage and frequency control [5, 6, 8, 23–27].

## 1.2.2 Voltage and Current Quality

The voltage quality is the first power quality aspect that is shown in Fig. 1.3. The voltage quality at the generator terminals is determined by the events and the equipments connected to the grid, therefore a voltage disturbances could impact the generators and lead to equipment damage [1, 2, 28, 29]. The second aspect of PQ is the current quality that is illustrated in Fig. 1.3. This figure shows also that the current produced by the generator could impact the power system and the equipments [1, 2, 29]. To resume, voltage quality is how the load or the end-user equipment is affected by the power system. The current quality is how the power system is affected by the end-user equipment or load. In the next, a review of several PQ disturbances and their origins and consequences is presented.

## 1.2.3 Disturbances

The electrical power systems are three-phase systems that have a mutual coupling between phases. A balanced three-phase systems are sinusoidal waveforms, where the three-phases have the same fundamental frequency that is equal to the nominal value (50 Hz or 60 Hz). Furthermore, voltages amplitudes and phase shift between phases are equal to 1 pu and  $120^\circ$ , respectively [30–32]. If one of these requirements is not satisfied, the system is considered as unbalanced [31, 33]. In real power systems, frequency and phasor (amplitude and initial phase) deviate significantly from their nominal values. These sudden deviations are called disturbances. These disturbances can be classified into two classes: power quality variation and event [2, 31]. The PQ variation is defined as steady-state disturbance, which is a small deviation<sup>1</sup> from its nominal value. For instance, the voltage and frequency

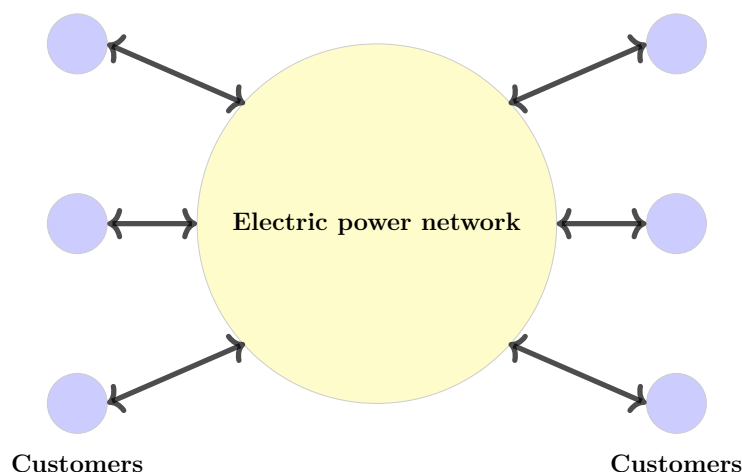


Figure 1.2: Electrical power system architecture.

<sup>1</sup>The value of small or large deviation is defined by international standards, such as the IEEE 1159, IEC 61000-4-30, and EN 50160 [34–36].

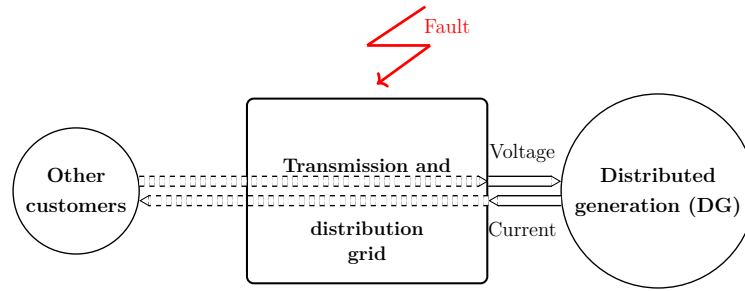


Figure 1.3: Voltage/Current quality and distributed generation [1].

variations are a PQ variations. While, the PQ event is a large deviation<sup>1</sup> from its nominal value. The supply interruption or outage, voltage sag and swell are the most severe PQ events [12, 37].

### 1.2.3.1 Voltage variations

This section presents several power quality variations that will be discussed with their origin and consequences.

#### 1.2.3.1.1 Frequency variations

In real power system, the fundamental frequency value is not always equal to the nominal value (50 Hz or 60 Hz) with frequency deviation less than  $\pm 1$  Hz [36]. Frequency is recorded by the PQ measurements periodically [38]. For example, the measurement estimates frequency once time per second. The number of frequency recorded per week can be obtained by a simple computation:  $7 \times 24 \times 60 \times 60 = 604800$  frequency values. This allows having more information on the probability distribution, such frequency average and standard deviation. A measured frequency variations illustration is given by Fig. 1.4. Several consequences of frequency variations are mentioned as follow:

- Motor speed variation: electrical machines, especially motors speed is affected by frequency variations.
- Rate of change of frequency (ROCOF): a high ROCOF value leads to lose many generator units. This could lead to lose the energy balance.

#### 1.2.3.1.2 Voltage amplitude variations

The voltage variations are a small variations of the voltage amplitude due to the load variation, distributed generation, etc. [31]. The amplitude variations could impact the lifetime and performance of the end-user equipments. These variations can be classified into two classes that are called overvoltage and undervoltage. Overvoltage or undervoltage refers respectively to higher or lower voltage than nominal one at which the power system

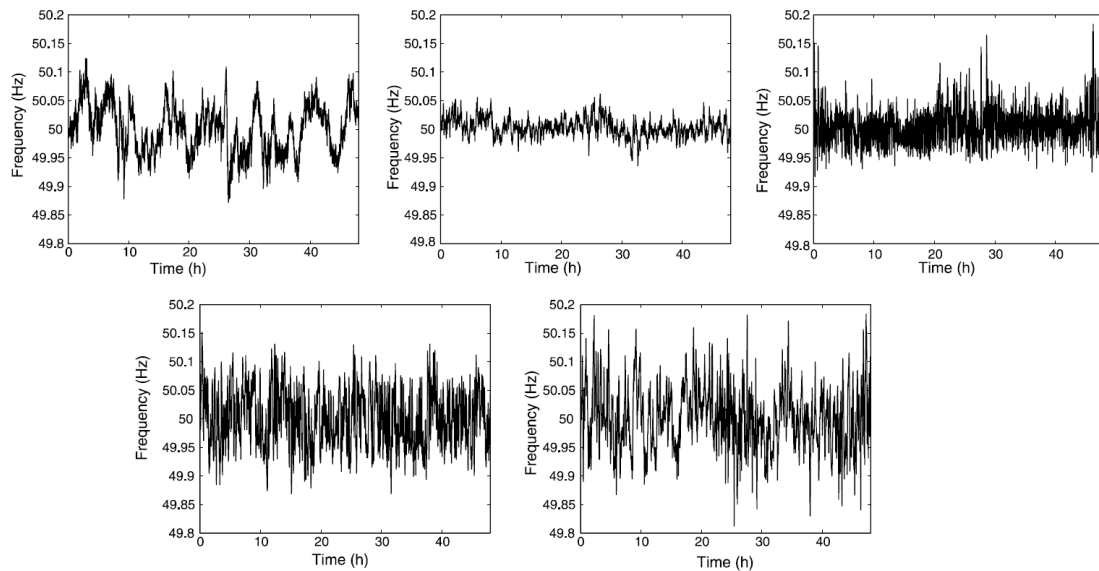


Figure 1.4: Frequency variations measured in Sweden (top left), in Spain (top center), on the Chinese east coast (top right), in Singapore (bottom left), and in Great Britain (bottom right) [2].

can operate effectively. For instance, overvoltage is when the voltage reaches 110%-120% of the nominal one for a longer than one minute. The consequences of these variations on the power system and end user equipments can be presented as follows:

- Causing potential equipment overheating.
- Starting torque of induction motors can be reduced due to undervoltage.
- Electronic equipment performances decrease critically due to an undervoltage.
- Light and life of fluorescent and incandescent lamps are critically impacted by the amplitude variations.

To minimise their effects, the voltage is controlled by several ways such as capacitor banks and transformer tap changers that are installed on the transmission lines [1]. Figure 1.5 presents an illustration of overvoltage.

### 1.2.3.1.3 Waveform distortion: harmonic, inter-harmonic, and nonperiodic distortion

The waveform distortion definition seems to one of voltage or current quality. It is a deviation of the voltage or current waveform from the nominal value. It causes several consequences such as transformer overheating, capacitor problems, electronic equipment malfunction, etc. [17, 39, 40]. The waveform distortion includes many forms that are harmonic, inter-harmonic, and nonperiodic distortion. The harmonic is the most studied since it dominants in most case. Harmonics are waveforms at multiples of the fundamental

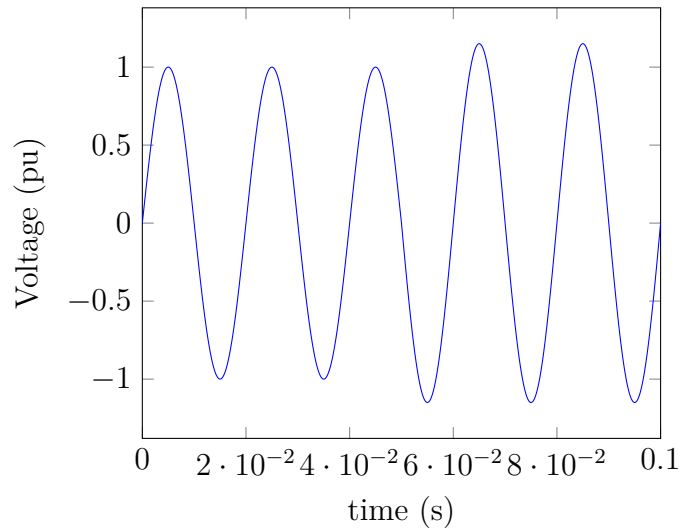


Figure 1.5: Overvoltage.

frequency and are caused by nonlinear loads. Harmonic distortion can be decomposed in two parts, odd harmonic that is dominant in supply voltage and load current and even harmonic that is normally rather small [41]. The total harmonic distortion (THD) is most commonly used for quantifying the harmonic amount on the signal and it is defined by IEC Standard 61000-4-7 [42] as follows

$$THD_F(\%) \triangleq 100 \alpha \frac{\sqrt{\sum_{h=2}^{\infty} a_{mh}^2}}{a_m}, \quad (1.1)$$

where  $a_{mh}$  and  $a_m$  correspond to the amplitude of the  $h^{th}$  order harmonic and fundamental component, respectively. The quantity  $\alpha > 0$  controls THD of the signal.

### 1.2.3.2 Events

Power quality events are a significant deviations from the nominal values. The three most severe PQ events are discussed in this section, they are interruptions, voltage sags, and voltage swells [2].

#### 1.2.3.2.1 Interruption

Interruption is a voltage or current waveform that has amplitude close or equal to zero. Typical thresholds<sup>2</sup> have been defined by several international standards to detect an interruption that are 1% and 10% of the nominal value [34–36]. Interruptions are caused by one- or multi-phase disconnection from the power system. Several causes may lead to

<sup>2</sup>The threshold value is the voltage r.m.s value defined in order to determine the start and end of an event. It can be expressed in volts or as per unit (percentage) value of the reference voltage.



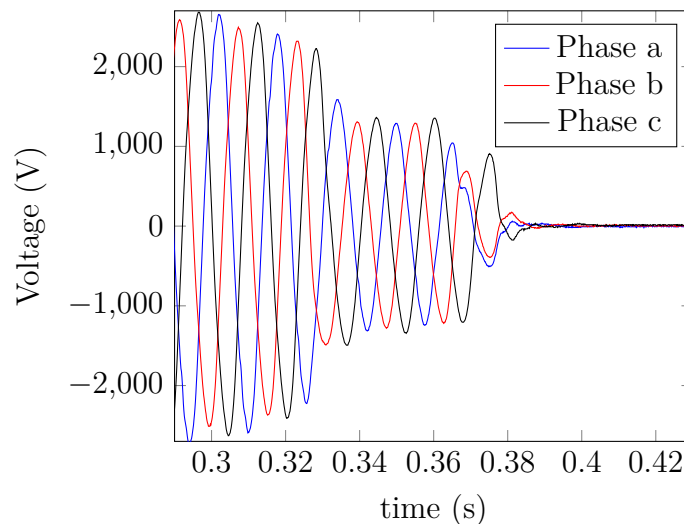


Figure 1.6: Interruption due to lightning (Event 2857) [3].

this disconnection such as circuit breaker opening, short circuit, etc. Figure 1.6 presents an interruption due to lightning. The used real data are obtained from the DOE/EPRI National Database of Power System Events (event-code: 2857) [3].

During an interruption the voltage at the customer interface or at the measurement location is zero. To measure an interruption, one has to wait until an interruption occurs. This is done automatically in most power quality monitors by comparing the estimated voltage amplitude with the threshold. In the case when the estimated voltage amplitude is less than the threshold for longer than a certain time, the monitor detects the start of an interruption. The end of the interruption is detected when the voltage amplitude rises above the threshold again. The duration of the interruption is obtained as the time difference between beginning and ending of the event.

#### 1.2.3.2.2 Voltage sag and swell

Voltage sag<sup>3</sup> is a decrease in the voltage amplitude between 0.9 and 0.1 pu of the nominal value for a short time that is between one half-cycle and one minute [34]. Voltage sag is considered as one of the main power quality issues. In fact, voltage sag critically degrades the performance and efficiency of customer load. The IEC 61000-4-30 standard characterizes voltage sag by two parameters: residual voltage and duration. These two parameters can not provide a complete explanation of sag behaviour, therefore other signal characteristics have been introduced in literature such as phase angle jump and three-phase characteristics. An illustration of voltage sag waveform due to a two-phase fault is given in Fig. 1.7. The used real data are obtained from the DOE/EPRI National Database of Power System Events (event-code: 0284) [3].

<sup>3</sup>The term sag is used mainly in US technical publications, while dip is normally preferred by the IEC.

Opposite to sag, swell is an increase in the voltage amplitude between 1.1 and 1.8 pu of the nominal value. In the next subsection, power quality monitoring and its international standards will be discussed in more details.

### 1.2.4 Monitoring

The electrical power system community is trying to address several challenges, including stability issue [43–45]. In fact, the existing power system can not address this critical issue due to its hierarchical topology. As a result, this could have a substantial influence on power quality by affecting voltage and frequency control [5, 16]. In order to overcome these challenges, the future smart grid is expected to address the limitations of the existing system. In particular, the control strategies applied to smart grid become of high interest and should be pervasive [46]. Moreover, the smart grid is required to improve efficiency, reliability, and safety through automated control and modern communication technologies. Last but not least, the future smart grid is expected to be self-healing and resilient to system anomalies [23–26, 47, 48]. In this context, power quality monitoring is the backbone of control strategies applied to smart grid. PQ monitoring is considered as the most efficient strategy used to ensure availability, reliability, and safety of the electrical power systems. Fig. 1.8 illustrates an example of control strategy applied to smart grid based on phasor measurement units (PMUs). This control strategy can be decomposed into four tasks that are: measurement-substations that consist in the extraction of the power quality parameters such frequency, amplitude, and phase angle. Substation automation refers to use data from intelligent electronic devices (IEDs). IEDs have several functions within power systems such as controlling and monitoring the power

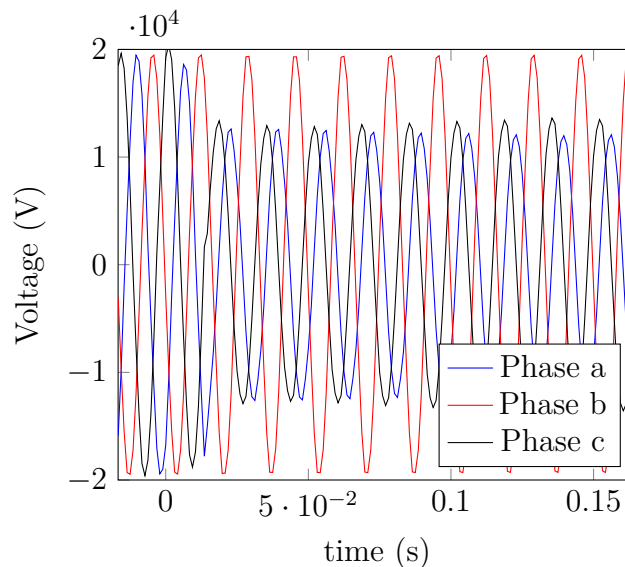


Figure 1.7: Voltage sag (Event 0284) [3].

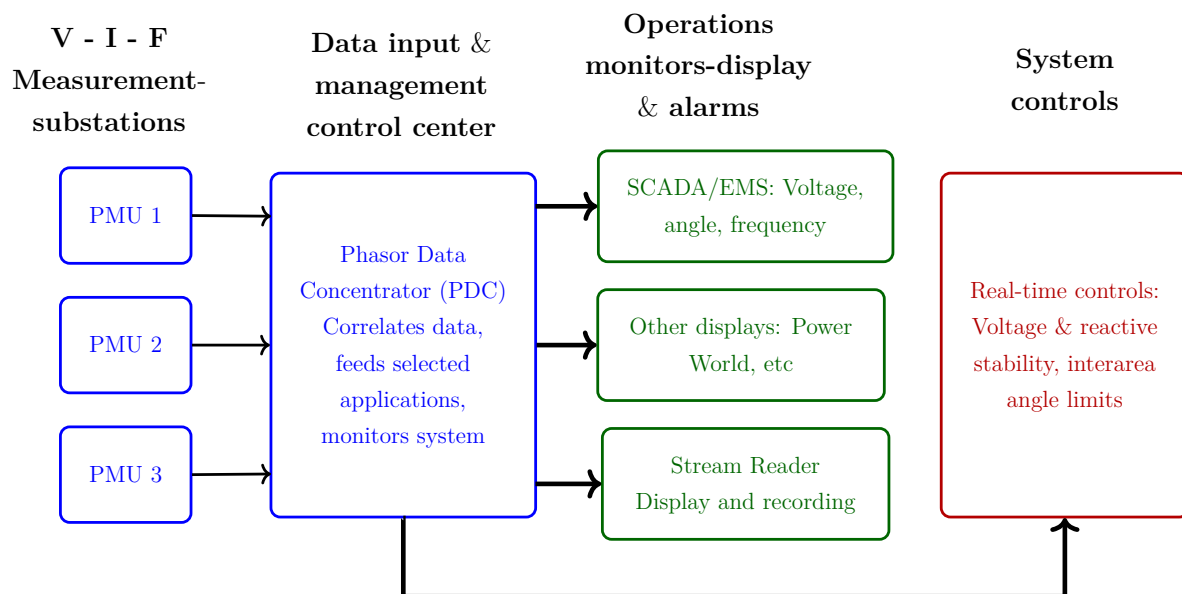


Figure 1.8: Example of control strategy applied to power system based on phasor measurement units (PMUs).

system devices and also protecting the personnel and equipments. PMUs, digital relays, and modern protective relay are the most known IEDs. The supervisory control and data acquisition (SCADA) infrastructure and energy management system (EMS), installed at control centers, allowed to monitor the power systems.

In this control strategy, the PQ parameters are extracted using the phasor measurement units, which are deployed at different substations. Data obtained from several PMUs are collected by phasor data concentrator (PDC), which is located in the data input & management control center, for nourishing the SCADA by their scalar data. In operations monitors, these data are supervised, controlled, and acquiesced for representing the power system state. Finally, system controls are the act of automatically controlling the power system via measurement instrumentation and control devices for improving the power systems stability with the help of state estimation (SE) programs embedded in EMSs.

As mentioned previously, in this thesis work two tasks are chosen to be focused upon that are the estimation and classification. The estimation task can be applied in the measurement instruments (PMUs) to estimate the voltage parameters. The classification task can be applied as a post-processing tool for transient characterization in disturbance detection in intelligent electronic devices. The other blocks of the control strategy are beyond of this work scope.

In practical cases is not easy to distinguish between the event and variation, which is considered as a difficult task to achieve [2]. For instance, the voltage sag (event) can be considered as an extreme case of the voltage amplitude variation. Therefore, a triggering mechanism is required to start recording the event by determining its starting and ending points. In contrast to event, the variation does not require triggering. In this context, the

rms voltage is used as a basic measurement parameter for voltage sags. In this regard, the voltage sags post-processing requires rms values and duration that are defined by the international standards such as EN 50160 and IEEE 1159 [34, 36]. If these parameter values do not meet the standard limits, then the monitoring instruments record the required information of the event. In particular, it is difficult to find a suitable triggering mechanism for some extreme events like transient. A general PQ monitoring scheme is shown in Fig. 1.9 that consists of several tasks of PQ monitoring, where the conversion from analog signal to sampled signal is the first task. The measurement device block includes

- Instrument transformers
- Analogue anti-aliasing filters
- Sampling and digitizing
- Digital anti-aliasing and down sampling

The anti-aliasing is used to avoid all components that their frequencies are above of  $\frac{1}{2}$  of the sampling frequency (Nyquist frequency). Power systems have a high voltage and current values that can not be directly measured. Consequently, an instrument transformers is required to reduce these high values. This instrument transform is working under a low frequencies such 50 Hz and 60 Hz. In fact, several PQ disturbances like transient and harmonic have a high frequency components that require the use of a high frequency measurements. In such case, Rogowski coils and resistive voltage are capable to achieve good accuracy with higher frequency components.

Several typical threshold and duration values of a triggering-based on rms voltage for event detection are given in Fig. 1.10. This figure shows a vertical axis that presents the reference voltage in percentage of the threshold, where the nominal voltage is considered as a reference. The duration is given by the horizontal axis that starts at the instant when the rms voltage exceeds the threshold.

There are two types of power quality monitoring that should be distinguished:

- Monitoring the supply at different locations at the same time by estimating an *average power quality*. This is called power quality survey.
- Monitoring the supply at one site by estimating the power quality at that specific site.

Statistical processing block allows to compute the number of events per year and per site per year. This can be useful for a *power quality surveys*. In the case when an event is detected, a PQ processing computes and storages several indices of this event

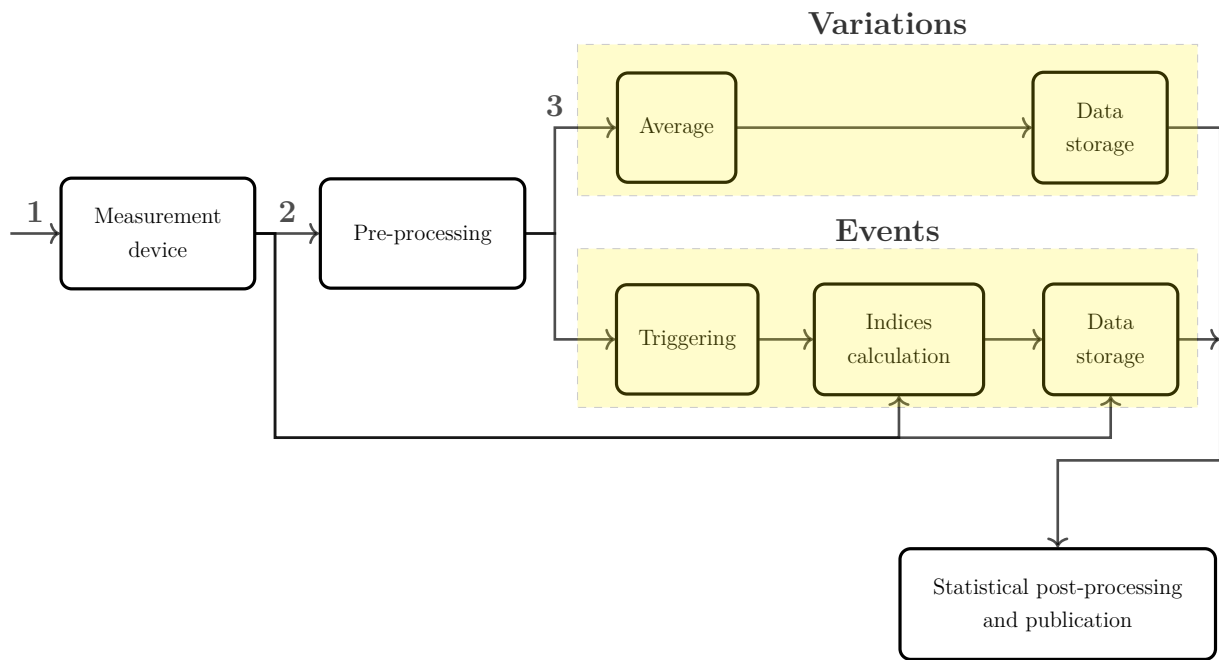


Figure 1.9: Power quality measurements device: (1) signal input (voltage or current), (2) sampled and digitized signal, (3) quantity for further processing.

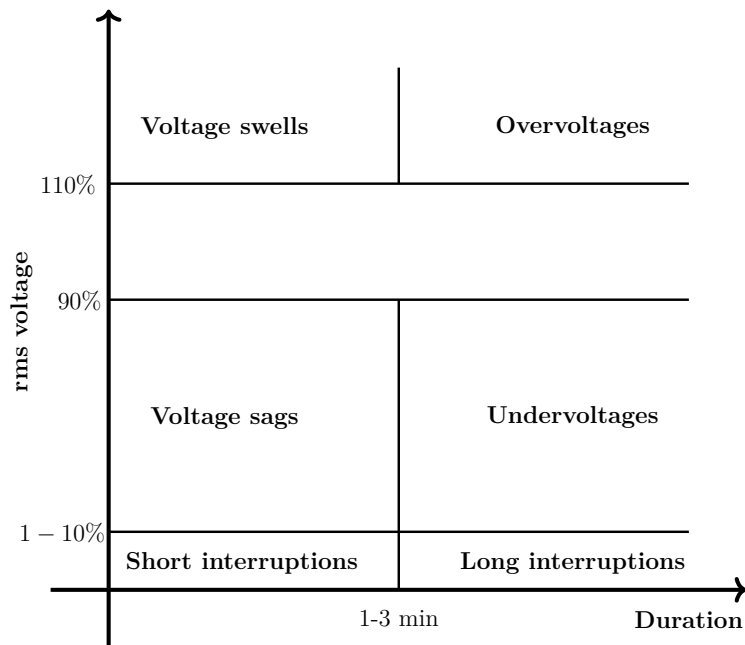


Figure 1.10: Example of threshold values triggering-based on rms voltage for event detection.

i.e. amplitude and duration. These data can be used later for diagnostics and computing additional indices. In this context, a huge number of data could be resulted, however only the event amplitude and duration are used for quantifying the power system performances. Finally, average values of the rms voltage are extracted over a certain interval.

The aim of the next subsection is to present the purpose of power quality standardization.

### 1.2.5 Standards

In the last decades, several international standards have been elaborated, in order to satisfy the PQ requirements of voltage and current in a power system. Specifically, these standards provide the limits and tolerance variations of the frequency and voltage. Measurement methods and thresholds are also defined to characterize various PQ disturbances. Appendix A lists various PQ variations and events, their characterization methods and possible causes.

The increased interest in power quality standards can be explained by the following reasons

- **Nominal conditions definition.** As mentioned in previous subsections, the frequency and voltage are not exactly equal to 50/60 Hz and 1 pu, respectively. In this context, it becomes imperative to describe this phenomena by a term such *nominal frequency and voltage*. In European standard EN 50160 [36], it could be said that the nominal frequency and voltage are equal to 50/60 Hz and 1 pu, respectively. In contrast, this nominal voltage does not give a correct information about the real voltage value that could have a deviation from the nominal value. Therefore, most countries use standard that provides acceptance variation in term of rms voltage.
- **Terminology definition.** Standards provide also a definition of the various phenomena with the characterization method of their parameters. This will facilitate the comparison and communication between various PQ monitoring systems.
- **PQ problems limitation.** The main objective of a PQ monitoring is to limit the number of PQ problems. This objective can be achieved by improving the power system performance.

In this context, there are two known organisations for developing standards on power quality, which are the international electrotechnical commission (IEC) and institute of electrical and electronics engineers (IEEE). For instance, the IEC standard provides a complete requirements on electromagnetic compatibility (EMC) for power quality. EMC is defined as the ability of a device, equipment, or system to function satisfactorily in its electromagnetic environment without introducing intolerable electromagnetic disturbances to anything in that environment [49]. IEEE 519 standard describes the requirements for harmonic distortion [50].

Several disturbances occur variations in amplitude (or rms values) with respect to nominal value during an interval time. The IEEE 1159 and European EN 50160 standards classify the PQ disturbances according to thresholds of the rms values of voltage and current deviation with respect to nominal values during the time of disturbance as shown in Tables 1.1 and 1.2. The IEC 61000-4-30 standard [35] provides a description of the

measurement methods and interpretation of PQ parameters in power system of 50/60 Hz.

The main emphasis in the PQ monitoring is on the extraction of relevant disturbances parameters. The main disturbance parameters are frequency and phasor (amplitude and phase angle). For this purpose, PMU is used to estimate power system frequency and phasor. The following section deals with a description of the phasor measurement unit with its standard.

## 1.3 Phasor Measurement Units (PMUs)

In this section, we shall provide an overview of power quality measurement that called phasor measurement unit and summarize its main points. In the following, we will discuss the requirements defined by the standards of this measurement.

### 1.3.1 Definition

Phasor measurement units have become one of the most advanced measurement technology applied in the power grid and are predicted to become a very vital part of power systems state estimation. They can be used to validate system performance and control equipment settings [38]. Moreover, PMUs can be a stand-alone or functional unit within another physical unit such as a protective relay or a power system data recorder [51].

Phasor measurement units provide synchrophasor and positive sequence voltages and currents with respect to the global time reference. Global position systems (GPSs) are used to provide the time-tags to the PMU measurements [38]. In addition, local frequency and rate of change of frequency can also be provided by PMU measurements. A general synchrophasor representation of a sinusoidal waveform can be shown by Fig. 1.11.

The reporting instant, represented by a time-tag ( $t = 0$ ), defines the reference for the phasor representation of the measured signal input. The phasor representation is com-

Table 1.1: Power quality disturbances classification.

PQ Disturbance	Duration	Voltage values
Sag	$> \frac{1}{2}$ cycles	0.1 to 0.9 pu
Swell	$> \frac{1}{2}$ cycles	1.1 to 1.8 pu
Outage	$> \frac{1}{2}$ cycles	$< 0.1$ pu
Flicker	$> \frac{1}{2}$ cycles	0.9 to 1.1 pu
Harmonic	-	$THD > 5\%$
Interharmonic	-	

Table 1.2: Interruption definitions in standard documents.

Standard	Term	Definition
IEEE 1159	Interruption	Voltage below 10% of nominal
	Sustained interruption	Longer than 3 s
	Momentary interruption	$\frac{1}{2}$ cycle to 3 min
	Temporary interruption	3 s to 1 min
IEEE 1250	Instantaneous interruption	Shorter than 30 cycles
	Momentary interruption	$\frac{1}{2}$ to 2 s
	Temporary interruption	2 s to 2 min
	Sustained interruption	longer than 2 min
EN 50160	Short interruption	Shorter than 3 min
	Long interruption	Longer than 3 min
IEEE 1366	Momentary interruption	Shorter than 5 min
	Sustained interruption	Longer than 5 min

posed of an amplitude equal to the rms value,  $X$ , and a phase angle  $\varphi$ . If all PMUs use a common and accurate timing references and related to a common frequency, then their measurements can be comparable and the phase angle differences between phasors are accurate. This is the main advantage of PMUs over conventional measurements [52, 53].

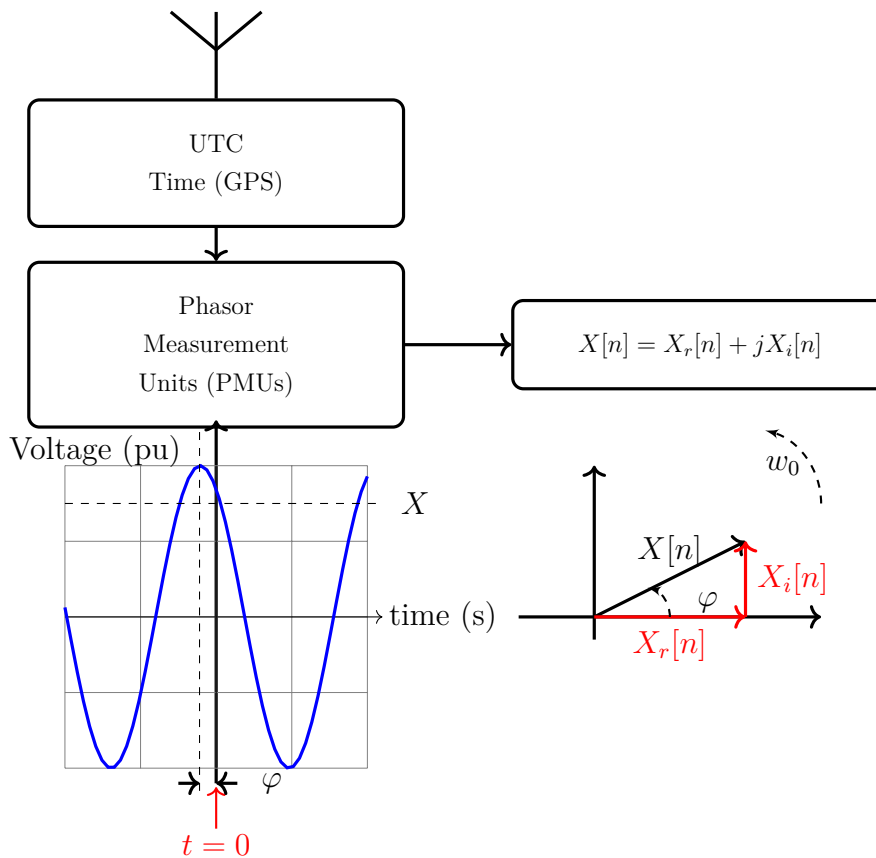


Figure 1.11: Synchrophasor representation of a sinusoid signal.



For ensuring reliability and interoperability among PMUs made by different manufacturers, the IEEE commission has defined a PMU industry standards that defines synchrophasor and frequency requirements for compliant PMUs. In the next subsection, this standard will be described.

### 1.3.2 Standards

Herein, we describe the standard of phasor measurement units, which is called C37.118. This standard provide the requirements of phasor, frequency, and rate of change of frequency (ROCOF) measurements under steady state and dynamic conditions. It specifies also time tag and synchronization requirements for measurement of the three-phase power system. Moreover, the PMU standard specifies methods for evaluating these measurements and requirements under steady-state and dynamic conditions [52].

The phasor measurements performance and the off-nominal frequencies requirements under steady state conditions have first defined in the 2005 version of the standard, C37.118-2005 [54,55]. In addition, this standard version does not provide the generalized definition of synchrophasor or frequency and ROCOF compliance. The PMUs standard has been reviewed and improved into C37.118.1-2011 [52] (and its amendment C37.118.1-2014 [56]) to utilize dynamic synchronized measurement. The revision version provides a definition of the synchrophasor, measurement requirements, and test conditions under steady state and dynamic conditions. This IEEE standard is designed only for phasor measurement units at the transmission level, while no standard has been developed yet for synchrophasor measurement devices at the distribution level.

According to C37.118-2014, the PMU requirements can be classified into two classes: P-class is intended for measurement applications that requires fast response to dynamic events, and M-class focuses on the estimation performances. Under off-nominal frequency, the estimation algorithms used by PMUs have to meet the requirements for a frequency deviation of  $\pm 5$  mHz from the nominal value. The concept of off-nominal frequency is illustrated in Fig. 1.12, where a sinusoid off-nominal signal frequency is considered and observed at intervals  $[0, T_0, 2T_0, \dots, NT_0]$ .  $T_0 = \frac{1}{f_0}$  corresponds to the fundamental period,  $f_0$  is the fundamental frequency, and  $[0, X_0, 2X_0, \dots, NX_0]$  are the phasors representation. In the case when the frequency signal ( $f$ ) is different and less than two times of the nominal value ( $f_n$ ) ( $f \neq f_n$  and  $f < 2f_0$ ), the estimated phasor is presented by a constant amplitude, while the phase angles of the phasors sequence change uniformly. In this context, the synchrophasor depends on the time, therefore the PMU shall receive time from an accurate time reference in order to keep all estimation performance criteria defined by PMU standard within the required limits. A complete process of the phasor measurement units is presented in Fig. 1.13. The estimation criteria defined in the PMU standard will be presented in the next subsection.

### 1.3.3 Estimation Performances Evaluation

Phasor measurement units shall provide a correct estimation of the signal input parameters such as fundamental phasor (amplitude and initial phase) and frequency under steady state and dynamic conditions. The standard requirements that are specified by the total vector error (TVE), frequency error (FE), and the rate of change of frequency (ROCOF) error (RFE) values for the phasor, frequency, and ROCOF measurements, respectively, are described in more detail in the next subsections.

#### 1.3.3.1 Frequency and ROCOF measurement evaluation

Considering a signal model of a three-phase voltage system expressed as follows

$$X_m(t) = a_m \cos(\phi_m(t)), \quad (1.2)$$

where  $m \in \{a, b, c\}$  corresponds to the phase index for three-phase voltage system.  $a_m$  is the maximum amplitude and  $\phi(t)$  corresponds to the phase angle at instant  $t$ . The frequency computation can be expressed in terms of the phase angle ( $\phi$ ) as follows

$$f(t) = \frac{1}{2\pi} \frac{d\phi(t)}{dt}, \quad (1.3)$$

and the ROCOF is defined as

$$ROCOF(t) = \frac{df(t)}{dt}. \quad (1.4)$$

The frequency and ROCOF errors are defined by C37.118-2014 standard for evaluating the frequency estimation performance of the synchrophasor measurement.

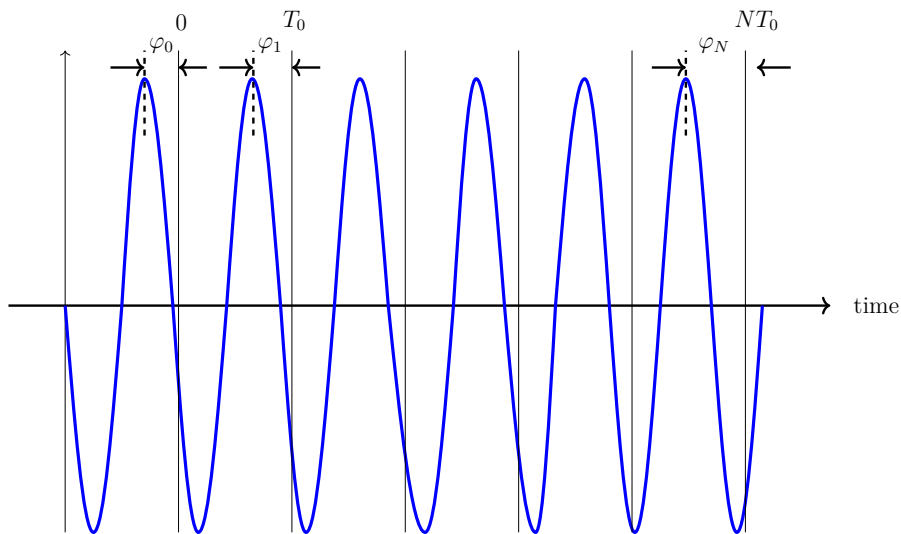


Figure 1.12: Phase angle change under off-nominal frequency conditions.

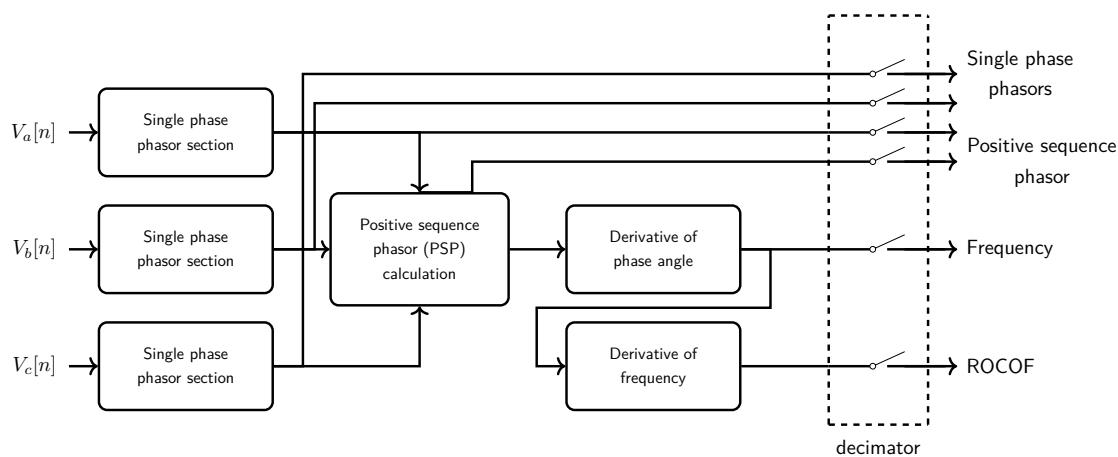


Figure 1.13: Complete PMU signal processing model.

The FE is expressed as

$$FE(t) = |f_0(t) - \hat{f}_0(t)|, \quad (1.5)$$

and the RFE is given by

$$RFE(t) = \left| \frac{df_0(t)}{dt} - \frac{d\hat{f}_0(t)}{dt} \right|, \quad (1.6)$$

where  $f_0$  and  $\hat{f}_0$  correspond to the real and estimated frequency.

The phasor measurement units have to meet the FE and RFE requirements specified by the C37.118-2014 standard. This also defines the test conditions and equipment for steady state and dynamic conditions. The FE and RFE requirements are specified for each class (P- and M-classes). If one of this requirement is not respected by PMU, then the PMU is not compliant with the C37.118-2014 standard. The FE and RFE requirements for both classes under steady state are given by Table 1.3. Under dynamic conditions, we present the condition test used for determining the bandwidth of the synchrophasor measurement. This test uses a sinusoidal amplitude and phase modulation. The signals can be expressed as follows

$$X_m(t) = a_m [1 + k_x \cos(wt)] \times \cos [w_0 t + k_a \cos(wt - \pi)], \quad (1.7)$$

where  $a_m$  corresponds to the amplitude of the input signal,  $w_0$  and  $w$  are the nominal and the modulation angular frequencies in  $\frac{rad}{s}$ , respectively.  $f_m = \frac{w}{2\pi}$  is the modulation frequency in Hz,  $m \in \{a, b, c\}$  corresponds to the phase index for three-phase voltage system.  $K_x$  and  $K_a$  refer to the amplitude and the phase angle modulation factors, respectively. This modulation tests shall be performed with  $w$ ,  $k_x$ , and  $k_a$  over the frequency ranges specified in Table 1.4.

We have provided a brief summary of the PMU standard. Several details of the synchrophasor definition and requirement are provided in the standard document [56].

Table 1.3: Steady-state frequency and ROCOF measurement requirements.

Influence quantity	Reference Condition	Error requirements for compliance			
		P-class		M-class	
Signal frequency	Frequency = $f_0$ ( $f_{nominal}$ ) Phase angle constant	Range: $f_0 \pm 2.0$		Range: $f_0 \pm 2.0$ Hz for $F_s \leq 10$ $\pm \frac{F_s}{5}$ for $10 \leq F_s < 25$ $\pm 5.0$ Hz for $F_s \geq 25$	
		Max FE	Max RFE	Max FE	Max RFE
		0.005 Hz	0.01 $\frac{Hz}{s}$	0.005 Hz	0.01 $\frac{Hz}{s}$
Harmonic distortion (same as Table 3 in C37.118-2011) (single harmonic)	< 0.2% THD	1% each harmonic up to 50 <sup>th</sup>		10% each harmonic up to 50 <sup>th</sup>	
		Max Fe	Max RFE	Max Fe	Max RFE
	$F_s > 20$	0.005 Hz	0.01 $\frac{Hz}{s}$	0.025 Hz	0.01 $\frac{Hz}{s}$
	$F_s \leq 20$	0.005 Hz	0.01 $\frac{Hz}{s}$	0.025 Hz	0.01 $\frac{Hz}{s}$

Table 1.4: Frequency and ROCOF performance requirements under modulation tests.

Modulation level, reference condition, range (use the same modulation levels and ranges under the reference conditions specified in Table 5 in C37.118-2011 standard)	Error requirements for compliance			
	P-class		M-class	
	Max FE	Max RFE	Max FE	Max RFE
$F_s > 20$	0.06 Hz	3 $\frac{Hz}{s}$	0.3 Hz	30 $\frac{Hz}{s}$
$F_s \leq 20$	0.01 Hz	0.2 $\frac{Hz}{s}$	0.06 Hz	2 $\frac{Hz}{s}$

### 1.3.3.2 Total vector error (TVE) evaluation

For simplifying the compliance specification, the standard C37.118-2014 has combined the amplitude and angle error into total vector error. The total vector error is provided to evaluate the estimation performance of the synchrophasor measurement. This error criterion can be expressed in terms of the difference between the real and the estimated phasor. By considering this synchrophasor representation  $\bar{X} = X_r + jX_i$ , the TVE value is given by

$$TVE[n] \triangleq \sqrt{\frac{\left(\widehat{X}_r[n] - X_r[n]\right)^2 + \left(\widehat{X}_i[n] - X_i[n]\right)^2}{X_r^2[n] + X_i^2[n]}}, \quad (1.8)$$

where  $X_r[n]$  and  $X_i[n]$  correspond to real and imaginary components of the fundamental phasor at the instant  $n$ , respectively.  $\widehat{X}_r[n]$  and  $\widehat{X}_i[n]$  correspond to the real and imaginary components of the estimated phasor at the instant  $n$ , respectively. This comparison between the real and estimated phasor must be done at the same time tag. The maximum value of the TVE is set to 1% by the C37.118-2014 standard. This allowed error is

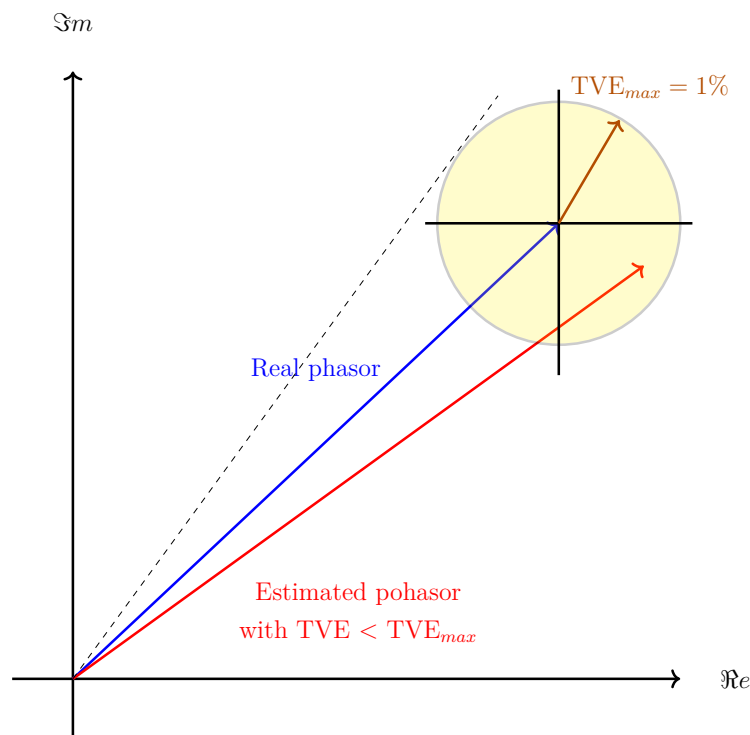


Figure 1.14: Synchrophasor accuracy required by synchrophasor standard.

represented by a circle in Fig. 1.14, knowing that its origin is the end of the real phasor and its radius is 1%.

Under steady state conditions, the signal parameters are considered constant for evaluating the synchrophasor measurement performance. Under dynamic conditions, the input signal could not be a pure sine wave. In this case, a comparison between the input signal and the estimated one by the measurement at the same time is required by the C37.118-2014 standard. The measurement time can be considered as the middle of the measurement window when the phase angle is constant or increasing across the measurement window. In the case when the phase angle is time-varying, it is required to use a signal model that assumes the angle phase changes.

The synchrophasor requirements for P- and M-classes under steady state conditions are given by Tables 1.5. Table 1.6 presents the standard requirements for TVE under dynamic conditions for modulation tests.

In the following section, a state of the art of existing feature extraction techniques for PQ monitoring is reviewed.

Table 1.5: Steady-state synchrophasor measurement requirements.

Influence quantity	Reference Condition	Minimum range of influence quantity over which PMU shall be within given TVE limit			
		P-class		M-class	
		Range	Max TVE %	Range	Max TVE %
Signal frequency range- $f_{dev}$ (test applied nominal +deviation: $f_0 \pm f_{dev}$ )	$F_{nominal}$ ( $f_0$ )	$\pm 2.0$ Hz	1	$\pm 2.0$ Hz for $F_s < 10$ $\pm \frac{F_s}{5}$ for $10 \leq F_s < 25$ $\pm 5.0$ Hz for $F_s \geq 25$	1
The above signal frequency range tests are to be performed over the given ranges and meet the given requirements at three temperatures: $T = \text{nominal } (23^\circ C)$ , $T = 0^\circ C$ , and $T = 50^\circ C$					
Signal voltage magnitude	100% rated	80% to 120% rated	1	10% to 120% rated	1
Signal current magnitude	100% rated	10% to 200% rated	1	10% to 200% rated	1
Phase angle with $ f_{in} - f_0  < 0.25$ Hz	Constant or slowly varying angle	$\pm \pi$ radians	1	$\pm \pi$ radians	1

## 1.4 Spectral Estimation Techniques for Power Quality Monitoring

In this section, a comprehensive and critical literature review is presented for spectral estimation techniques for the estimation of the power quality disturbances parameters. The required techniques for spectral analysis can be classified into two main categories: the non-parametric and parametric methods (also known as model-based methods). Herein, we focus on these methods under stationary conditions and their extension to non-stationary conditions.

### 1.4.1 Non-Parametric Methods

Non-parametric spectral estimation analyses the data without making any assumptions about the data and hence are called non-parametric.

#### 1.4.1.1 Zero-Crossing transform

The standard IEC 61000-4-30 proposes a frequency estimator based on the zero-crossing technique. This technique estimates the frequency using the time between two zero crossings of voltage signal. Zero crossing is defined as the change of the signal from positive

Table 1.6: Synchrophasor measurement bandwidth requirements using modulated test signals.

Influence quantity	Reference Condition	Minimum range of influence quantity over which PMU shall be within given TVE limit			
		P class		M class	
		Range	Max TVE (%)	Range	Max TVE (%)
$k_x = 0.1,$ $k_x = 0.1$ radian	100% rated signal magnitude, $f_{nominal}$	Modulation frequency 0.1 to lesser of $\frac{F_s}{10}$ or 2 Hz	3	Modulation frequency 0.1 to lesser of $\frac{F_s}{5}$ or 5 Hz	3
$k_x = 0,$ $k_x = 0.1$ radian	100% rated signal magnitude, $f_{nominal}$		3		3

to negative value (or vice versa) as shown in Fig. 1.15.

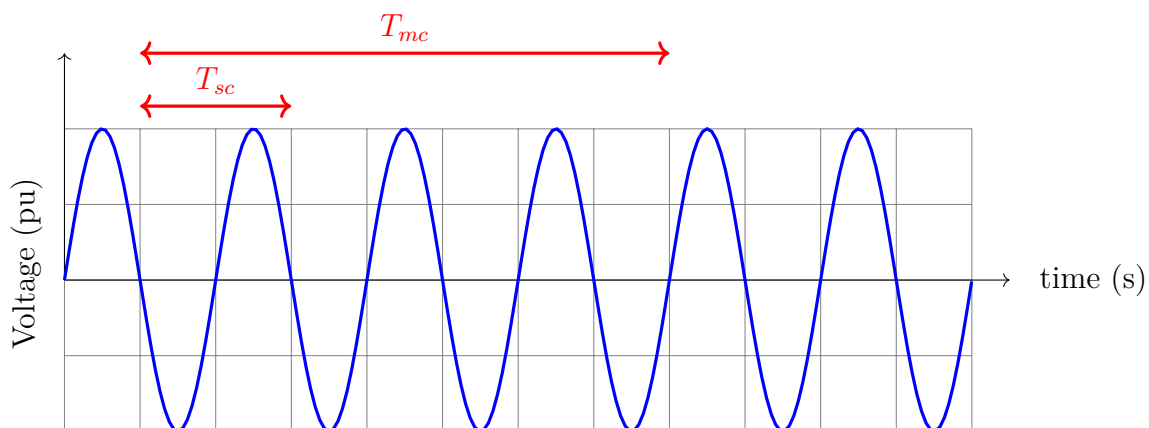


Figure 1.15: Zero-crossing approach illustration.

The first step is based on the computation of the time between two or several zero crossings in the same direction. From Fig. 1.15, the frequency can be obtained as follows

$$\hat{f}_0 = \frac{1}{T_{sc}}, \quad (1.9)$$

where  $T_{sc}$  is the time between two consecutive zero crossings in the same direction. In the case of  $N_{zc}$  zero crossings in the same direction, the frequency can be estimated by

$$\hat{f}_0 = \frac{N_{zc}}{T_{mc}}, \quad (1.10)$$

where  $T_{mc}$  is the time between  $N_{zc}$  zero crossing.

Nevertheless, this technique is sensitive to distorted signals, harmonics, inter-harmonics,

and other power quality disturbances [13].

#### 1.4.1.2 RMS and peak voltage techniques

Several classical techniques allow to determine the voltage amplitude. Herein, we interest by two techniques for voltage amplitude characterization, which are the root mean square (rms) and peak voltage techniques. The rms technique allows to obtain the amplitude by using the rms value of the voltage over a multiple of one half-cycle of the power system frequency. The rms voltage can be expressed in term of the instantaneous voltage,  $V(t)$ , over a given period of time  $T$

$$V_{rms} = \sqrt{\frac{1}{T} \int_0^T V^2(t) dt}, \quad (1.11)$$

Alternatively, the peak voltage component allows also to obtain the amplitude. The peak voltage as a function of time can be obtained as follows

$$V_{peak} = \max_{0 < \tau < T} |v(t - \tau)| \quad (1.12)$$

Power quality monitors obtain the rms voltage once every cycle or once every few cycles. A power quality monitor will usually calculate the rms value once every cycle and thus will give an overestimation of the event duration such voltage sag [31].

The root mean square and peak voltage techniques are simple and well-proven techniques. However, these techniques do not provide any estimate of the phase angle parameter and are quite sensitive to noise. To overcome these issues, many estimation algorithms are based on Fourier transform (FT).

#### 1.4.1.3 Fourier transform and its extensions

The Fourier transform (FT) is the most widely used computation algorithm for stationary signals by extracting spectrum at specific frequencies. The signal to be analysed is modeled by sum of sinusoids signals with different frequencies. The Fourier transform allows to estimate the frequency components without any information of the time at which the frequency components appear. Several papers and books are devoted to the Fourier transforms [57, 58].

The Fourier transform of a continuous time signal  $x(t)$  is given by [57, 59]

$$X(f) = \int_{-\infty}^{\infty} x(t) e^{-j2\pi ft} dt, \quad (1.13)$$

In sampled data systems, the analysis of signal is performed by the discrete time Fourier transform (DTFT). The DTFT is usually implemented using the fast Fourier transform



(FFT) over a short signal length. The FFT is computed at discrete steps in the frequency domain with an input signal that is sampled at discrete instants in the time domain.

Let assume that the signal length contains the  $N$  measurements or samples from a sampled voltage or current signal in an equal interval  $t_n$

$$t_n = n\Delta t = \frac{nT_w}{N}, \quad (1.14)$$

where  $n$  is an integer number ( $n = 0, 1, \dots, N-1$ ).  $N$  corresponds to the number of samples within the measurement window  $T_w$ . The DTFT phasor estimator is given by

$$\hat{V} = \frac{1}{N} \sum_{n=0}^{N-1} x[n]e^{-j\hat{w}n}, \quad (1.15)$$

where the angular frequency,  $w$ , estimator is given by

$$\hat{w} = \arg \max_w \frac{1}{N} \left| \sum_{n=0}^{N-1} x[n]e^{-j\omega n} \right|^2. \quad (1.16)$$

In fact, the use of the DTFT over a finite length of infinite signal can be interpreted as multiplying an infinitely continuous signal with a rectangular window function defined by

$$w[n] = \begin{cases} 1 & \text{if } |n| \leq \frac{1}{2}T_w. \\ 0 & \text{otherwise.} \end{cases} \quad (1.17)$$

As mentioned before, the DTFT computation requires the use of data window that implies truncation of the sampled data. This leads to errors in the Fourier transform computation from the sampled data, which is known as the leakage effect. In power system applications is preferred to use a rectangular windowing function due to its simplicity.

The benefits of the DTFT are its simple implementation, low computational complexity, accuracy, and immunity against harmonic components under stationary conditions. Indeed, DTFT leads to high accuracy estimation under stationary conditions, when the fundamental frequency is close to the nominal one. However, its accuracy has several limitations under off-nominal frequency, amplitude, or phase variations [60].

## 1.4.2 Parametric Methods

The spectral estimation methods of this subsection are based on parametric models, such as sinusoidal and autoregressive-moving average (ARMA) models. These methods are known as parametric or model-based methods and they assume that the signal satisfies a generating model with known functional form. These methods have been developed to overcome drawbacks of non-parametric methods. The selection of appropriate model for

the process is based upon:

- A priori knowledge about how the process is generated
- Experimental results indicate that a particular model works well.

Once the signal model is selected, the next step is to estimate the signal parameters from the given data. The signal's spectral characteristics of interest are then derived from the estimated model. In the cases where the used model is a close approximation of the real model, a highest estimation performances can be obtained over a significantly less data as compared to those in non-parametric methods. The limitation of these methods only depends on the matching between the true and theoretical signal model.

The parametric methods can be classified into two parts: 1) parametric methods for discrete or line spectra such as those associated with sinusoidal signal buried in additive noise. 2) parametric methods for rational spectra that form a dense set in the class of continuous spectra.

#### 1.4.2.1 Discrete spectra

The spectral estimation based-parametric model for discrete spectra reduces to the estimation of signal parameters and can be decomposed into two steps: 1) the estimation of the frequency ( $f_0$ ) from the set of observations, which is the main difficult step. 2) Estimation of the other parameters that can be reformulated as a simple linear regression problem.

These methods include subspace techniques that are also called high-resolution techniques. These subspace techniques include MUSIC (MUltiple SIngle Classification) and ESPRIT (Estimation of Signal Parameters via Rotational Invariance Techniques) approaches. MUSIC approach allows to estimate the frequency components from a sinusoidal model. However, the drawbacks of this approach are its Failing to resolve closely spaced signals at low SNRs and its high computational burden. ESPRIT approach has been proposed to reduce this high computational burden. The ESPRIT method uses also sinusoidal models and estimates the frequency components. ESPRIT is a signal subspace-based technique, while MUSIC is noise subspace-based techniques. Both techniques are widely used to analysis the harmonics and inter-harmonics in the power system. These two methods have achieved good performance for inter-harmonic estimation [2]. Moreover, they can be used to estimate frequency for transient voltages and currents [2].

However, both techniques require the knowledge of the number of frequency components in the signal. Moreover, their performances critically degrade under high noisy environment.

### 1.4.2.2 Continuous spectra

In previous subsection, we discussed the spectral estimation for discrete spectra that is used to characterize the disturbances such harmonic and inter-harmonic. Otherwise, some disturbances signals could be described by continuous spectra, especially when the number of harmonic or inter-harmonic is not limited and can be a band-limited distortions. For instance, this include the current and the high frequency components occurred by an arc furnace and active rectifiers, respectively. However the main barrier is the limited knowledge on the cause of high frequency components in power systems [13]. This makes hence the interpretation becomes difficult. In this subsection, a brief description of the useful continuous spectra methods is performed.

Autoregressive (AR) model is a simple and used model, where autoregressive moving average (ARMA) model is more general rational model. For more details, the reader could refer to [61]. The parametric methods for continuous spectra include the linear prediction techniques such as Prony. Instead of estimating the signal parameters from the data, these techniques model the data as the output of a linear system driven by white noise. Then, the parameters of the linear system can be estimated using ARMA model. It can be observed that the Prony method performances are equivalent to those of the MUSIC and ESPRIT [13]. For the theoretical considerations, one can refer to [61, 62]. However, most signals of PQ disturbances possess a discrete spectra, where the frequency components at discrete frequencies.

### 1.4.3 Discussion: parametric methods versus non-parametric methods

The non-parametric methods are well used for the frequency and phasor estimation. These methods require a long data window for achieving a good resolution, however, this window leads to the leakage effect. In power quality applications, the recorded signal is finite that presents the major limitation of the non-parametric methods [13].

On the other hand, the parametric methods or based-model methods require a priori information about how the process is generated. In the cases where the used model is a close approximation of the real model, a highest estimation performances can be obtained over a significantly less data as compared to those in non-parametric methods. However, the limitation of these methods only depends on the matching between the true and theoretical signal model.

As highlighted previously, several power quality events are non-stationary signals. In such conditions, Fourier transform-based techniques are not suitable to analyse these non-stationary signals. Therefore, PQ estimation is usually performed by using non-stationary methods. These methods can be classified into two categories: non-parametric

methods and parametric methods. Non-parametric methods include time-frequency or time-scale representation [61, 63–67, 70–84]. Parametric methods include non-stationary high-resolution techniques and non-stationary MLE techniques [2, 85, 86]. These techniques should use a sliding window in order to handle the non-stationarity of the signal. The signal is considered to be stationary over each window, which is a short duration of time. The estimation of the time-varying parameters can then be performed over each block by shifting the data window (block). Therefore, the estimated parameters are time-varying since they depend on the window number.

Several advanced techniques have been proposed to analyze the PQ disturbances under non-stationary conditions. Hilbert-Huang transform (HHT) is one of recent advances in signal processing techniques. HHT is based on Hilbert transform (HT) and Empirical Mode Decomposition (EMD) techniques [70]. Empirical Mode Decomposition is a time–frequency analysis method that decomposes the signal into number of intrinsic mode functions (IMFs) [71]. Then, the Hilbert transform analysis these IMFs to estimate the instantaneous frequency (IF), amplitude (IA), and phase (IP). HT main advantage is that it requires a single phase signal for extracting the instantaneous frequency and amplitude. The Hilbert transform can detect the presence of the fault, however it suffers from border effects that may lead to incorrect information of the event. Moreover, it can be difficult to interpret under fast signal modulation, i.e. when the Bedrosian condition is not satisfied. On the other hand, the EMD presents several drawbacks such as mode mixing that may lead to a wrong intrinsic mode functions (IMF) decomposition and border effect. A Hilbert-Huang transform based algorithm for PQ disturbance classification was proposed in [73]. It has a special focus on the the PQ events that are sag, swell, harmonics, spikes, notches, flicker, and transients. The probabilistic neural network (PNN) technique is used to classify the corresponding event. A PQ assessment approach expands a distorted signal into its intrinsic mode oscillations was proposed in [72]. A comparison is performed between the proposed technique and S-transform. The obtained results showed a good classification accuracy for detection of PQ disturbance, such as voltage spike and notch. Under non-stationary conditions, it is become imperative to separate between different components of frequency for identify the cause of PQ disturbances. For such purpose, a combination between EMD and Hilbert transform to detect the cause of voltage sag was proposed in [74]. Then, PNN classifier is used for identifying the voltage sag cause and type.

## 1.5 Power Quality Disturbances Classification Techniques

Power system complexity does not only require signal processing techniques for identifying signal parameters, but also for identifying and classifying special class of system behaviour. The estimated parameters can be used as inputs of the classification techniques whose output is the disturbance type. PQ disturbances classification is of great important in the PQ monitoring. Among several techniques of PQ disturbance classification, we focus on the most commonly techniques. These techniques can be classified into two classes: 1) classical techniques and 2) pattern recognition techniques [87, 88]. In the literature, others classification techniques have been proposed, and the reader could refer to [89–98].

### 1.5.1 Classical Techniques

Most classical techniques use two parameters for classifying the power quality disturbances (i.e., amplitude (residual voltage) and duration) [2]. These techniques do not use the phase angle and other parameters. Moreover, they are suitable for single-phase measurements. Electrical power systems are three-phase signals that require the use of classification techniques for multi-channel measurements through the lowest residual voltage and the longest duration of all the channels [2]. In this subsection, we describe the commonly classical techniques for disturbances classification, specifically voltage sags [2, 99, 100].

#### 1.5.1.1 ABC classifier

ABC classification technique is used to classify the unbalanced voltage sags. Regarding voltage sag, there are seven types that are denoted with letters from A to G and are defined in [99]. These sags types are illustrated by Fig. 1.16. The dashed arrows present the balanced three-phase voltages and the solid ones correspond to the sags types caused by the three-phase system fault(s). For instance, Voltage sags due to symmetrical faults occur the same sag in the three-phase, which is called balanced sags and is refereed as type A. The values of voltage sag differ from a complex pre-fault voltage in phase  $a$  ( $E$ ), and a voltage in the faulted phase or between the faulted phases ( $V$ ) [99]. ABC classification is a simple approach used for voltage sags classification. However, This technique is not able to extract the voltage sag parameters.

#### 1.5.1.2 Symmetrical component classifier

Symmetrical component classifier allows to identify the six voltage sags among the C and D types [100]. Regarding sags sub-types, an illustration of the six sag sub-types among C and D types are illustrated in Fig. 1.17. To classify the corresponding sag sub-type,

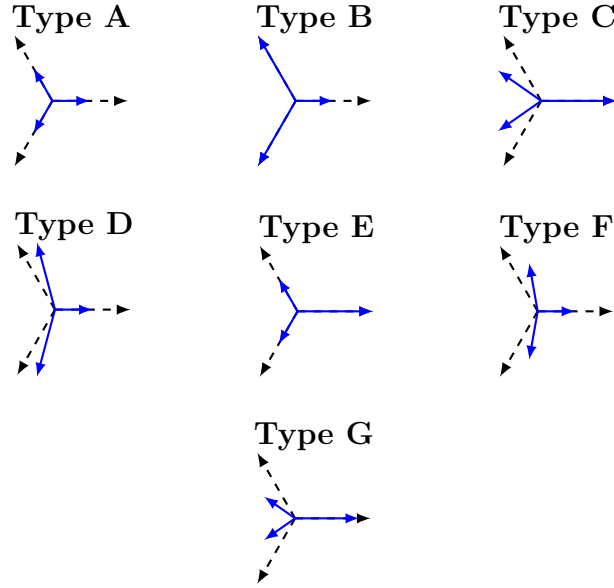


Figure 1.16: ABC classification: voltage sags types.

we use the angle between the drop in positive- and negative-sequence voltages ( $V_1$  and  $V_2$ ) [100]. The angle is given by

$$T = \frac{1}{60^\circ} \arg \left( \frac{V_2}{1 - V_1} \right), \quad (1.18)$$

where  $T$  is rounded to the nearest integer. This angle allows to identify the corresponding sag type

$$\begin{aligned} T = 0 & \quad \text{Type } C_a \\ T = 1 & \quad \text{Type } D_c \\ T = 2 & \quad \text{Type } C_b \\ T = 4 & \quad \text{Type } D_a \\ T = 5 & \quad \text{Type } C_c \\ T = 6 & \quad \text{Type } D_b \end{aligned} \quad (1.19)$$

These classical techniques are very sensitive to large variations in amplitude or phase angle, and a small error in frequency estimation may lead to an erroneous sag type. In such conditions, it is imperative to use other advanced classifiers for PQ monitoring. In the next subsections, a review is performed for the classifiers-based pattern recognition.

## 1.5.2 Pattern Recognition Techniques

Pattern recognition is the act of taking in raw data and taking an action based on the category of the pattern. It has become of great important in electrical engineering field and it has evolved highly sophisticated neural and cognitive systems for such tasks.

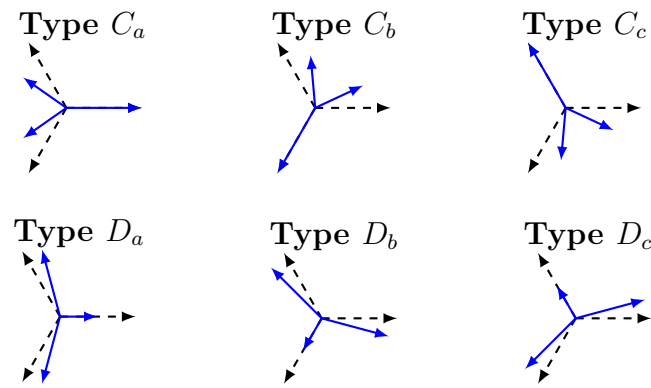


Figure 1.17: Six sub-types of three-phase unbalanced voltage sags among C and D types.

These techniques can be used for the applications where there is a few knowledge of the events characteristics and the systems. Hence, data learning is a practical way to analysis the PQ disturbances. Several techniques for pattern recognition of the PQ disturbances have been proposed. These techniques include: artificial neural network (ANN), Fuzzy expert system, genetic algorithm, and support vector machine [89, 92, 101–105]. In fact, the main advantage of a pattern recognition machine is its capability of learning by examples and generalization. Pattern recognition has been applied in power systems for PQ disturbances classification, protection, and consumer profile identification.

### 1.5.2.1 Artificial neural network

Artificial neural networks have widely been used for classifying several PQ disturbances and they proved a good performance for solving the PQ disturbances classification. The multilayer perceptron (MLP) is the most used structure of the ANN. Figure 1.18 illustrates network graph of a multilayer perceptron. Neurones are grouped into layers and the inputs and outputs are grouped in the first and last layers, respectively. Hidden neurons allow to perform a non-linear transformation of the input data into a new space. The different classes of the pattern recognition can be separated from each other in this new space [106]. The main advantage of ANN techniques is their ability to self-learn the pattern recognition of those relationships and their applicability to several systems. The classification techniques based-ANN have been applied to harmonic, interruption, and several PQ disturbances classification.

Several research papers have dealt with PQ monitoring and events classification based on ANNs [79, 107–109, 109–113]. In [107] an automatic classifier of the PQ disturbances was proposed. This classifier is based on the FFT and discrete wavelet transform (DWT) based MLP neural network. A PQ disturbances classifier based on wavelet transform (WT) and MLP neural network with three layers was proposed in [108]. In [109], the authors proposed an adaptive linear network (ADALINE) and FFNN for classifying several PQ disturbances. ADALINE allows to estimate the harmonic and inter-harmonic components

for obtaining the THD and rms values. FFNN was used for classifying the several PQ disturbance such as flicker, spikes, transient.

### 1.5.2.2 Support vector machine

A support vector machine (SVM) was proposed in the late 1970<sup>s</sup> and is based on statistical learning theory used for classification and pattern recognition [114, 114, 115], such as forecasting, dependency estimation, and intelligent machines. The SVM is based on two main steps that are: 1) a non-linear transform of the input data is performed into a high-dimensional feature space. Then, 2) optimal hyperplane determination in a high- or infinite-dimensional space allows to classify the input data in this high-dimensional space. The SVM requires also a learning stage as ANN. Several published techniques in the literature have proven that these techniques are suitable for classification and pattern recognition [116–124]. A classifier based on DWT and space vector machine for classifying several PQ disturbances was proposed in [116]. In [117], a classifiers based on SVM for PQ disturbances classification was proposed. The SVM classifiers were One-Versus-One (OVO) and One-Versus-Rest (OVR) suitable for there cognition of the multi class problems. The multi class SVM techniques suffer due to the size of the network, heuristic solution scheme, and complicated data preparation. The authors proposed in [118] a disturbances-Versus-Normal (DVN) approach for multi class SVM. A classification technique for real-time PQ events was proposed in [125]. This technique was based on DWT for feature extraction and one versus one multi class SVM as a binary classifier.

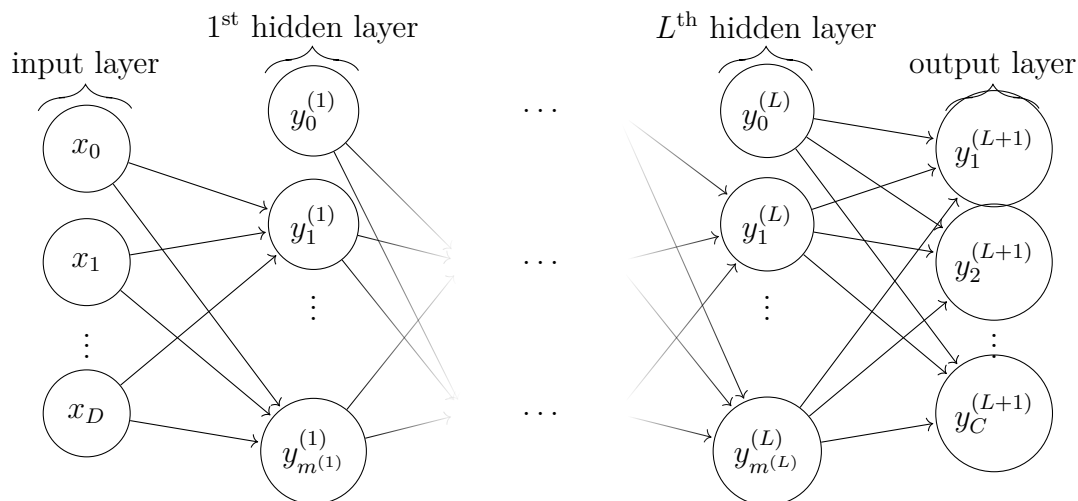


Figure 1.18: Network graph of a  $(L+1)$ -layer perceptron with  $D$  input units and  $C$  output units. The  $l^{\text{th}}$  hidden layer contains  $m^{(l)}$  hidden units.



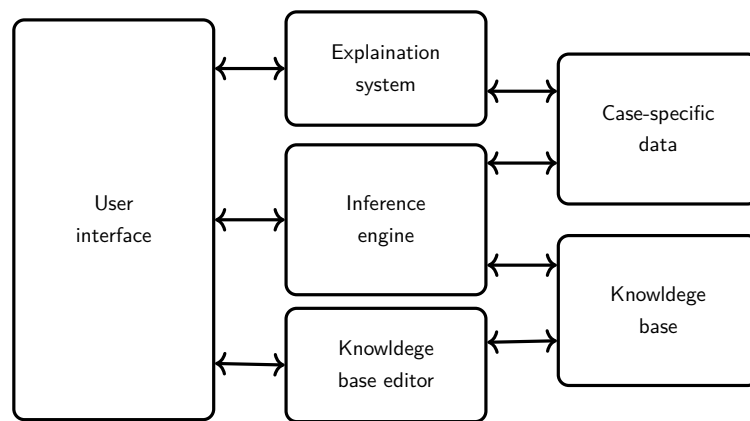


Figure 1.19: Illustration of a rule-based expert system architecture.

### 1.5.2.3 Fuzzy expert systems

Fuzzy logic systems inspired by human reasoning to generalize the binary logic under uncertainty. Fuzzy set maps the objects in the concern domain to their membership values in the set using a function. The triangular and trapezoidal functions are the most used membership functions. The particular application of AI used in the diagnostic module is called an expert system [126]. Fuzzy Expert System (FES) is the one that use two elements ( i.e., fuzzy sets and fuzzy rule base), instead of boolean sets for reasoning about data. A fuzzy set can be fully defined by its membership functions and fuzzy rules offer human-like reasoning capabilities and provide transparent interface mechanism.

The PQ disturbances classification based on expert systems requires knowledge from human experts and involves automatically extracting the relevant information by computers. This knowledge is often heuristic in nature, which is difficult to be used by computer.

The typical structure of an expert system is rule-based expert system as shown in Fig. 1.19. This structure consists of the following blocks: the user interface presents the interface where input data are sent into system, such the PQ monitoring output. Its outputs are the classification results. Interface engine performs the reasoning between the expert system knowledge (or rules) and the data from a particular problem. The explanation of the reasoning to the user is performed by explanation system. Knowledge base editor allows a human expert to update or check the rules and the knowledge base contains all the rules. The data provide by the user is stocked in case-specific data, this latter includes also partial additional information from the measurements. An illustration of rule-based expert system for event classification of PQ disturbances is given in Fig. 1.20. This architecture is able to classify the corresponding event from the input recorded data. The expert system uses rules from the knowledge base and then it gives the corresponding event class.

There are several expert systems for PQ disturbances classification [127–138]. The authors proposed in [127] a disturbances algorithm based on principle component analysis (PCA)

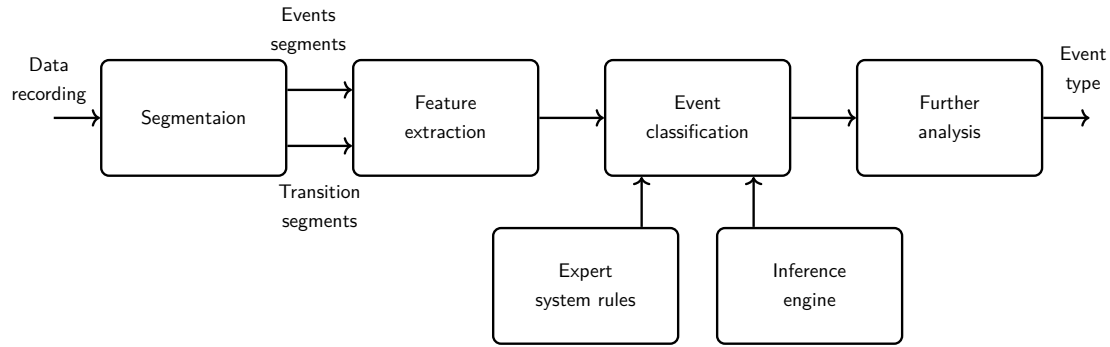


Figure 1.20: Illustration of rule-based expert system for event classification of PQ disturbances.

and neuro-fuzzy classifier. In [128], a PQ events recognition systems that integrated the noise suppression algorithm, feature extraction based on the Parseval's Theorem, and the neuro-fuzzy classifier was developed and tested using both simulated noise-riding data of various disturbance events and actual field data. In [129], the authors proposed an algorithm for detection and classification various PQ disturbances, which is based on fuzzy decision tree. The authors proposed in [130] a disturbance classifier based on DWT, Kalman filter, and fuzzy expert system.

#### 1.5.2.4 Genetic algorithm

Feature selection or optimization algorithm are used to obtain the suitable feature and discover the redundant feature of the disturbances. In classifier based-feature selection algorithms, a feature is selected from the feature extraction stage that has the best suitable recognition rate. Several algorithms are used in the feature selection process such as genetic algorithm (GA).

Genetic algorithm is an iterative search heuristic based on the evolutionary ideas of natural selection [139]. GA is widely used to solve the optimization problems by finding the optimum solutions [140]. GA uses a string structures that are Chromosomes, which are a binary digits represent the encoding of the control parameters of a specific problem. Individual population is repeatedly modified, then a decision is taken using probabilistic rules. At each generation, GA selects parent that is a random individual from the actual population, which produces a children for the next generation. The poor solutions are eliminated by a competitive selection using GA (mutation and cross over). The main advantage of genetic algorithm is its ability to find the optimal solution over successive generation [140–146].

The authors proposed in [147] an automatic classifier based on Fuzzy k-nearest neighbour (FKNN) and genetic algorithms. The selection of the optimal feature is obtained by GA algorithm that allows to improve the classification accuracy. This accuracy was enhanced

using 16 better features from 96 features. In [148], a genetic and SVM algorithms were proposed to classify the PQ disturbances. The authors proposed in [149], a combination of the genetic algorithm and extension theory. The extension theory allows to provide a means for distance measurement and GA provides an optimal solution within a wide space.

However, the performances of all the above-presented techniques critically depend on the learning stage that requires a training database. The size of this latter must be sufficiently large to encompass different kinds of power quality conditions, which may be difficult to obtain in practice. Their performances also depend on many parameters and on the features extraction process. Furthermore, the learning stage requires relatively high computational complexity effort.

## 1.6 Conclusion

In this chapter, a state of the art of power quality disturbances characterization was performed. In particular, several feature extraction and classification techniques for power quality monitoring were reviewed.

Power quality involves voltage quality, which presents a voltage deviation from the nominal voltage. It involves also current quality that concerns its deviation from the nominal current. PQ disturbances can be classified into two main classes: power quality variations and events. A distinction is made between the variation and the event, where a triggering mechanism is required to start recording the event by determining its starting and ending points. In fact, the triggering mechanism detects the event and extract additional information. A review of several standards for PQ was performed. These standards provide guidelines, recommendations, and frequency and phasor limits. The PQ standards allow to assure compatibility between the power system and the end-user equipments. The most known organisations for developing standards on power quality are IEC and IEEE. Regarding power quality monitoring, PMUs are used to extract frequency and phasor of the voltage at important substations for solving the PQ disturbance problems. Several frequency and phasor estimator requirements are provided by the IEEE standard C37.118.2011. Their performances are evaluated under steady-state and dynamic compliance conditions. Most of previously published techniques in frequency and phasor estimations are suboptimal, since they do not fully exploit the three-phase nature of the electrical signals. Moreover, the performances of these techniques critically degrade under off-nominal conditions.

Extracted parameters can be used as inputs for classification tool and disturbance detection in power systems. A state of the art of the existing PQ disturbance classification techniques was reviewed. Specifically, pattern recognition-based techniques (i.e. ANN,

SVM, etc.) critically depend on a learning stage that requires a training database and on a features extraction process. Moreover, these techniques particularly suffer from computation complexity.

To overcome the above-discussed issues and challenges, the use of advanced signal processing tool becomes obvious. In this context, the next chapter will deal with a parametric spectral estimation technique that is used to estimate the phasor and the frequency. The proposed technique fully exploits the multidimensional nature of the electrical signals and it is able to achieve good performances even under off-nominal conditions. Moreover, its design procedure is simple and particularly suitable for power grid monitoring.



## Chapter 2

# Phasor and Frequency Estimations

**T**HIS chapter presents a new signal processing-based technique for voltage parameters estimations. The proposed technique uses an optimization algorithm that allows to choose the suitable parameter (i.e. fundamental frequency). The benefits of the proposed estimators are also illustrated with real power system data obtained from the DOE/EPRI National Database of Power System Events. The above-mentioned points will be discussed in the next sections.

## 2.1 Introduction

Parameters estimation of the voltage signal, i.e. frequency and phasor, are of special interest in electric power systems. As it was mentioned in the previous chapter, voltage or current signals are expected to be pure sinusoidal waveforms at the fundamental frequency (50/60 Hz). However, the increasing amount of renewable energy sources will lead to unacceptable levels of power quality by producing additional disturbances. Therefore, each PQ disturbance has a substantial influence on the voltage and current signals. In this context, it becomes imperative to identify the cause of each disturbance by estimating their parameters. Motivated by this, spectral analysis of signals is a suitable approach for the power quality characterization.

In the literature, several techniques have been proposed to deal with the voltage spectral estimation (see section 1.4). Indeed, Fourier transform-based techniques are used to estimate the frequency and phasor of voltage. However, these techniques lead to poor estimation under noisy environment and require long data to achieve good resolution. Moreover, their performances critically degrade under off-nominal conditions. To overcome these limitations, parametric methods allow to achieve highest estimation performances over a significantly decreased data amount as compared to those in non-parametric methods.

In this context, this chapter describes a novel estimation technique based on a parametric method. This technique fully exploits the multidimensional nature of the electrical signals. The proposed technique is devoted to fundamental frequency and phasor parameters estimation. It is based on the least squares method, which is equivalent to the maximum likelihood estimator (MLE) under additive white Gaussian noise. It has been demonstrated that the maximum likelihood estimator is an asymptotically optimal estimator [150]. MLE performs better than traditional methods with highest statistical performance. This proposed technique requires the maximization of a 1-dimensional cost-function. For this purpose, we propose an optimization algorithm based on the Newton-Raphson optimization technique. This technique allows improving the performance of the frequency and phasor estimators and has lower computational complexity than classical techniques. The proposed estimator can be applied for real-time characterization

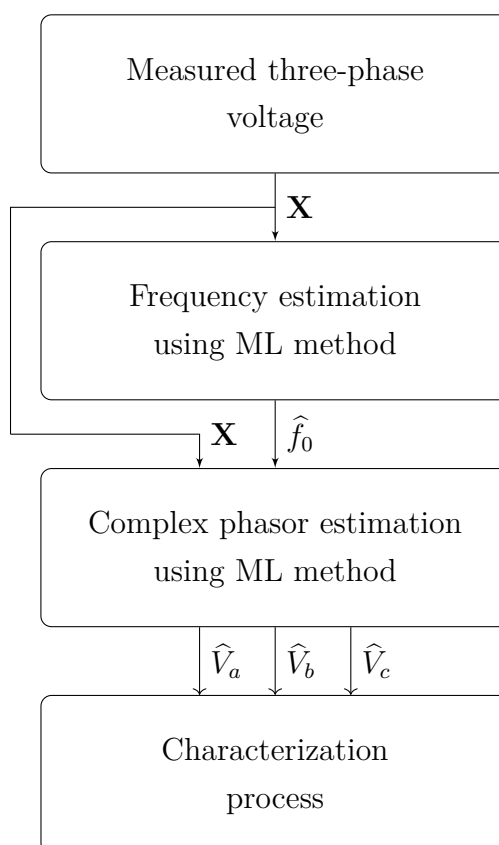


Figure 2.1: Flowchart of the proposed algorithm.

of processes since it uses the discrete-time signals. The proposed algorithm is illustrated by Fig. 2.1, where  $\mathbf{X}$  is the measurements matrix for the three-phase voltage system,  $\hat{f}_0$  corresponds to the estimated fundamental frequency, and  $\hat{V}_a$ ,  $\hat{V}_b$ , and  $\hat{V}_c$  are the estimated complex phasors, respectively.

In PMU standard C37.118 [52, 56], several frequency and phasor estimator requirements have been defined. The performance of the phasor, frequency, and rate of change of frequency (ROCOF) estimators are evaluated under steady-state and dynamic compliance conditions, with several criteria such as the Total Vector (TVE), Frequency (FE), and ROCOF (RE) Errors. In this chapter, we will focus on M-class that requires TVE and FE smaller than 1% and 5 mHz, respectively. A comparison of the TVE and FE performances according to the IEEE Std. C37.118.2011 requirements has been performed.

This chapter is organised as follows: first, the three-phase signal model and the proposed angular frequency and phasor estimators are presented including the maximum likelihood method. Then, an extension to non-stationary signals of these estimators is performed. Afterwards, the proposed optimization algorithm used for the frequency estimation is given. Finally, the benefits of the proposed estimators are illustrated with real power system data obtained from the DOE/EPRI National Database of Power System Events.



## 2.2 Parameters Estimations

In this study, a stationary signal over a small time window is used with additive noise. The IEEE 1159 standard recommends the use of half-cycle for the voltage sag and swell. In the forthcoming subsections, a signal and phasor models under noisy environment are presented. Based on the phasor model, we also describe the proposed maximum likelihood angular frequency and phasor estimators with their extension to non-stationary case.

### 2.2.1 Study hypotheses

In this study, we make the following hypotheses:

- H1: the input signal on phase  $m \in \{a, b, c\}$  is modelled as a sine wave that is corrupted by an additive noise.
- H2: the additive noise, as an approximation, is supposed to be a white Gaussian noise with zero mean and variance  $\sigma^2$ . This should be a good approximation for the electrical noise picked up in the wiring and signal conditioning circuits [151]. Moreover, white Gaussian noise is widely considered in the research of power quality issues [110].
- H3: the three-phase signals have the same fundamental frequency  $f_0$ .
- H4: the signal does not contain any harmonics<sup>1</sup>.

### 2.2.2 Signal model and phasor expression

Under the hypotheses H1-H4, the discrete time signal of phase  $m$  ( $m \in \{a, b, c\}$ ) in a three-phase voltage system can be expressed as (see [152])

$$V_m[k] = a_m \cos(kw_0 + \phi_m) + b_m[k], \quad (2.1)$$

where  $a_m$  and  $\phi_m$  are respectively the amplitudes and initial phases of each fundamental component of the three-phase voltage system.  $w_0 = w_n + \delta = (2\pi f_0)$  corresponds to the fundamental angular frequency,  $w_n$  is the nominal angular frequency, and  $\delta$  refers to angular frequency deviation from the nominal angular frequency (i.e.,  $100\pi$  or  $120\pi$   $rd/s$ ).  $f_0$  is the fundamental frequency. Finally,  $b_m[k]$  refers to the additive noise. The complex phasor of phase  $m$  can be expressed as follows

$$V_m = a_m e^{j\phi_m}. \quad (2.2)$$

---

<sup>1</sup>If it is not the case, we use a low pass-filter to respect this hypothesis.

It should be mentioned that under nominal conditions, the phase shift between phases is equal to  $120^\circ$  and  $a_m = 1$  pu. If one of these requirements is not satisfied, the system is considered as unbalanced [31, 33].

In practice, the signal parameters could be estimated from the measured three-phase voltage. Let consider that the voltage sensors record  $N$  consecutive samples of the electrical signal  $V_m[k]$ , where  $k = 0, 1, \dots, N-1$ . Using matrix notations, the signal model in (2.1) can be expressed as

$$\mathbf{X} = \mathbf{G}(w_0)\mathbf{S} + \mathbf{B}, \quad (2.3)$$

where

- $\mathbf{X}$  and  $\mathbf{B}$  are  $N \times 3$  matrices containing the recorded and noise samples, respectively. These matrices are defined by

$$\mathbf{X} = \begin{bmatrix} x_a[0] & x_b[0] & x_c[0] \\ \vdots & \vdots & \vdots \\ x_a[N-1] & x_b[N-1] & x_c[N-1] \end{bmatrix}, \quad (2.4)$$

$$\mathbf{B} = \begin{bmatrix} b_a[0] & b_b[0] & b_c[0] \\ \vdots & \vdots & \vdots \\ b_a[N-1] & b_b[N-1] & b_c[N-1] \end{bmatrix}, \quad (2.5)$$

- $\mathbf{G}(w_0)$  is a  $N \times 2$  matrix that only depends on the unknown fundamental angular frequency  $w_0$ . This matrix is defined as

$$\mathbf{G}(w_0) = \begin{bmatrix} 1 & 0 \\ \cos(w_0) & \sin(w_0) \\ \cdot & \cdot \\ \cdot & \cdot \\ \cdot & \cdot \\ \cos(w_0(N-1)) & \sin(w_0(N-1)) \end{bmatrix}. \quad (2.6)$$

- $\mathbf{S}$  is a  $2 \times 3$  real-valued matrix containing the amplitudes and initial phases of the three-phase voltage system. This matrix is defined by

$$\mathbf{S} = \begin{bmatrix} a_a \cos(\phi_a) & a_b \cos(\phi_b) & a_c \cos(\phi_c) \\ -a_a \sin(\phi_a) & -a_b \sin(\phi_b) & -a_c \sin(\phi_c) \end{bmatrix}. \quad (2.7)$$

In the next section, we propose a parametric estimators that uses the three-phase signal model in (2.1). This proposed estimators allow to estimate the angular frequency ( $w_0$ )

and phasor ( $V_m$ ) from the input three-phase signals  $\mathbf{X}$ .

### 2.2.3 Least squares estimations

The main objective of this present section is to estimate the voltage parameters, i.e. angular frequency and phasor, from the input three-phase signals,  $\mathbf{X}$ . In this context, we propose the use of Maximum Likelihood estimator (MLE). MLE corresponds to least square estimator when the noise is white Gaussian noise. This spectral estimation based-parametric model can be decomposed into two steps: first, the estimation of angular frequency from  $\mathbf{X}$  is the main difficult step. Then, the estimated phasor can be obtained once the angular frequency is estimated. These two steps are described in the next subsections.

#### 2.2.3.1 Angular frequency estimation

This frequency estimator, based on the maximum likelihood principle, is the most popular approach to obtaining practical estimator. Moreover, its performance is optimal for a small recorded data. The maximum likelihood estimator is defined as the value of angular frequency ( $w_0$ ) that maximizes the log-likelihood function. In the case when a closed form expression for MLE can not be found, then a grid search or an iterative maximization of the log-likelihood function can be exploited. If the grid search is not practical, then the iterative approaches such as Newton-Raphson can be used. The value that is maximizing the asymptotic log-likelihood function is the estimated angular frequency. The optimization algorithm based on the Newton-Raphson method is described in the forthcoming section. In particular, the estimation of  $w_0$  ( $\hat{w}_0$ ) is obtained by the following maximization

$$\{\hat{w}_0, \hat{\mathbf{S}}\} = \arg \max_{w, \mathbf{S}} \mathcal{L}(\mathbf{X}; w, \mathbf{S}), \quad (2.8)$$

where  $\hat{\mathbf{S}}$  is the estimation of  $\mathbf{S}$  and  $\mathcal{L}(\mathbf{X}; w, \mathbf{S}) = \log(p(\mathbf{X}; w, \mathbf{S}))$  is the log-likelihood function of  $\mathbf{X}$ .  $p(\mathbf{X}; w, \mathbf{S})$  is the probability density function (pdf) of  $\mathbf{X}$  that is given by

$$p(\mathbf{X}; w, \mathbf{S}) = \frac{1}{(2\pi\sigma^2)^{\frac{N}{2}}} \times \exp \left[ -\frac{1}{2\sigma^2} (\mathbf{X} - \mathbf{G}(w_0)\mathbf{S})^T (\mathbf{X} - \mathbf{G}(w_0)\mathbf{S}) \right], \quad (2.9)$$

where  $(.)^T$  denotes the matrix transpose. It is assumed that the signal is corrupted by a white Gaussian noise (hypothesis H2 is hold). In particular, the maximization of  $\mathcal{L}(w)$  with respect to  $w$  reduces to the following minimization

$$\{\hat{w}_0, \hat{\mathbf{S}}\} = \arg \min_{w, \mathbf{S}} \mathcal{L}(\mathbf{X}; w, \mathbf{S}) = \arg \min_{w, \mathbf{S}} \|\mathbf{X} - \mathbf{G}(w)\mathbf{S}\|_F^2, \quad (2.10)$$

where  $\|\cdot\|_F^2$  is the Frobenius norm. By simplifying the cost function, we obtain

$$\begin{aligned}\|\mathbf{X} - \mathbf{G}(w)\mathbf{S}\|_F^2 &= (\mathbf{X} - \mathbf{G}(w)\mathbf{S})^T (\mathbf{X} - \mathbf{G}(w)\mathbf{S}) \\ &= (\mathbf{X}^T - \mathbf{S}^T \mathbf{G}^T(w)) (\mathbf{X} - \mathbf{G}(w)\mathbf{S}) \\ &= \mathbf{X}^T \mathbf{X} - \mathbf{S}^T \mathbf{G}^T(w) \mathbf{X} - \mathbf{X}^T \mathbf{G}(w) \mathbf{S} + \mathbf{S}^T \mathbf{G}^T(w) \mathbf{G}(w) \mathbf{S},\end{aligned}\tag{2.11}$$

The first-derivative of the cost-function with respect to  $\mathbf{S}$  is given by (please refer to reference [153])

$$\frac{\partial \mathcal{L}(\mathbf{X}; w, \mathbf{S})}{\partial \mathbf{S}} = -2\mathbf{G}^T(w)\mathbf{X} + 2\mathbf{G}^T(w)\mathbf{G}(w)\mathbf{S}.\tag{2.12}$$

Finally, by setting the derivative in (2.12) to 0, we obtain the maximum likelihood estimator of  $\mathbf{S}$ . It is defined as follows

$$\hat{\mathbf{S}} = (\mathbf{G}^T(w)\mathbf{G}(w))^{-1} \mathbf{G}^T(w)\mathbf{X},\tag{2.13}$$

where  $(\cdot)^{-1}$  denotes the matrix inverse. The most challenge step for estimating the phasors  $\mathbf{S}$  is the estimation of  $w_0$ . By replacing the  $\mathbf{S}$  by  $\hat{\mathbf{S}}$  in the equation (2.10), we obtain

$$\mathcal{L}(\mathbf{X}; w, \mathbf{S}) = \mathbf{X}^T \left( \mathbf{I}_N - \mathbf{G}(w) (\mathbf{G}^T(w)\mathbf{G}(w))^{-1} \mathbf{G}^T(w) \right) \mathbf{X}\tag{2.14}$$

By neglecting the terms  $\mathbf{X}^T \mathbf{X}$ , which is not depending on  $w_0$ , it can be checked that the estimation of  $w_0$  is obtained by

$$\hat{w}_0 = \arg \max_w \mathcal{J}(w),\tag{2.15}$$

where

$$\mathcal{J}(w) \triangleq \text{Tr}[\mathbf{X}^T \mathbf{G}(w) (\mathbf{G}^T(w)\mathbf{G}(w))^{-1} \mathbf{G}^T(w) \mathbf{X}],\tag{2.16}$$

and  $\text{Tr}[\cdot]$  is the trace of an  $N$ -by- $N$  square matrix, and is defined to be the sum of the elements on the main diagonal.

Regarding the angular frequency estimation, the main challenge step relies on the optimization of the cost function defined in (2.15). In this context, numerical methods could be used for estimating the  $w_0$  and then phasors ( $\mathbf{S}$ ) since the maximum can not found analytically. Initially, this estimator requires the maximization of a cost-function in a 7-dimensional space. However, as the phasors  $\mathbf{S}$  are linearly separable, the estimation of  $w_0$  and  $\mathbf{S}$  can be decoupled into two steps [154]. First, the nonlinear parameter  $w_0$  can be obtained by maximizing a 1-dimensional function. In the forthcoming section, we propose an iterative algorithm based on Newton-Raphson for the cost-function optimization. Then, the estimation of  $\mathbf{S}$  can be derived using a simple closed form expression. This proposed estimator based on ML method leads to highest performance under white Gaussian

noise and even under colored noise [61]. In special cases, this estimator overcomes the classical technique such discrete time Fourier transform in term of frequency resolution. It is worth mentioning that the computation of  $\mathcal{J}(w)$  requires matrix inversion of  $\mathbf{G}^T(w)\mathbf{G}(w)$ . The  $\mathbf{G}(w)$  could be large matrix, therefore matrix inverse needs more computational time. It should be mentioned that an approximate form expression of the MLE can be obtained when the signal length is multiple to half-cycle or it is large. Using the expression of  $\mathbf{G}(w)$  in (2.6),  $\mathbf{G}^T(w)\mathbf{G}(w)$  can be decomposed as [155]

$$\begin{aligned}\mathbf{G}^T(w)\mathbf{G}(w) &= \frac{1}{2} \sum_{k=0}^{N-1} \begin{bmatrix} 1 + \cos(2kw) & \sin(2kw) \\ \sin(2kw) & 1 - \cos(2kw) \end{bmatrix} \\ &= \frac{N}{2} \mathbf{I}_{22} + \frac{1}{2} \begin{bmatrix} \Re(q(w)) & \Im(q(w)) \\ \Im(q(w)) & -\Re(q(w)) \end{bmatrix},\end{aligned}\tag{2.17}$$

where  $\mathbf{I}_{22}$  is the identity matrix of size  $2 \times 2$  and  $q(w)$  is defined as

$$q(w) = \sum_{k=0}^{N-1} e^{2j\omega k} = \frac{\sin(Nw)}{\sin(w)} e^{j\omega(N-1)}.\tag{2.18}$$

In the case when the number of samples,  $N$ , is equal to an integer multiple of the fundamental half-period, we have

$$N = \frac{lF_s}{2f} = \frac{l\pi}{\omega} \quad l \in \mathbb{N},\tag{2.19}$$

then

$$\sin(Nw) = \sin(l\pi) = 0\tag{2.20}$$

Using (2.20), the scalar  $q(w)$  defined in (2.18) is equal to

$$q(w) = \frac{\sin(Nw)}{\sin(w)} e^{j\omega(N-1)} = 0.\tag{2.21}$$

In the case when  $N$  is sufficiently large and  $N \neq \frac{lF_s}{2f}$ , the scalar  $q(w)$  is generally non-zero but can be neglected as compared to  $\frac{N}{2}$  when  $\omega$  is not near 0 or  $1/2$  [150]. Using this result,  $\mathbf{G}^T(w)\mathbf{G}(w)$  can be approximated by

$$\mathbf{G}^T(w)\mathbf{G}(w) \approx \frac{N}{2} \mathbf{I}_{22}.\tag{2.22}$$

Note that this approximation is exact when  $N = \frac{lF_s}{2f}$ . Using (2.22), the cost-function in

(2.16) can be computed without any matrix inversion and can be approximated by

$$\mathcal{J}(w) \approx \frac{2}{N} \text{Tr} \left[ \mathbf{X}^T \mathbf{G}(w) \mathbf{G}(w)^T \mathbf{X} \right] = \frac{2}{N} \|\mathbf{G}^T(w) \mathbf{X}\|_F^2. \quad (2.23)$$

The approximate cost-function expression can be simplified using the definition of  $\mathbf{G}(w)$  and  $\mathbf{X}$ , then we obtain

$$\begin{aligned} \mathcal{J}(w) &\approx \frac{2}{N} \\ &\left\| \sum_{k=0}^{N-1} \begin{bmatrix} x_a[k] \cos(kw) & x_b[k] \cos(kw) & x_c[k] \cos(kw) \\ x_a[k] \sin(kw) & x_b[k] \sin(kw) & x_c[k] \sin(kw) \end{bmatrix} \right\|_F^2 \\ &= 2 \sum_{m=1}^3 P_m(w), \end{aligned} \quad (2.24)$$

where  $P_m(w)$  corresponds to the periodogram of  $\mathbf{x}_m[k]$  and is defined as

$$P_{x_m}(w) \triangleq \frac{1}{N} \left| \sum_{k=0}^{N-1} x_m[k] e^{-j\omega k} \right|^2. \quad (2.25)$$

By maximizing (2.24) instead of (2.16), the resulting estimator is called the DTFT angular frequency estimator. In the case when signal length is equal to a multiple of the fundamental half-period or it is sufficiently large, the cost-function can be reduced to a sum of discrete time Fourier transform. In such conditions, the approximate cost-function is considered as an attractive choice since it has a much lower computation complexity than the ML cost-function. Indeed, the ML cost-function involves many matrix multiplication operations that need more time burden, while the approximate one involves less number of matrix multiplication operations. Finally, when the signal length is a multiple of a half-cycle, the approximate cost-function is an attractive choice for PQ applications, where the periods of transients in power system is very short. Indeed, it leads to the same performance as the ML cost-function with a much lower computational cost. However, the performance of the DTFT critically depend on the signal length  $N$ .

### 2.2.3.2 Phasor estimation

Once the fundamental frequency is estimated, the maximum likelihood estimator of the phasors,  $\mathbf{S}$ , is given by [154, 156]

$$\hat{\mathbf{S}} = \left( \mathbf{G}^T(\hat{w}_0) \mathbf{G}(\hat{w}_0) \right)^{-1} \mathbf{G}^T(\hat{w}_0) \mathbf{X}, \quad (2.26)$$

where  $\hat{\omega}_0$  corresponds to the ML (or DTFT) estimator of  $\omega_0$ . Using the definition  $\mathbf{S}$ , the ML estimator of the phasor is therefore given by

$$[\hat{V}_a, \hat{V}_b, \hat{V}_c] = [1 \quad -j] \hat{\mathbf{S}}. \quad (2.27)$$

Similarly to the angular frequency estimator, it is also possible to derive a low complexity estimator by using the approximation (2.22) in (2.26). After some simplifications, we obtain

$$\hat{V}_m \approx \frac{2}{N} \sum_{k=0}^{N-1} x_m[k] e^{-j\hat{\omega}_0 k}. \quad (2.28)$$

This approximate estimator is called the DTFT phasor estimator.

### 2.2.4 Extension to non-stationary case

In the previous section, we considered disturbances that are statistical time invariant or stationary. The presented method is based on the stationary assumption. In fact, stationary signals are not existing in real power systems since the three-phase signals are affected by small and large variations (events). In such conditions, the signal parameters are time-varying. These small and relatively slow statistical changes can be addressed by using a short-time analysis as illustrated by Fig. 2.2. In Fig. 2.2, the analysis is performed on several signal blocks with a window length of  $N_s$  samples. The signal is considered to be stationary over each window, which is a short duration of time. Then, the signal parameters are estimated over each window by a shifting in time of the window. Therefore, the estimated parameters are time-varying since they depend on the window number. By considering an overlapping parameter  $0 \leq q < 1$ , the  $l^{th}$  signal block can be modeled as

$$\mathbf{X}_l = \mathbf{G}(w_l)\mathbf{S}_l + \mathbf{B}_l, \quad (2.29)$$

where

- $\mathbf{X}_l$  and  $\mathbf{B}_l$  are  $N_s \times 3$  matrices containing the recorded and noise samples, respec-

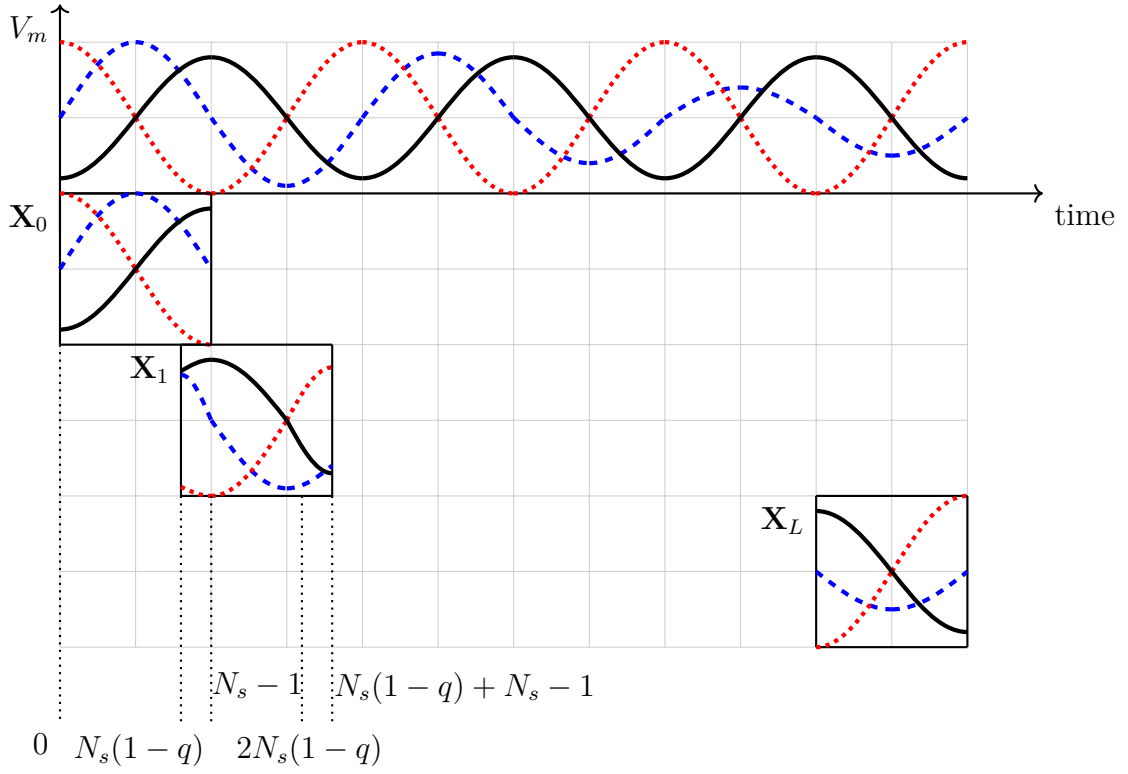


Figure 2.2: Concept of sliding window under quasi-stationary conditions.

tively. These matrices are defined by

$$\mathbf{X}_l = \begin{bmatrix} x_a[N_b] & x_b[N_b] & x_c[N_b] \\ \vdots & \vdots & \vdots \\ x_a[N_e] & x_b[N_e] & x_c[N_e] \end{bmatrix}, \quad (2.30)$$

$$\mathbf{B}_l = \begin{bmatrix} b_a[N_b] & b_b[N_b] & b_c[N_b] \\ \vdots & \vdots & \vdots \\ b_a[N_e] & b_b[N_e] & b_c[N_e] \end{bmatrix}, \quad (2.31)$$

where  $N_b = lN_s(1 - q)$ ,  $N_e = lN_s(1 - q) + N_s - 1$ .

- $\mathbf{G}(w_l)$  is a  $N_s \times 2$  matrix that only depends on the unknown fundamental angular frequency  $w_l$ . This matrix is defined as

$$\mathbf{G}(w_l) = \begin{bmatrix} \cos(w_l N_b) & \sin(w_l N_b) \\ \vdots & \vdots \\ \cos(w_l N_e) & \sin(w_l N_e) \end{bmatrix}, \quad (2.32)$$

- $\mathbf{S}_l$  is a  $2 \times 3$  real-valued matrix containing the amplitudes and initial phases of the



three-phase voltage system. This matrix is defined by

$$\mathbf{G}(w_l) = \begin{bmatrix} a_{al}\cos(\phi_{al}) & a_{bl}\cos(\phi_{bl}) & a_{cl}\cos(\phi_{cl}) \\ -a_{al}\sin(\phi_{al}) & -a_{bl}\sin(\phi_{bl}) & -a_{cl}\sin(\phi_{cl}) \end{bmatrix}. \quad (2.33)$$

Under non-stationary conditions, the estimation problem can be modeled as a statistical problem by using splitting the signal ( $\mathbf{X}$ ) into small signal blocks ( $\mathbf{X}_l$ ). The estimation of the fundamental angular frequency  $w_l$  using MLE can be obtained by

$$\hat{w}_l = \arg \max_w \mathcal{J}(w_l), \quad (2.34)$$

where

$$\mathcal{J}(w_l) \triangleq \text{Tr}[\mathbf{X}_l^T \mathbf{G}(w_l) \mathbf{G}^\dagger(w_l) \mathbf{X}_l], \quad (2.35)$$

where  $\mathbf{G}^\dagger(w_l)$  is the pseudo-inverse of  $\mathbf{G}(w_l)$  i.e.  $\mathbf{G}^\dagger(w_l) = (\mathbf{G}^T(w_l)\mathbf{G}(w_l))^{-1}\mathbf{G}^T(w_l)$ .

The proposed estimator can estimate the fundamental angular frequency under non-stationary conditions since the signal is divided into small window lengths. Then, the phasors can be estimated by the following expression

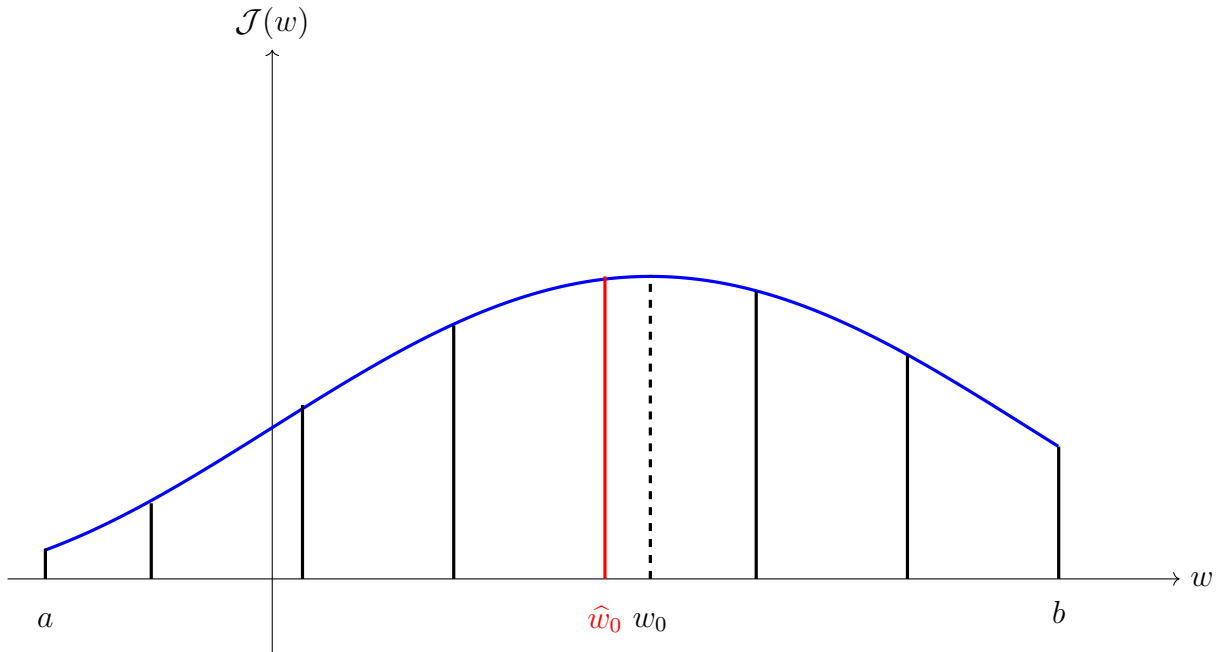
$$[\hat{V}_{al}, \hat{V}_{bl}, \hat{V}_{cl}] = \begin{bmatrix} 1 & -j \end{bmatrix} \hat{\mathbf{S}}_l. \quad (2.36)$$

Regarding the estimation of the angular frequency and phasors in (2.15) and (2.27), one should note that the most challenging step is the maximization of the non-linear cost-function  $\mathcal{J}(w)$ . In the next section, we propose an iterative approach based on the Newton-Raphson iterative technique to perform this task.

## 2.3 Cost-Function Optimization Method

This section is concerned with the problem of cost-function optimization, i.e. finding the maximum value of the cost-function. This is due the fact that the fundamental angular frequency is determined as the maximum of the cost-function. Indeed, this function is one-dimensional parameter that will be optimized. In this study,  $w_0$  should be positive and close to the nominal angular frequency. Then, the safest way to maximize the exact (or approximate) cost-function  $\mathcal{J}(w)$  is to perform a grid-search over an interval  $[a, b]$  as shown in the Fig. 2.3. An enough small spacing between  $w$  values guarantee to obtain the best solution ( $\hat{w}_0$ ).

In the consecutive subsections, we will present two optimization methods, i.e. Downhill Simplex and an iterative approach-based Newton-Raphson methods. These methods will explicit use of 1 dimensional minimization.

Figure 2.3: Grid search over the  $[a, b]$  interval.

### 2.3.1 Downhill Simplex Method

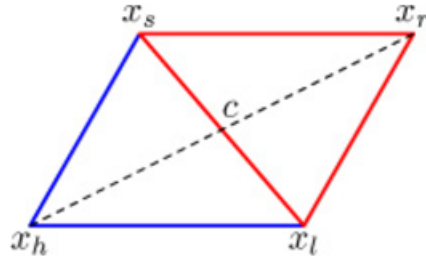
For optimizing the one-dimensional function is to use the Downhill simplex optimization method. This method is due to Nelder and Mead [157] and it is commonly applied for finding the minimum or maximum of a one- or multi-dimensional cost-function. Downhill simplex is used to nonlinear optimization problems that do not require any derivative information. It is heuristic search method, which does not guaranteed to be optimal [158, 159].

This presented method could search a one-dimensional minimizer that finds a minimum for a problem specified by

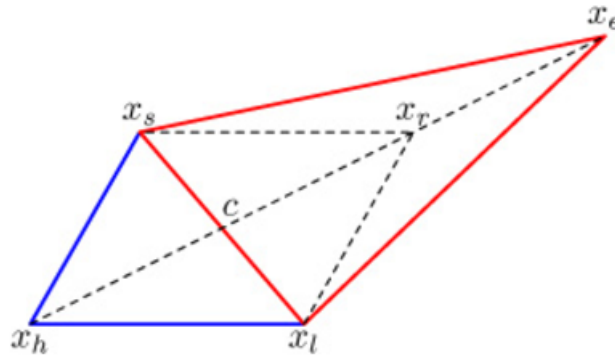
$$\min_w \mathcal{J}(w) \quad \text{where, } w_1 < w < w_2. \quad (2.37)$$

The Nelder-Mead technique is provided with MATLAB<sup>®</sup> environment by the *Fminsearch* algorithm. This standard algorithm allows to use an arbitrary values, which describe the simplex movement in the merit space. Simplex is a geometric construct that is used to achieve the optimization of the function (i.e., minimization). *Fminsearch* obtains the minimum by making a simplex around the initial guess  $w_0$  by adding 5% of each component  $w_0(i)$  to  $w_0$ . A search of the unknown parameter is performed by a moving simplex. Three factors are used by this method to move the simplex that are alpha (reflection moves), beta (contraction moves), and gamma (expansion moves).

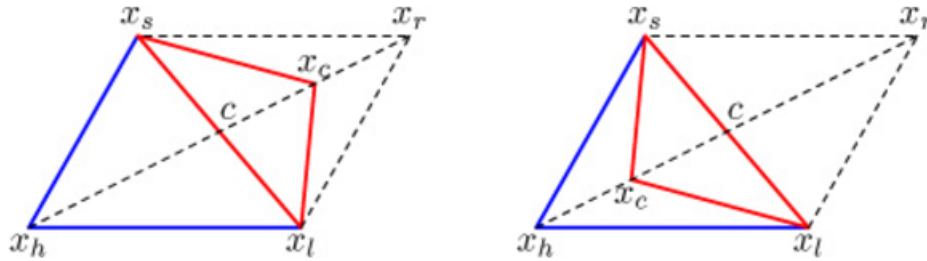
- Reflection moves compute the reflection point  $x_r := c + \alpha(c - x_h)$  and  $\mathcal{J}_r := \mathcal{J}(x_r)$ . If  $\mathcal{J}_l \leq \mathcal{J}_r < \mathcal{J}_s$ , accept  $x_r$  and terminate the iteration.



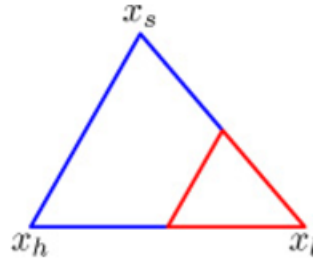
- Expansion moves compute expansion point  $x_e := c + \gamma(x_r - c)$  and  $\mathcal{J}_e := \mathcal{J}(x_e)$ . If  $\mathcal{J}_e \leq \mathcal{J}_r$ , accept  $x_e$  and terminate the iteration. Otherwise, if  $\mathcal{J}_e \geq \mathcal{J}_r$ , then they accept  $x_r$  and terminate the iteration.



- Contraction moves compute the contraction point  $x_c$  by using the better of the two points  $x_h$  and  $x_r$ .
  - Outside, if  $\mathcal{J}_s \leq \mathcal{J}_r < \mathcal{J}_h$ , compute  $x_c := c + \beta(x_r - c)$  and  $\mathcal{J}_c := \mathcal{J}(x_c)$ . If  $\mathcal{J}_c \leq \mathcal{J}_r$ , accept  $x_c$  and terminate the iteration. Otherwise, we should perform a shrink transformation.
  - Inside, if  $\mathcal{J}_r \geq \mathcal{J}_h$ , compute  $x_c := c + \beta(x_h - c)$  and  $\mathcal{J}_c := \mathcal{J}(x_c)$ . If  $\mathcal{J}_c < \mathcal{J}_h$ , accept  $x_c$  and terminate the iteration. Otherwise, we should perform a shrink transformation.



- Shrink computes  $n$  new vertices  $x_j := x_l + \delta(x_j - x_l)$  and  $\mathcal{J}_j := \mathcal{J}(x_j)$ , for  $j = 0, \dots, n$ , with  $j \neq l$ .



This optimization method is considered as robust one, but it has a limited convergence speed compared to other modern methods. It focuses on continuous numerical methods and can lead to local solutions [160, 161]. Unfortunately, this method can be computationally prohibitive.

## 2.3.2 Newton-Raphson Method

We concluded the previous subsection by showing how the Downhill simplex method could be used to solve the optimization problem. The method developed was suitable and safest to optimize the cost-function, but it can be computationally prohibitive to obtain an accurate estimation of  $w_0$ . To reduce the computational time, we propose to use an iterative maximization procedure called the Newton-Raphson algorithm (NRA).

An initial estimate of the root is found by drawing a graph of the function in the neighbourhood of the root. This estimate is then improved by using a technique known as the Newton-Raphson method. The method is based upon a knowledge of the tangent to the curve near the root. It is an iterative method that can be used repeatedly to continually improve the accuracy of the root.

### 2.3.2.1 Newton-Raphson iteration

Once reason for the great interest in Newton-Raphson method is the importance of being able to obtain the solution in few iterations. In fact, the evaluation of an iterative method invariably focuses on how quickly the iterates ( $w_k$ ) converge. This could reduce the computation time, which makes it as an attractive choice for short transient analysis. If the initial value is close to the true maximum, the Newton-Raphson algorithm can reach the maximum of  $\mathcal{J}(w)$  in several iterations [162].

This method can maximize the cost-function when the derivative function is zero. This can be expressed as follows

$$\nabla \mathcal{J}(w) = 0, \quad (2.38)$$

where,  $\nabla \mathcal{J}(w)$  corresponds to the first-derivative of the cost-function.

For the solution in (2.38), we assume that there is an initial guess that is  $w_0$ . In the case

when  $\nabla \mathcal{J}(w)$  is linear near initial guess, then it could be approximated by

$$\nabla \mathcal{J}(w) \approx \nabla \mathcal{J}(w_0) + \nabla^2 \mathcal{J}(w)|_{w=w_0}. \quad (2.39)$$

Using the (2.39) to solve for the zero  $w_1$ , then  $\nabla \mathcal{J}(w_0)$  is equal to zero and solving for  $w_1$ , we obtain

$$\hat{w}_1 = w_0 - \frac{\nabla \mathcal{J}(w)}{\nabla^2 \mathcal{J}(w)} \Big|_{w=w_0}, \quad (2.40)$$

We consider again the new guess  $w_1$ , then we repeat the same procedure for finding the new zero. Figure 2.4 shows that with several iterations the guesses converge to the real zero of  $\nabla \mathcal{J}(w)$ . Generally, this algorithm is defined as

$$\hat{w}_{n+1} = w_n - \frac{\nabla \mathcal{J}(w)}{\nabla^2 \mathcal{J}(w)} \Big|_{w=w_n}, \quad (2.41)$$

where,  $\nabla^2 \mathcal{J}(w)$  corresponds to the second-derivative of the cost-function. These derivatives are defined by

$$\nabla \mathcal{J}(w) = \frac{\partial \mathcal{J}(w)}{\partial w}, \quad (2.42)$$

and

$$\nabla^2 \mathcal{J}(w) = \frac{\partial^2 \mathcal{J}(w)}{\partial w^2}. \quad (2.43)$$

An initial guess close to the maximum is required, in order that the iteration converges to this maximum. In the next subsections, we focus on the first- and second-derivative of the exact and approximate cost-functions defined in (2.16) and (2.23), respectively.

### 2.3.2.2 Derivatives of the exact cost-function

Let us focus on the exact cost-function in (2.16). The first-derivative of the inverse  $\mathbf{A}^{-1}(w)$  is given by [153]

$$\nabla \mathbf{A}^{-1}(w) = -\mathbf{A}^{-1}(w) \frac{\partial \mathbf{A}(w)}{\partial w} \mathbf{A}^{-1}(w). \quad (2.44)$$

Using this result, the first-derivative of the cost-function can be obtained as follows

$$\begin{aligned} \nabla \mathcal{J}(w) = & Tr \left[ \mathbf{X}^T \left( 2 \frac{\partial \mathbf{G}(w)}{\partial w} \mathbf{Y}^{-1}(w) \mathbf{G}^T(w) \right. \right. \\ & \left. \left. - \mathbf{G}(w) \mathbf{Y}^{-1}(w) \mathbf{W}(w) \mathbf{Y}^{-1}(w) \mathbf{G}^T(w) \right) \mathbf{X} \right], \end{aligned} \quad (2.45)$$

where  $\mathbf{Y}(w) = \mathbf{G}^T(w) \mathbf{G}(w)$  and  $\mathbf{W}(w) = \frac{\partial \mathbf{Y}(w)}{\partial w}$  is the first-derivative of  $\mathbf{Y}(w)$  with respect to the fundamental angular frequency. Regarding the second-derivative, it can be checked

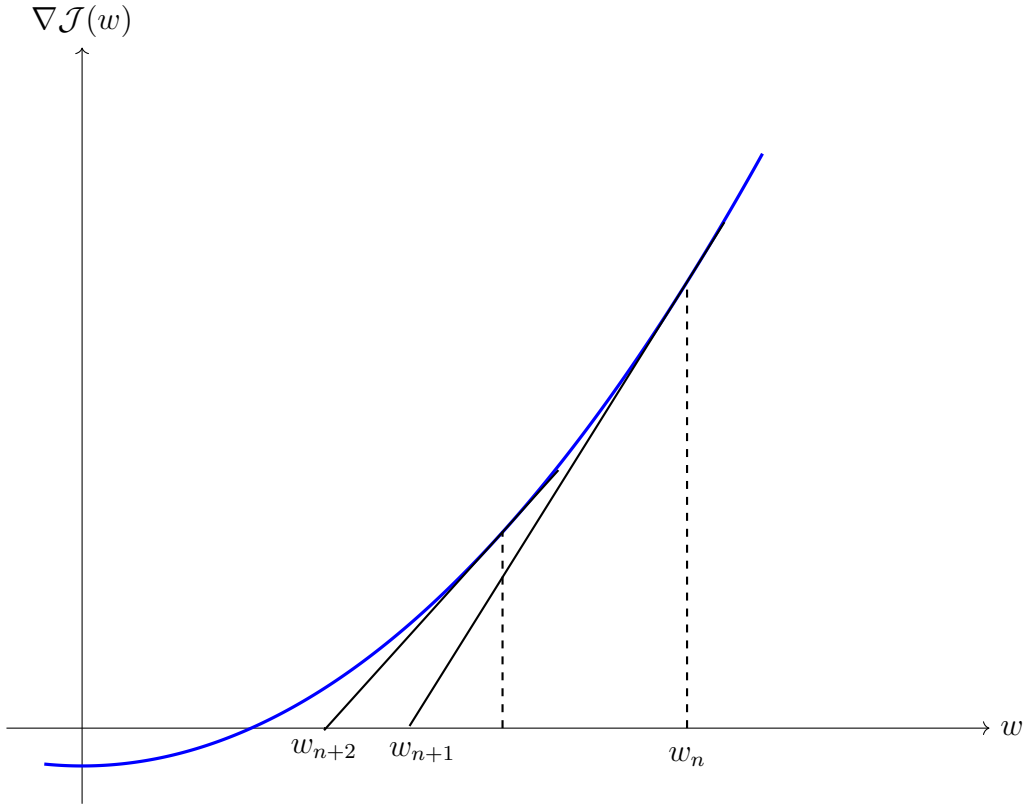


Figure 2.4: Newton-Raphson method for finding a function zero.

that

$$\begin{aligned}
 \nabla^2 \mathcal{J}(w) = & \text{Tr} \left[ \mathbf{X}^T \left( 2 \frac{\partial^2 \mathbf{G}(w)}{\partial w^2} \mathbf{Y}^{-1}(w) \mathbf{G}^T(w) \right. \right. \\
 & + 2 \frac{\partial \mathbf{G}(w)}{\partial w} \mathbf{Y}^{-1}(w) \frac{\partial \mathbf{G}(w)^T}{\partial w} \\
 & - 4 \frac{\partial \mathbf{G}(w)}{\partial w} \mathbf{Y}^{-1}(w) \mathbf{W}(w) \mathbf{Y}^{-1}(w) \mathbf{G}^T(w) \\
 & + 2 \mathbf{G}(w) \mathbf{Y}^{-1}(w) \mathbf{W}(w) \mathbf{Y}^{-1}(w) \mathbf{W}(w) \mathbf{Y}^{-1}(w) \mathbf{G}^T(w) \\
 & \left. \left. - \mathbf{G}(w) \mathbf{Y}^{-1}(w) \frac{\partial \mathbf{W}(w)}{\partial w} \mathbf{Y}^{-1}(w) \mathbf{G}^T(w) \right) \mathbf{X} \right].
 \end{aligned} \tag{2.46}$$

The computation of the first- and second-derivative requires the evaluation of the derivatives of  $\mathbf{G}(w)$  and  $\mathbf{Y}(w)$ . Using the definition of  $\mathbf{G}(w)$  in (2.6), it can be verified that

$$\begin{aligned}
 \left[ \frac{\partial \mathbf{G}(w)}{\partial w} \right]_{k+1,1} &= -k \sin(kw), \\
 \left[ \frac{\partial \mathbf{G}(w)}{\partial w} \right]_{k+1,2} &= k \cos(kw).
 \end{aligned} \tag{2.47}$$

and

$$\begin{aligned} \left[ \frac{\partial^2 \mathbf{G}(w)}{\partial w^2} \right]_{k+1,1} &= -k^2 \cos(kw), \\ \left[ \frac{\partial^2 \mathbf{G}(w)}{\partial w^2} \right]_{k+1,2} &= -k^2 \sin(kw). \end{aligned} \quad (2.48)$$

where  $[\cdot]_{u,v}$  corresponds to the matrix element located at the  $u^{\text{th}}$  row and  $v^{\text{th}}$  column.

As  $\mathbf{Y}(w) = \mathbf{G}^T(w)\mathbf{G}(w)$ , the matrix  $\mathbf{Y}(w)$  can be decomposed as

$$\mathbf{Y}(w) = \begin{bmatrix} \sum_{k=0}^{N-1} \frac{1+\cos(2kw)}{2} & \sum_{k=0}^{N-1} \frac{\sin(2kw)}{2} \\ \sum_{k=0}^{N-1} \frac{\sin(2kw)}{2} & \sum_{k=0}^{N-1} \frac{1-\cos(2kw)}{2} \end{bmatrix}. \quad (2.49)$$

It follows that the first- and second-derivative of  $\mathbf{Y}(w)$  are respectively given by

$$\mathbf{W}(w) = \begin{bmatrix} -\sum_{k=0}^{N-1} k \sin(2kw) & \sum_{k=0}^{N-1} k \cos(2kw) \\ \sum_{k=0}^{N-1} k \cos(2kw) & \sum_{k=0}^{N-1} k \sin(2kw) \end{bmatrix}, \quad (2.50)$$

$$\frac{\partial \mathbf{W}(w)}{\partial w} = \begin{bmatrix} -\sum_{k=0}^{N-1} 2k^2 \cos(2kw) & -\sum_{k=0}^{N-1} 2k^2 \sin(2kw) \\ -\sum_{k=0}^{N-1} 2k^2 \sin(2kw) & \sum_{k=0}^{N-1} 2k^2 \cos(2kw) \end{bmatrix}. \quad (2.51)$$

### 2.3.2.3 Derivatives of the approximate cost-function

Let us focus on the approximate cost-function in (2.23). The first-derivative of the approximate cost-function is given by

$$\nabla \mathcal{J}(w) = \frac{4}{N} \text{Tr} \left[ \mathbf{X}^T \frac{\partial \mathbf{G}(w)}{\partial w} \mathbf{G}^T(w) \mathbf{X} \right], \quad (2.52)$$

where  $\frac{\partial \mathbf{G}(w)}{\partial w}$  is the first-derivative of matrix  $\mathbf{G}(w)$ . The second-derivative of the approximate cost-function can be shown to be

$$\nabla^2 \mathcal{J}(w) = \frac{4}{N} \text{Tr} \left[ \mathbf{X}^T \left( \frac{\partial^2 \mathbf{G}(w)}{\partial w^2} \mathbf{G}^T(w) + \frac{\partial \mathbf{G}(w)}{\partial w} \frac{\partial \mathbf{G}^T(w)}{\partial w} \right) \mathbf{X} \right], \quad (2.53)$$

where the first- and second-derivative of the matrix  $\mathbf{G}(w)$  are provided in (2.47) and (2.48), respectively.

## 2.4 Simulation and Experimental Results

In this section, the performances of the two proposed estimators are compared: the first estimator is based on the exact cost-function and is provided in (2.16) and (2.27), while the second estimator is based on the approximate cost-function and is provided in (2.24)

Table 2.1: Simulation parameters.

$a_a$	$a_b$	$a_c$	$\phi_a$	$\phi_b$	$\phi_c$
1 pu	1 pu	1 pu	0°	120°	240°

and (2.28). For the sake of brevity, these two estimators are called LS and DTFT in the next subsections. Regarding the cost-function optimization, two algorithms are also compared: the downhill simplex method (*fminsearch*) with a termination tolerance of  $10^{-4}$  [157], and the proposed Newton-Raphson algorithm with 4 iterations.

### 2.4.1 Monte Carlo Simulation Results

Monte Carlo simulations have been carried out to evaluate the estimators performances. As recommended by the IEEE Standard C37.118 [52, 56], the performance of the phasor and frequency estimators is evaluated using the TVE and FE criteria. Under additive white Gaussian noise, the following simulations present the mean of the TVE and FE criteria. These criteria are evaluated through  $N_{mc} = 1000$  Monte Carlo trials by generating signals according to signal model (2.1). In each simulation, the fundamental frequency is set to  $f_0 = 55$  Hz, which is the worst case value reported in the IEEE Standard C37.118, and the sampling frequency is set to  $F_s = 48 \times f_n = (48 \times 60)$  Hz = 2880 Hz, where  $f_n$  is the nominal frequency. The amplitudes and initial phases of the three complex phasors are given in Table 2.1. Then, the mean TVE for the phase  $m$  and the mean FE are estimated by

$$TVE_{m,mean} \triangleq \frac{1}{N_{mc}} \sum_{n=1}^{N_{mc}} \frac{|V_m - \widehat{V}_m[n]|}{|V_m|}, \quad (2.54)$$

and

$$FE_{mean} \triangleq \frac{1}{N_{mc}} \sum_{n=1}^{N_{mc}} |\widehat{f}_0[n] - f_0|, \quad (2.55)$$

where  $\widehat{V}_m[n]$  and  $\widehat{f}_0[n]$  corresponds to the estimated phasor and estimated frequency for the  $n^{th}$  Monte Carlo trial. In the next subsections, the mean TVE for the first phase and FE of the proposed estimators are analyzed for different signal lengths, harmonic and inter-harmonic distortion, off-nominal frequency deviation, and Signal to Noise Ratio (*SNR*), where the *SNR* is defined as

$$\eta = \frac{1}{6\sigma^2} \sum_{k=0}^2 a_k^2, \quad (2.56)$$

and  $\sigma^2$  corresponds to the noise variance.



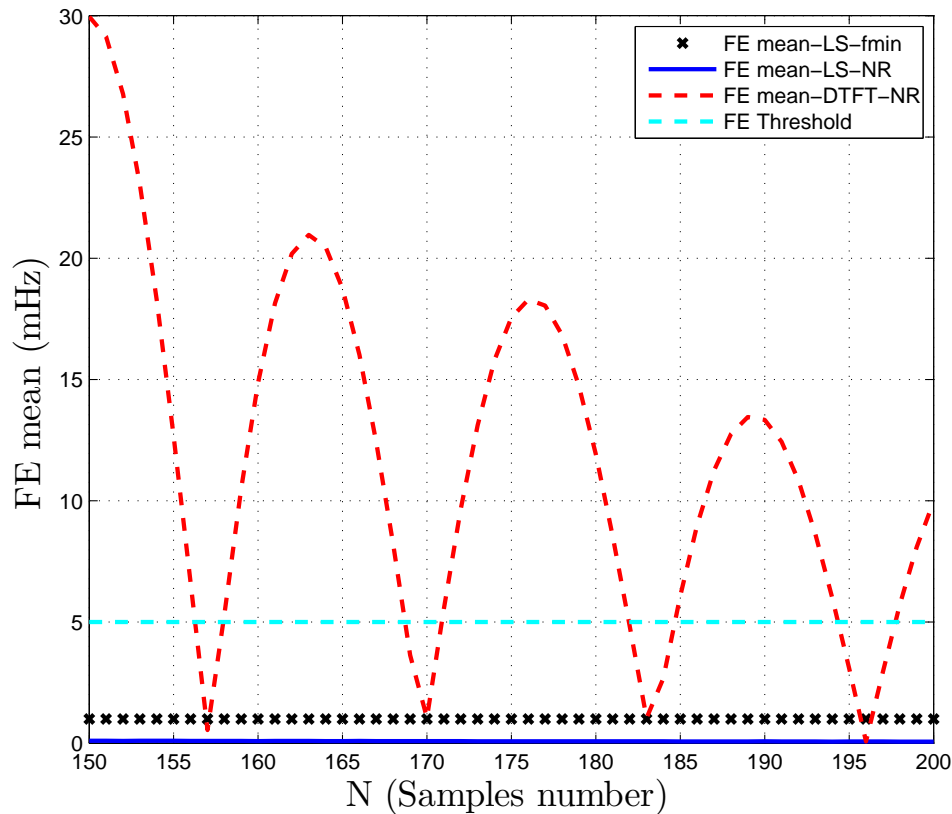


Figure 2.5: Mean FE versus  $N$  with noiseless signals ( $SNR = 150$  dB): comparison between LS and DTFT using NRA with LS using *fminsearch* estimations.

#### 2.4.1.1 Frequency error. Effect of the number of samples $N$

Figure 2.5 presents the Average Frequency Error ( $FE_{mean}$ ) versus  $N$ . This figure clearly shows that the LS-NR estimator outperforms the other techniques. The  $FE_{mean}$  obtained with the LS-fmin estimator is slightly above the  $FE_{mean}$  obtained with the LS-NR method whatever the signal length is. For particular values of  $N$ , we observe that the LS-NR and DTFT-NR techniques have similar performance. Indeed, as demonstrated in Section II, the exact cost-function (2.16) is equal to the approximate cost-function (2.23) when  $N$  is equal to a multiple of the half-period or when it is large. This figure also shows that the accuracy requirement of the IEEE Standard [52, 56], which is set to 5 mHz, seems to be respected on average for the LS-NR and LS-fmin estimators whatever the signal length is.

#### 2.4.1.2 Frequency error. Effect of signal to noise ratio ( $SNR$ )

Figure 2.6 illustrates the influence of the  $SNR$  on the estimator performances when  $N = 240$  samples. We observe that the LS-NR estimator seems to outperform the other techniques whatever the  $SNR$  is. We also note that the  $FE_{mean}$  of the proposed estimators decreases when the  $SNR$  increases. The LS-NR and LS-fmin estimators lead to a mean FE

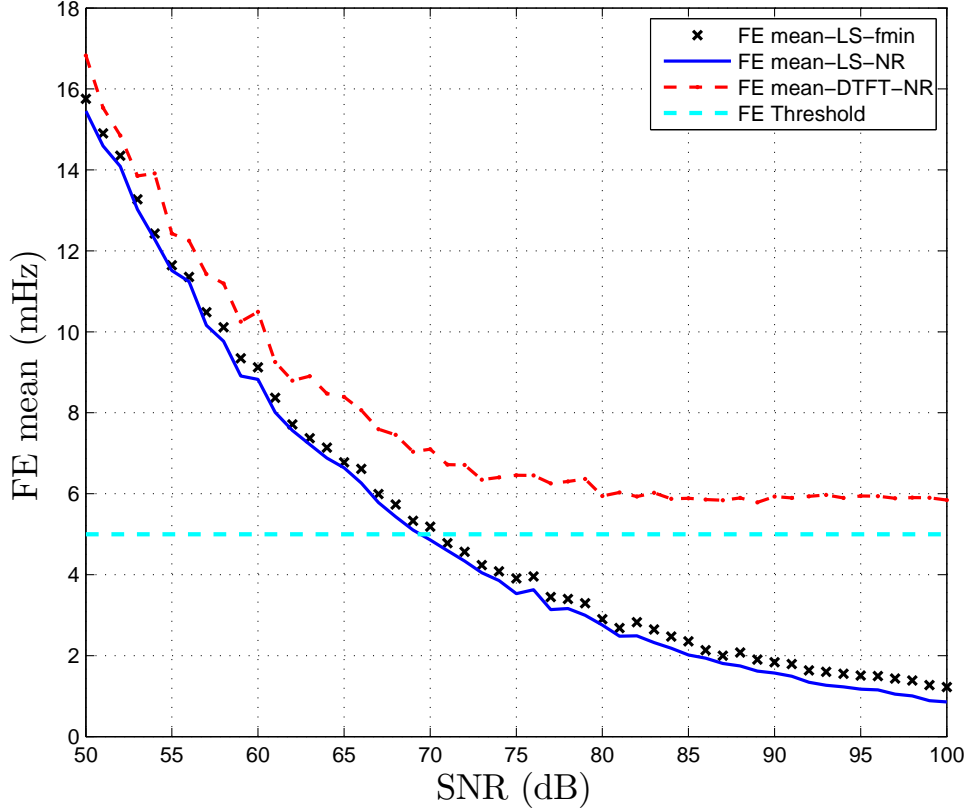


Figure 2.6: Mean FE versus  $SNR$  for  $N = 240$  samples: comparison between LS and DTFT using NRA with LS using *fminsearch* estimations.

lower than 5 mHz when the  $SNR$  is greater than 70 dB. While, the DTFT estimator leads to a frequency error more than 5 mHz whatever the  $SNR$  is. It can be also noted that for a  $SNR$  lower than 70 dB, the mean FE is larger than the IEEE standard limit. For the low- $SNR$  scenario, a larger number of samples  $N$  is required to meet the requirement of the IEEE standard.

### 2.4.1.3 Total vector error. Effect of off-nominal frequency deviation

This subsection evaluates the influence of the frequency error on the phasor estimator performance. In the following simulation, the (normalized) angular frequency is set to  $w_0 = \omega_n + \delta$  where  $\omega_n = \frac{120\pi}{F_s}$  corresponds to the nominal angular frequency and  $\delta$  refers to the angular frequency deviation. The phasor estimation is obtained by setting  $\hat{w}_0 = \omega_n$  in (2.26) or (2.28). Under noiseless conditions, it is demonstrated in Appendix G that the TVE expression at off-nominal frequency can be approximated by

$$TVE_m = \frac{\|\mathbf{M}(w_n, \delta)\mathbf{s}_m\|}{a_m}, \quad (2.57)$$

where  $\mathbf{s}_m = [a_m \cos(\phi_m), -a_m \sin(\phi_m)]^T$  and  $\mathbf{M}(w_n, \delta) = \mathbf{I}_{22} - (\mathbf{G}^T(w_n)\mathbf{G}(w_n))^{-1} \mathbf{G}^T(w_n)\mathbf{G}(w_n + \delta)$  for the ML phasor estimator, or  $\mathbf{M}(w_n, \delta) = \mathbf{I}_{22} - \frac{2}{N} \mathbf{G}^T(w_n)\mathbf{G}(w_n + \delta)$  for the

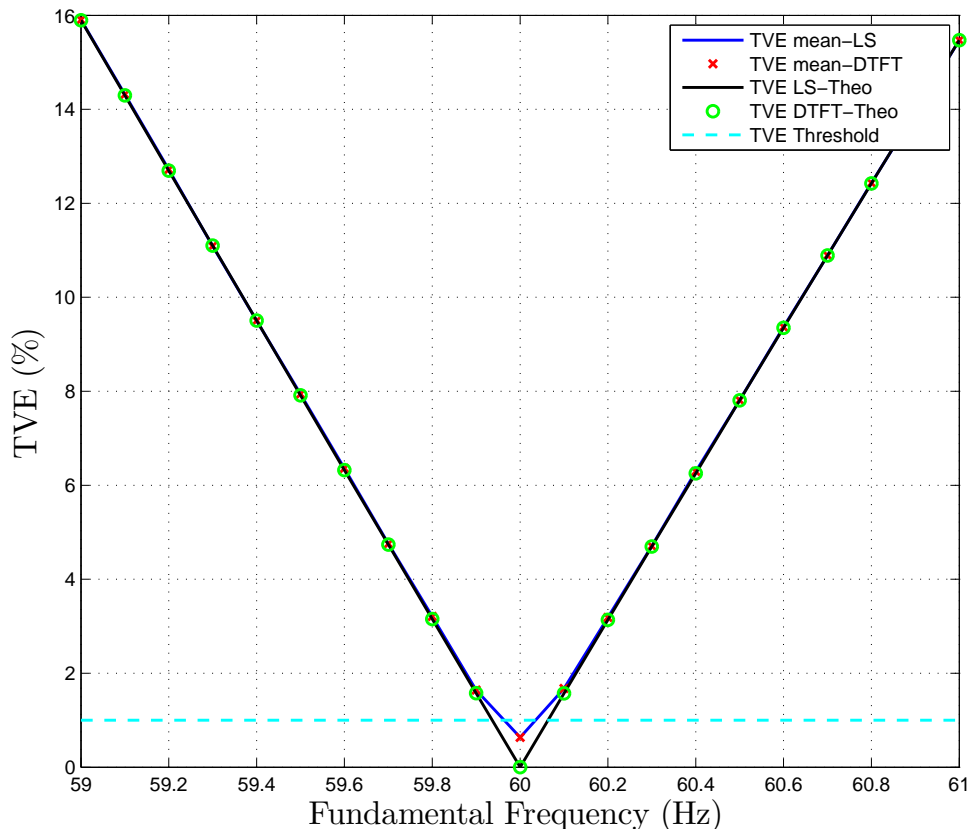


Figure 2.7: TVE and Mean TVE versus frequency deviation for  $N = 144$  samples and  $SNR = 50$  dB: comparison between LS and DTFT estimations.

DTFT phasor estimator.

Figure 2.7 shows the mean TVE and the theoretical TVE values of the proposed estimators versus fundamental frequency deviation for  $N = 144$  samples and at  $SNR = 50$  dB. The  $TVE_{mean}$  values are evaluated through Monte Carlo simulations while the theoretical ones are computed from (2.57). It is obvious that all the experimental TVE mean and the theoretical TVE increase steadily when the frequency deviation increases. Under nominal conditions ( $f_0 = 60$  Hz), the estimation error of the LS and DTFT technique is due to the Gaussian noise. Under off-nominal conditions, we observe that the frequency deviation drives the estimation error. Therefore, these simulations emphasize the importance of the frequency estimation before phasor estimation.

#### 2.4.1.4 Total vector error with frequency estimation. Effect of off-nominal frequency deviation

Figure 2.8 shows the mean TVE of LS- and DTFT-NR estimators versus fundamental frequency deviation for  $N = 144$  samples under noiseless conditions ( $SNR = 150$  dB). The fundamental frequency is first estimated by using the LS-NR or DTFT-NR algorithm before phasor estimation. In this context, it is clear that the LS-NR estimator outper-

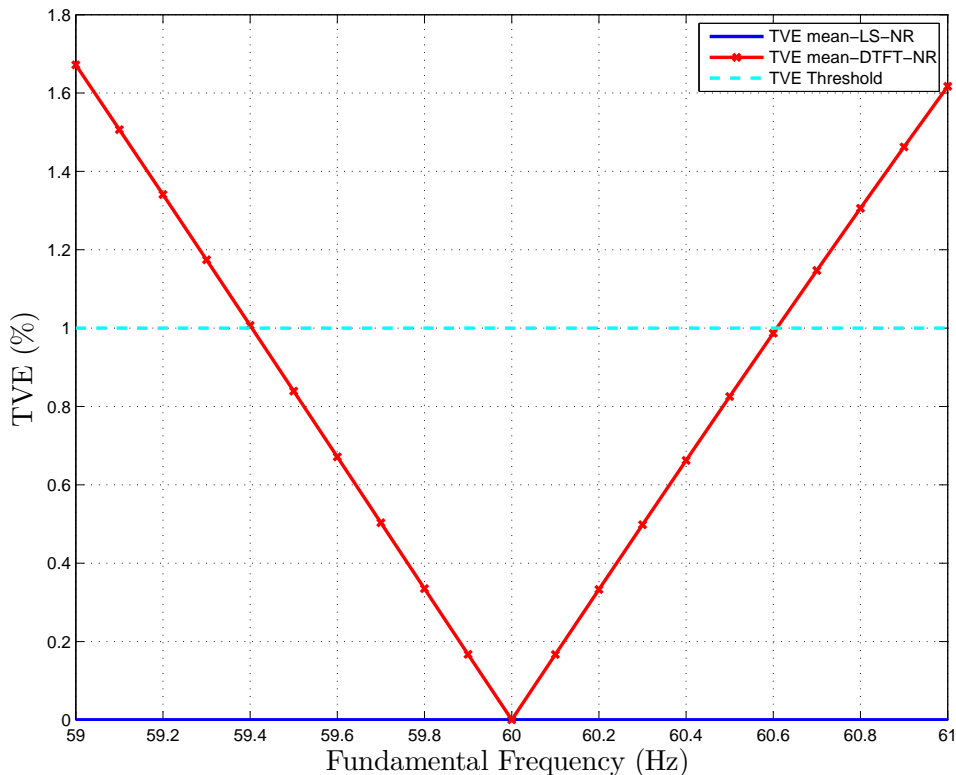


Figure 2.8: Mean TVE versus frequency deviation for  $N = 144$  samples: comparison between LS and DTFT using NRA estimations.

forms the DTFT-NR technique. It can also be observed that the fundamental frequency deviation critically degrades the DTFT-NR estimator performance even with frequency estimation.

#### 2.4.1.5 Total vector error with frequency estimation. Effect of the number of samples $N$

Figure 2.9 shows the mean Total Vector Error ( $TVE_{mean}$ ) versus  $N$ . It can be observed that the LS-NR estimator seems to outperform the other estimators. When the number of samples  $N$  is close to a multiple of the half of signal period ( $N = 209$  or  $N = 236$  samples), it can be seen that the DTFT-NR estimator performs well. Indeed, it is possible to prove that the exact cost-function (2.16) is equal to the approximate cost-function in (2.23) for these particular values of  $N$ . This simulation also shows that both LS-NR and LS-fmin techniques seem to respect on the average the accuracy limit defined by the IEEE standard, which is equal to  $TVE < 1\%$ . When, the number of samples is close to a multiple of the half of signal period, the DTFT-NR estimator can also meet this requirement.

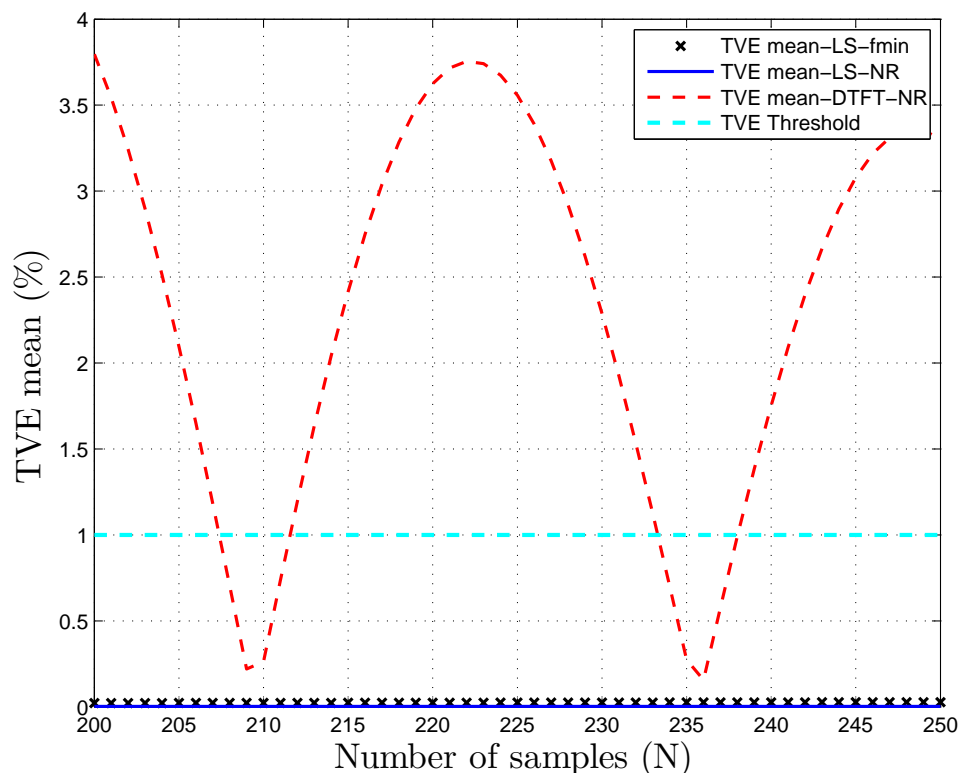


Figure 2.9: Mean TVE versus  $N$  with noiseless signals ( $SNR = 150$  dB): comparison between LS and DTFT using NRA with LS using *fminsearch* estimations.

#### 2.4.1.6 Total vector error with frequency estimation. Effect of signal to noise ratio ( $SNR$ )

Figure 2.10 shows the mean Total Vector Error ( $TVE_{mean}$ ) versus  $SNR$  for  $N = 240$  samples. It can be observed that the LS-NR and LS-fmin estimators achieve the higher performances. It can be seen that for moderate  $SNR$  levels ( $\geq 48$  dB), the LS-NR and LS using *fminsearch* estimators meet on the average the standard requirements. In particular, the  $TVE_{mean}$  of these two estimators becomes negligible for a high  $SNR$  value. Regarding the DTFT technique, this estimator does not seem to meet the standard requirements even for high  $SNR$  values.

#### 2.4.1.7 Total vector error with frequency estimation. Effect of harmonics and inter-harmonics

In power systems, harmonics are mainly due to nonlinear loads and constitute a big issue that should be taken in consideration [163]. By adding harmonics in (2.1), we obtain the

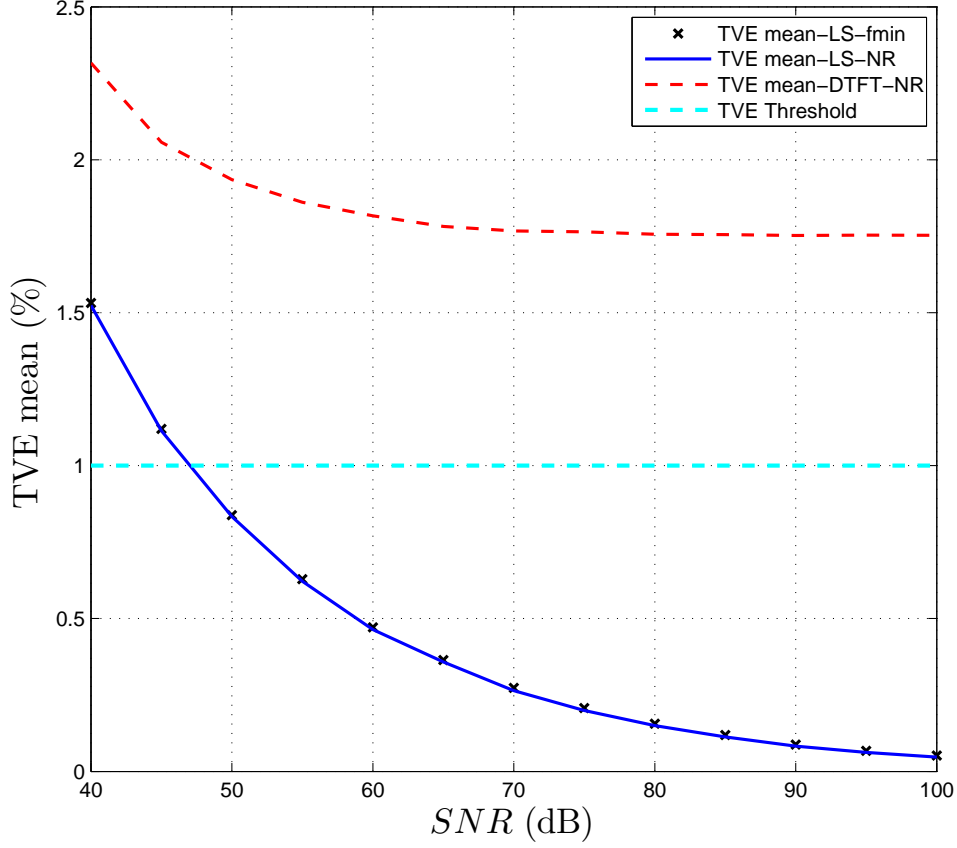


Figure 2.10: Mean TVE versus  $SNR$  for  $N = 240$  samples: comparison between LS and DTFT using NRA with LS using *fminsearch* estimations.

following signal model

$$\begin{aligned}
 x_m[k] &= a_m \cos(kw_0 + \phi_m) \\
 &+ \alpha \left( \sum_{h=2,3,4\dots} a_{mh} \cos(hkw_0 + \phi_{mh}) \right) + b_m[k],
 \end{aligned} \tag{2.58}$$

where  $a_{mh}$  and  $\phi_{mh}$  correspond to the amplitude and initial phase of the  $h^{th}$  order harmonic, respectively. The quantity  $\alpha > 0$  controls the Total Harmonic Distortion (THD) of the signal. IEC Standard 61000-4-7 defines the THD as the ratio of the Root Mean Square (rms) sum of all the harmonic components to the RMS value of the first harmonic or fundamental [42]. This value is known as  $THD_F$  and is given by

$$THD_F(\%) \triangleq 100 \alpha \frac{\sqrt{\sum_{h=2}^{\infty} a_{mh}^2}}{a_m}. \tag{2.59}$$

In the following simulation, a constant three-phase amplitudes  $a_m = 1$  pu are assumed. The standard IEEE C37.118.2011 requires that each harmonic up to  $50^{th}$  should be added to the fundamental signal. Their amplitudes and the sampling frequency are set to  $a_{mh} =$

Table 2.2: TVE versus inter-harmonic components for  $N = 192$  samples and  $SNR = 150$  db.

	LS-NR	LS-fmin	DTFT-NR
$f_{ih1} = 30$ Hz	0.73%	0.76%	1.14%
$f_{ih2} = 85$ Hz	0.71%	0.80%	1.10%

10% pu and  $F_s = 144 \times 60$  Hz, respectively. Figure 2.11 shows the  $TVE_{mean}$  of the proposed estimators versus harmonic level for  $N = 72$  samples and at  $SNR = 80$  dB. The performances of these estimators are evaluated for different  $THD_F$  values by varying  $\alpha$ . It is shown that the performances of the proposed estimators are impacted by the presence of harmonic components. It is observed that LS-NR and LS-fmin estimation errors are steadily increasing when the  $THD_F$  increases. Indeed, this is due to model mismatch. It is also shown that the proposed LS-NR estimator outperforms the other estimators whatever the  $THD_F$  value is. Finally, LS-NR and LS-fmin estimators lead to a phasor error on the average less than 1%, while the DTFT technique does not seem to respect the standard limit (on the average).

In order to analyze the effect of inter-harmonics on the proposed estimators, two inter-harmonic components have been added to the fundamental sinusoid. The amplitudes of the two inter-harmonic components are set to  $a_{ih} = 5\%$  pu and their frequencies are equal to  $f_{ih1} = 30$  Hz and  $f_{ih2} = 85$  Hz, respectively. Table 2.2 shows the TVE of the proposed estimators for  $N = 192$  samples with noiseless signals. This table shows that the LS-NR and LSE using the *fminsearch* outperform the DTFT-NR. Finally, this figure shows that the accuracy requirement defined in the IEEE Standard for maximum phasor error (1%) is only respected for LS-NR and LS-fmin proposed estimators.

#### 2.4.1.8 Computation complexity

Figure 2.12 compares the computational complexity (in seconds) between the Newton-Raphson with 4 iterations and *fminsearch* algorithms. Both algorithms computational complexity are evaluated through 1000 Monte Carlo trials. The Newton-Raphson algorithm has lower computational complexity than the *fminsearch* technique whatever the number of samples  $N$  is. Furthermore, it can be seen that the computation time does not increase with the same rate. In particular, the computation complexity of the *fminsearch* technique highly increases with the number of samples  $N$ .

#### 2.4.1.9 Comparative study

In this section, we propose a comparison between the LS-NR and zero-crossing estimators. Figure 2.13 presents the Average Frequency Error ( $FE_{mean}$ ) of estimators versus  $N$  at

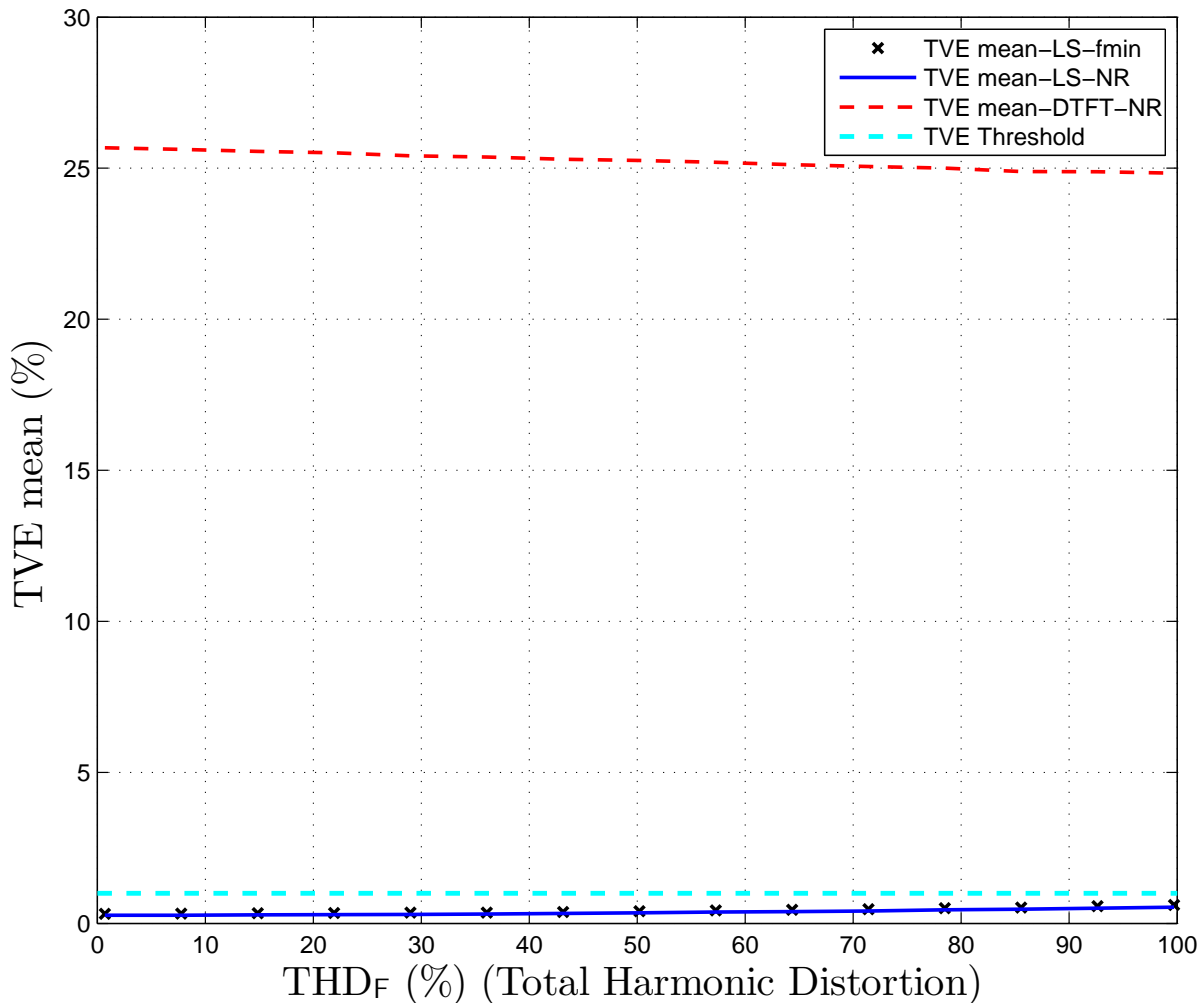


Figure 2.11: Mean TVE versus harmonic level for  $N = 76$  samples: comparison between LS and DTFT using NRA with LS using *fminsearch* estimations under harmonic environment.

$SNR = 150$  dB. This figure clearly shows that the LS-NR estimator outperforms the zero-crossing technique. The  $FE_{mean}$  obtained with the zero-crossing estimator is above the one obtained with the LS-NR estimator whatever the number of samples is. It can be observed that the accuracy requirement of the IEEE standard C37.118.2011 seems to be respected on average for the LS-NR and zero-crossing estimators whatever the number of sample is.

## 2.4.2 Experimental Results

In this section, the LS-NR, DTFT-NR, LS-fmin, and DTFT-fmin estimators performances are evaluated using real power system data obtained from DOE/EPRI National Database of Power System Events [3]. The disturbance event has the code 2911 and was collected on August 10, 2006. This disturbance corresponds to a voltage sag and swell caused by a transmission power fault. The window length  $N$  was set to 64 samples to allow



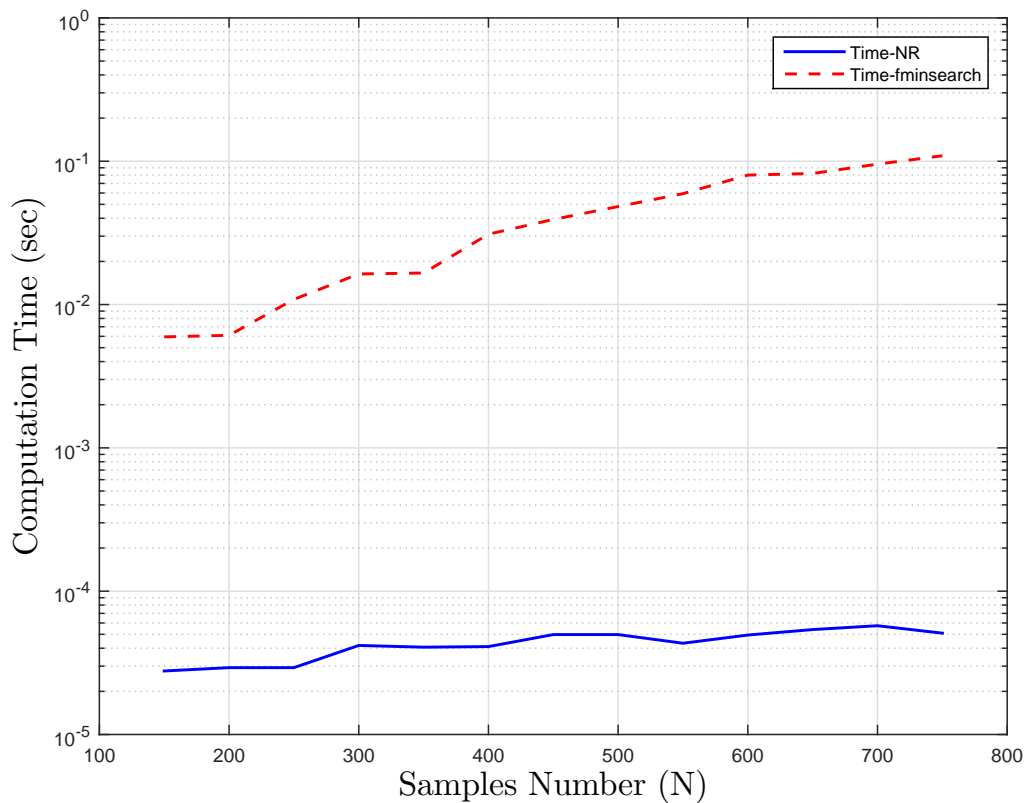


Figure 2.12: Computation time versus  $N$  for  $SNR = 55$  dB: comparison between *Newton-Raphson* and *fminsearch* algorithms.

the DTFT-NR and DTFT-fmin estimators working under favorable conditions. For this event, phasor parameters obtained with LS-NR, LS-fmin, DTFT-NR, and DTFT-fmin estimators are shown in Figs. 2.14 to 2.16. It can be observed that the system is working under balanced conditions before 0.04 s and after 0.12 s, and under unbalanced conditions between 0.04 s and 0.12 s. Under balanced conditions (pre-fault: before 0.04 s), all estimators seem to provide good estimations. After 0.12 s (post-fault), the LS-NR and LS-fmin estimators quickly converge to the nominal value with high estimation performance compared to the performance of the DTFT-NR and DTFT-fmin estimators. Under unbalanced conditions, the LS-NR and LS-fmin estimators show less fluctuations on the frequency, amplitudes, and phases estimations as compared to the DTFT-NR and DTFT-fmin. These fluctuations are mainly due to unbalanced conditions.

## 2.5 Conclusion

This chapter dealt with frequency and phasor estimations for electric power grid monitoring purposes. A new approach based on Maximum Likelihood estimator that exploits the multidimensional nature of the electrical signals, has been proposed. Regarding the frequency estimation, two techniques have been proposed: the Maximum Likelihood and the

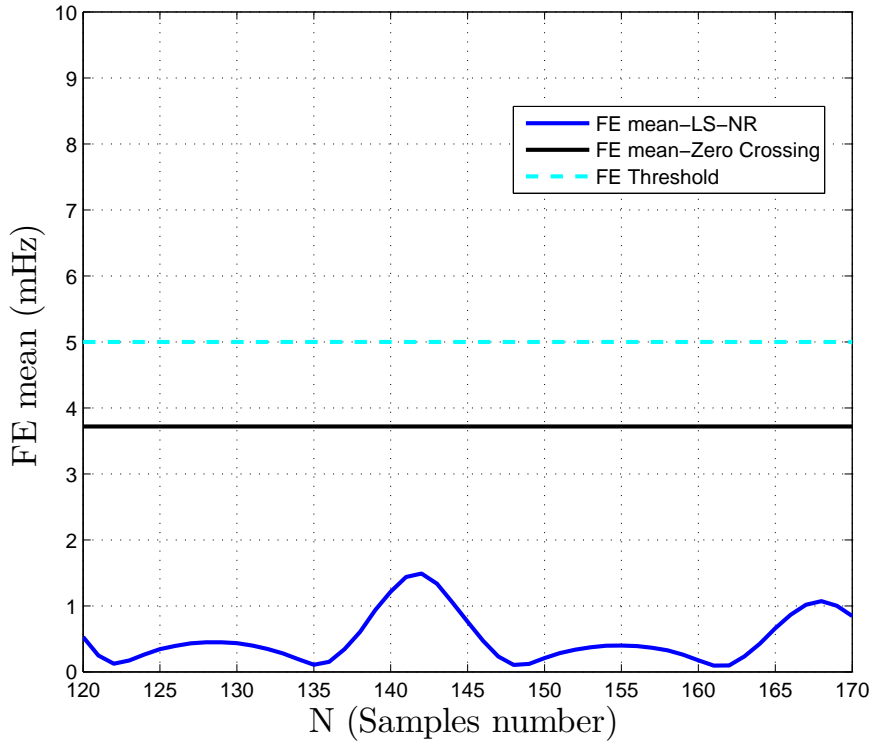


Figure 2.13: Mean FE versus  $N$  for  $SNR = 150$  dB: comparison between LS using NRA with zero-crossing estimations.

DTFT techniques. These techniques require the maximization of a 1-dimensional cost-function. To maximize this cost function, it has been proposed an optimization algorithm based on the Newton-Raphson method.

Simulation and experimental results have shown that the Maximum Likelihood-based Newton-Raphson estimator has better statistical performance than the DTFT approach, when the number of samples is not equal to a multiple of the fundamental half-period. These results have also proven that the proposed estimator clearly outperforms the DTFT approach in terms of TVE and FE, whatever the  $SNR$ , harmonics, inter-harmonics, and off-nominal frequency deviation are. Furthermore, simulation results have also shown that the proposed estimator and DTFT technique exhibit similar performances when the number of samples is equal to a multiple of the fundamental half-period. Regarding the requirements of the IEEE Standard C37.118, simulation results have proven that the proposed technique meets, on the average, the M-class requirements in terms of TVE and FE under steady-state conditions.

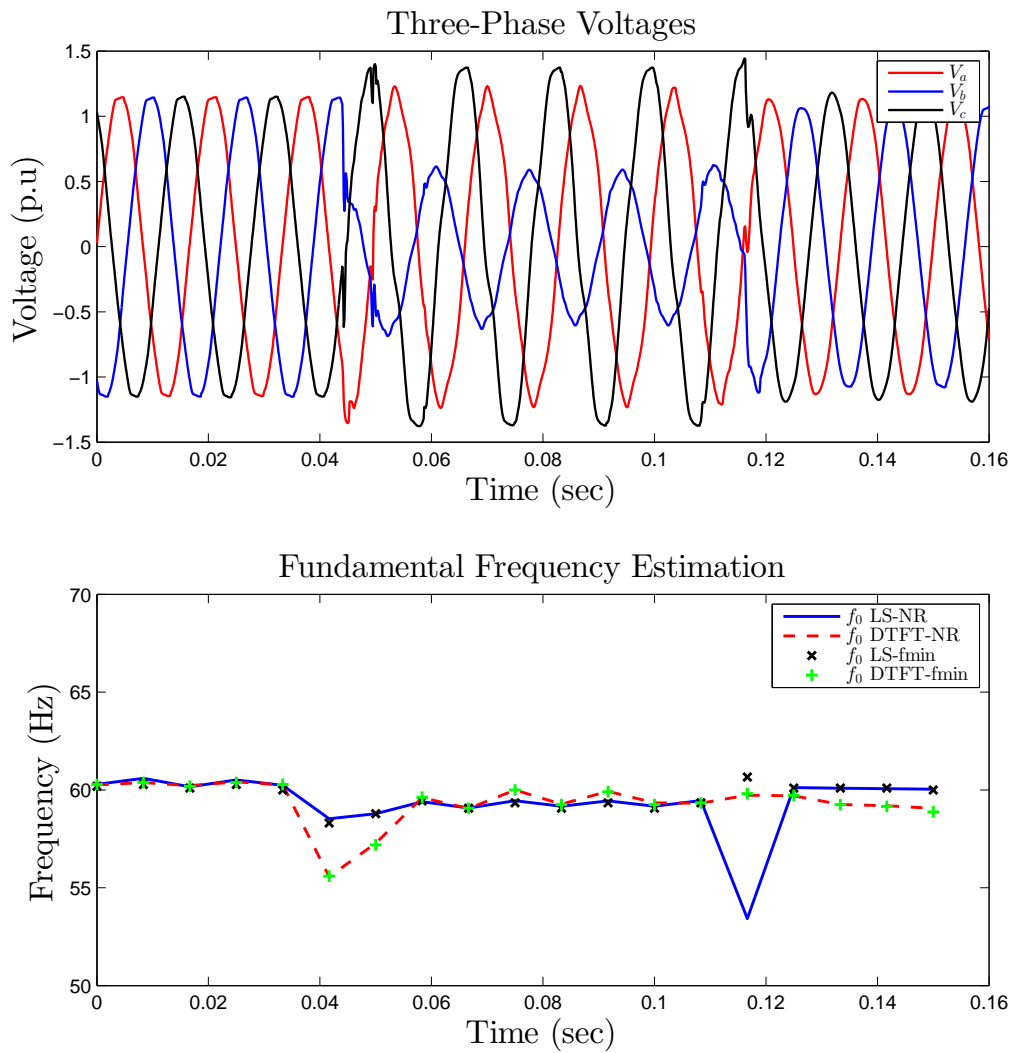


Figure 2.14: Three-Phase voltages and estimated frequency: comparison between LS and DTFT using NRA and *fminsearch* estimations.

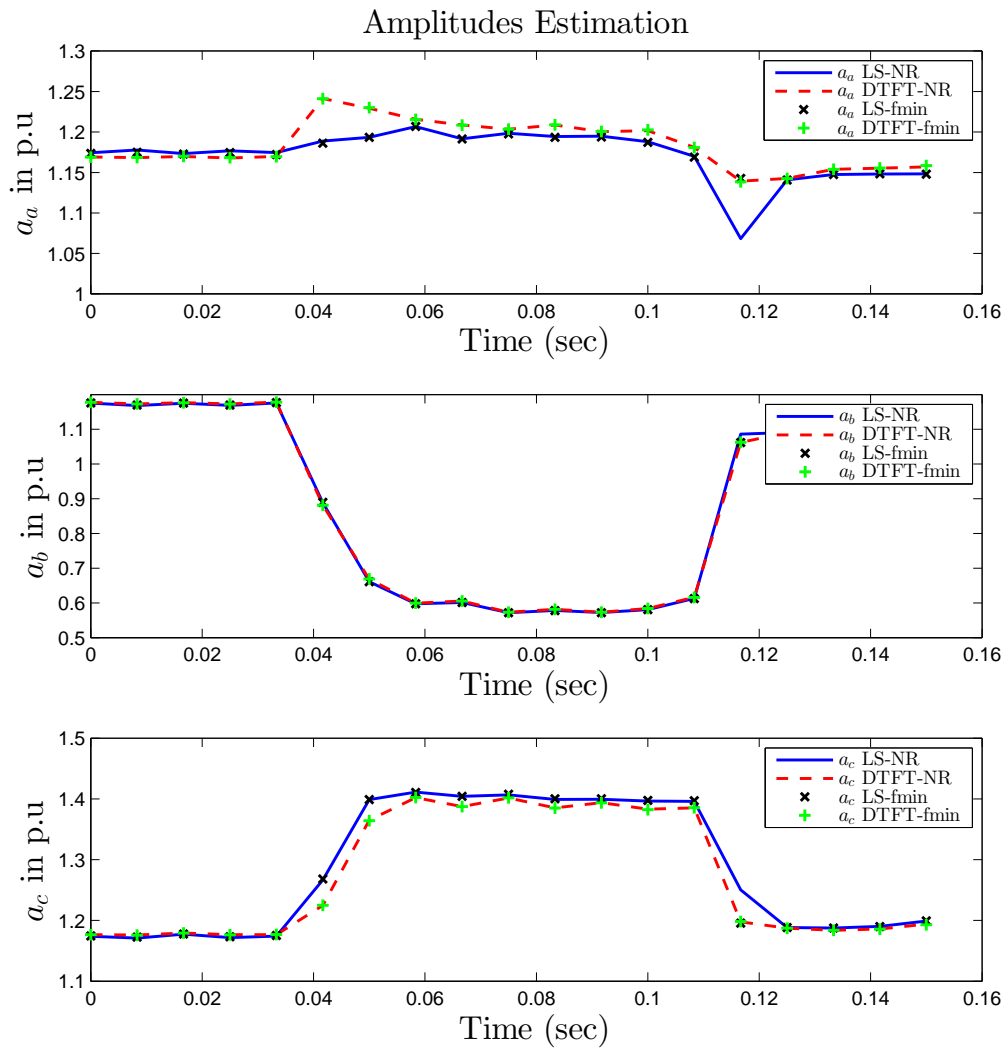


Figure 2.15: Amplitude variation of phasors: comparison between LS and DTFT using NRA and *fminsearch* estimations.

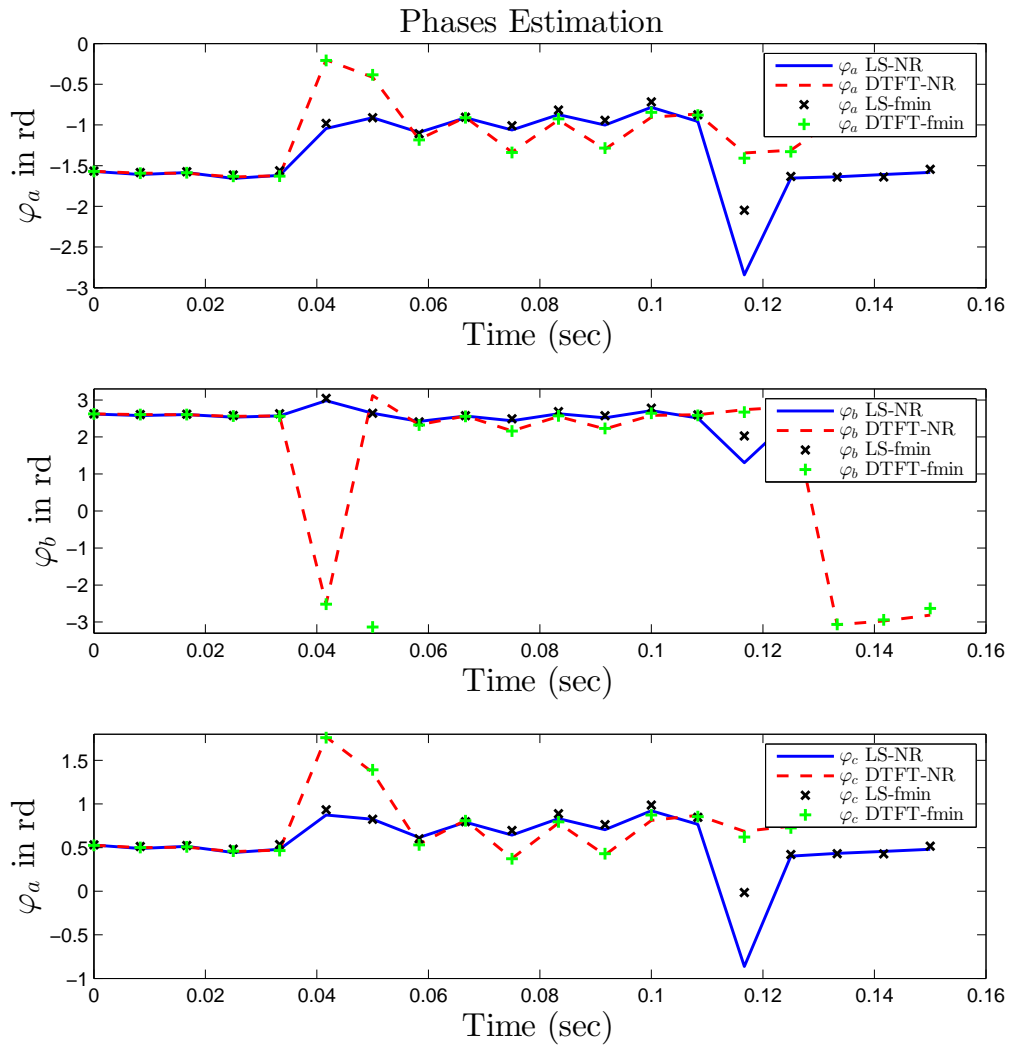


Figure 2.16: Phases variation of phasors: comparison between LS and DTFT using NRA and *fminsearch* estimations.



# Chapter 3

## Power Quality Disturbances

### Classification based on Model Order Selection

THIS chapter presents a new technique for power quality disturbances classification. The proposed technique focuses on voltage sags and swells signatures. First, the input signal is pre-classified into one of four pre-classes that depend on the number of non-zero symmetrical components. In this regard, several sag/swell signatures can be found in each class. Afterwards, the corresponding signature can be selected using the estimated symmetrical component values. In this study, the pre-classification task can be reformulated as a pure model order selection problem. To solve this problem, two pre-classifiers based on Information Theoretical Criteria are proposed. The former yields the highest statistical performances, while the latter has a lower computation complexity. The achieved simulations and experimental results clearly illustrate the effectiveness of the proposed algorithms for voltage sag and swell classification.

### 3.1 Introduction

This chapter proposes a new PQ classification technique based on the analysis of the three-phase signal. The proposed classifier can be applied as a post-processing tool for transient characterization and disturbance detection in power systems [164]. Similarly to the technique described in [165], the proposed classifier is based on *model order selection*. Nevertheless, unlike the method in [165], which mainly focuses on the detection problem, the proposed technique emphasizes on the classification problem. Specifically, the proposed classifier is able to identify the number of non-zero symmetrical components and to pre-classify the signal into four classes under quasi-stationary conditions. Indeed, it uses the estimate of the noise variance,  $\sigma^2$ , under different constraints that correspond to different symmetrical component configurations (which are described by classes  $\mathcal{C}_1$ ,  $\mathcal{C}_2$ ,  $\mathcal{C}_3$ , and  $\mathcal{C}_4$ ). For the estimation of the noise variance, a Maximum Likelihood estimator has been proposed. This estimator exploits four ML noise variance estimates, where each estimate corresponds to a particular symmetrical component configuration and provides information about the three-phase configuration, as depicted in Fig. 3.1.

Once the correct class is selected, the corresponding sag or swell can be identified using the estimated symmetrical components. The performances of the proposed algorithm are evaluated with synthetic and experimental data. Thus, an in-depth analysis of its sensitivity is carried out for different signal lengths, noisy environments, and quasi-stationary conditions. Then, its robustness is evaluated for different Total Harmonic Distortion (THD) values. After that, the classifier computation complexity is analyzed. Finally, a comparison is carried out between the proposed technique and two other classifiers, namely the symmetrical components and the three-phase three-angle algorithms.

This chapter is organized as follows. Section II presents the signal and phasor models. Section III describes the classification method for sags and swells signatures, then Section



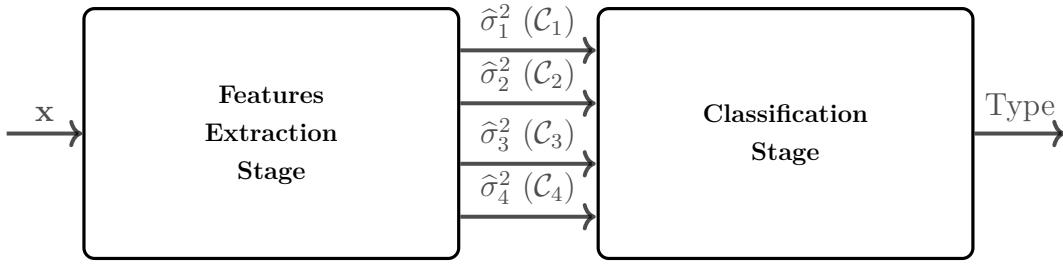


Figure 3.1: Overview of the proposed power quality disturbance classifier.

IV illustrates the effectiveness of the proposed technique evaluated using Monte Carlo simulations on synthetic signals and real power system data.

## 3.2 Signal and Phasor Models

The purpose of this section is to provide the signal and phasor models. Moreover, the four proposed classes and the nine sags and swells signatures are described.

### 3.2.1 Three-Phase Signals Model

The signal on phase  $m$  ( $m \in \{0, 1, 2\}$ ), as it is reported by the IEEE standard [152], can be expressed as follows

$$x_m[n] = a_m \cos(n\omega_0 + \varphi_m) + b_m[n], \quad (3.1)$$

where  $x_m[n]$  and  $b_m[n]$  refer to single-phase electrical signal and the additive noise, respectively.  $\omega_0$  is the system angular frequency,  $a_m$  and  $\varphi_m$  are respectively the amplitude and phase angle. The complex phasor associated to (2.1) is defined as

$$c_m \triangleq a_m e^{j\varphi_m}. \quad (3.2)$$

Assuming that the recorded signal is sampled at  $N$  consecutive samples ( $n = 0, 1, \dots, N-1$ ). The recorded three-phase signals can be expressed using the matrix notation

$$\mathbf{X} = \mathbf{GS} + \mathbf{B}, \quad (3.3)$$

where

- $\mathbf{X}$  and  $\mathbf{B}$  are  $N \times 3$  matrices containing the recorded and noise samples, respectively.

These matrices are defined by

$$\mathbf{X} = \begin{bmatrix} x_0[0] & x_1[0] & x_2[0] \\ \vdots & \vdots & \vdots \\ x_0[N-1] & x_1[N-1] & x_2[N-1] \end{bmatrix}, \quad (3.4)$$

$$\mathbf{B} = \begin{bmatrix} b_0[0] & b_1[0] & b_2[0] \\ \vdots & \vdots & \vdots \\ b_0[N-1] & b_1[N-1] & b_2[N-1] \end{bmatrix}, \quad (3.5)$$

- $\mathbf{A}$  is a  $N \times 2$  real-valued matrix which is defined by

$$\mathbf{G} = \begin{bmatrix} 1 & 0 \\ \cos(w_0) & \sin(w_0) \\ \vdots & \vdots \\ \cos((N-1)w_0) & \sin((N-1)w_0) \end{bmatrix}, \quad (3.6)$$

- $\mathbf{C}$  is a  $2 \times 3$  real-valued matrix containing the real and imaginary parts of the phasors and is defined by

$$\mathbf{S} = \begin{bmatrix} a_0 \cos(\varphi_0) & a_1 \cos(\varphi_1) & a_2 \cos(\varphi_2) \\ -a_0 \sin(\varphi_0) & -a_1 \sin(\varphi_1) & -a_2 \sin(\varphi_2) \end{bmatrix}. \quad (3.7)$$

In order to analyse the recorded signals  $\mathbf{X}$ , a vectorized version of matrix  $\mathbf{X}$  is presented. The vectorization operator, denoted as  $\text{vec}(\cdot)$ , is described by a linear transformation that converts the matrix into a column vector. More precisely,  $n \times m$  matrix can be vectorized by a  $nm \times 1$  column vector that is obtained by stacking the columns of the matrix on top of one another. Using the properties of the vectorization operator, the three-phase signal  $\mathbf{x} \triangleq \text{vec}(\mathbf{X})$  can be expressed into a  $3N \times 1$  column vector as

$$\mathbf{x} = (\mathbf{I}_3 \otimes \mathbf{G}) \mathbf{s} + \mathbf{b}, \quad (3.8)$$

where  $\mathbf{b} = \text{vec}(\mathbf{B})$ ,  $\mathbf{s} \triangleq \text{vec}(\mathbf{S})$ ,  $\mathbf{I}_3$  is the  $3 \times 3$  identity matrix, and  $\otimes$  corresponds to the Kronecker product.

### 3.2.2 Phasor Model and 4-Classes

This subsection deals with the analysis of phasors configuration. In power systems, the symmetrical components method has a great interest to analysis the three-phase power systems under balanced and unbalanced conditions. In particular, an asymmetrical system can be described through symmetrical components method [166]. In three-phase

power systems, the symmetrical components are denoted by the zero-sequence  $z_0$ , positive-sequence  $z_1$ , and negative-sequence  $z_2$ . Indeed, the power system analysis becomes more simpler since the obtained expressions are linearly independent. Within this context, the complex phasors  $s_0$ ,  $s_1$ , and  $s_2$  are decomposed using the symmetrical components method using Fortescue transform, the complex phasors  $s_0$ ,  $s_1$ , and  $s_2$  can be expressed as [167]

$$\begin{bmatrix} s_0 \\ s_1 \\ s_2 \end{bmatrix} = \begin{bmatrix} 1 & 1 & 1 \\ 1 & e^{4j\pi/3} & e^{2j\pi/3} \\ 1 & e^{2j\pi/3} & e^{4j\pi/3} \end{bmatrix} \begin{bmatrix} z_0 \\ z_1 \\ z_2 \end{bmatrix}. \quad (3.9)$$

The main advantage of decomposing the complex phasors into symmetrical components domain is to identify the power system state. Under balanced conditions, the phase shift between phases is equal to  $120^\circ$  and  $a_m = 1$  pu. In such conditions, the symmetrical components are sparse i.e.  $z_0 = z_2 = 0$ . Based on the three symmetrical components, we propose four different classes that are described as

- $\mathcal{C}_1$ : Zero- and negative-sequences are equal to 0 i.e.  $z_0 = z_2 = 0$ .
- $\mathcal{C}_2$ : Zero-sequence is equal to 0 i.e.  $z_0 = 0$ .
- $\mathcal{C}_3$ : Negative-sequence is equal to 0 i.e.  $z_2 = 0$ .
- $\mathcal{C}_4$ : All sequences are different from 0.

For the 4 classes, the real-valued vector  $\mathbf{s}$  in (3.8) that contains the real and imaginary parts of the complex phasors can be rewritten with respect to the real and imaginary parts of the symmetrical components as

$$\mathbf{s} = \mathbf{W}_k \mathbf{d}_k, \quad (3.10)$$

where the matrix  $\mathbf{W}_k$  and the *augmented* symmetrical components  $\mathbf{d}_k$  depend on the class number. For example, for Class  $\mathcal{C}_1$ , the vector  $\mathbf{s}$  can be decomposed as

$$\mathbf{s} = \underbrace{\begin{bmatrix} \mathbf{Q}_0 \\ \mathbf{Q}_1 \\ \mathbf{Q}_2 \end{bmatrix}}_{\mathbf{W}_1} \underbrace{\begin{bmatrix} \Re(z_1) \\ \Im(z_1) \end{bmatrix}}_{\mathbf{d}_1}, \quad (3.11)$$

where

$$\mathbf{Q}_k = \begin{bmatrix} \Re(e^{2jk\pi/3}) & \Im(e^{2jk\pi/3}) \\ \Im(e^{2jk\pi/3}) & -\Re(e^{2jk\pi/3}) \end{bmatrix}. \quad (3.12)$$

For the classes,  $\mathcal{C}_1$  to  $\mathcal{C}_4$ , the expressions of  $\mathbf{W}_k$  and  $\mathbf{d}_k$  are presented in Table 3.1.

Table 3.1: Expressions of  $\mathbf{W}_k$  and  $\mathbf{d}_k$  with respect to class  $\mathcal{C}_k$ .

Class	$\mathcal{C}_1$	$\mathcal{C}_2$	$\mathcal{C}_3$	$\mathcal{C}_4$
k	1	2	3	4
$\mathbf{W}_k$	$\begin{bmatrix} \mathbf{Q}_0 \\ \mathbf{Q}_1 \\ \mathbf{Q}_2 \end{bmatrix}$	$\begin{bmatrix} \mathbf{Q}_0 & \mathbf{Q}_0 \\ \mathbf{Q}_1 & \mathbf{Q}_2 \\ \mathbf{Q}_2 & \mathbf{Q}_1 \end{bmatrix}$	$\begin{bmatrix} \mathbf{Q}_0 & \mathbf{Q}_0 \\ \mathbf{Q}_0 & \mathbf{Q}_1 \\ \mathbf{Q}_0 & \mathbf{Q}_2 \end{bmatrix}$	$\begin{bmatrix} \mathbf{Q}_0 & \mathbf{Q}_0 & \mathbf{Q}_0 \\ \mathbf{Q}_0 & \mathbf{Q}_1 & \mathbf{Q}_2 \\ \mathbf{Q}_0 & \mathbf{Q}_2 & \mathbf{Q}_1 \end{bmatrix}$
$\mathbf{d}_k$	$\begin{bmatrix} \Re(z_1) \\ \Im(z_1) \end{bmatrix}$	$\begin{bmatrix} \Re(z_1) \\ \Im(z_1) \\ \Re(z_2) \\ \Im(z_2) \end{bmatrix}$	$\begin{bmatrix} \Re(z_0) \\ \Im(z_0) \\ \Re(z_1) \\ \Im(z_1) \end{bmatrix}$	$\begin{bmatrix} \Re(z_0) \\ \Im(z_0) \\ \Re(z_1) \\ \Im(z_1) \\ \Re(z_2) \\ \Im(z_2) \end{bmatrix}$

The proposed classification technique can be applied to the ABC classification [99]. This later provides seven sag signatures of three-phase unbalanced power system. These signatures are denoted with letters from A to G [99]. This classification has been extended by two other signature types H and I that correspond to a rise of the voltage in the non-faulted phase(s) [4]. All signatures are characterized by a complex pre-fault voltage,  $E$ , and a complex post-fault voltage,  $V$  [99]. Figure 3.2 illustrates the phasor configuration for each signature, where the dashed and solid arrows present the phasor configuration before and after fault, respectively. Each signature presents a voltage sag caused by a particular fault. Voltage sags A, B, and E are caused by three-phase, single-phase, and double-phase to ground faults, respectively, measured at the fault point. Sag C may be caused by phase-to-phase or by propagation of sag D via a transformer. Sags D and F are obtained from the propagation of sags C and E respectively via transformers or are provided from phase-to-phase measurements of sags B and E at the fault location. Sag G usually results from the propagation of sag F [168]. Type H is caused by phase to ground fault and type I is caused by double phase to ground fault.

Within this context, the nine signatures are pre-classified into 4-classes, where each class,  $\mathcal{C}_k$ , has at least two sag/swell signatures. Table 3.2 presents the link between the proposed classification technique and the nine sag/swell signatures. Once the correct class is selected, a symmetrical components-based classification technique can be used to select the corresponding sag or swell signature.

### 3.2.3 General Vectorized Signal Model

In this subsection, the general vectorized version of signal model is presented. By replacing the real-valued vector  $\mathbf{s}$  in (3.8), by its expression in (3.10), we obtain

$$\mathbf{x} = (\mathbf{I}_3 \otimes \mathbf{G}) \mathbf{W}_k \mathbf{d}_k + \mathbf{b}, \quad (3.13)$$

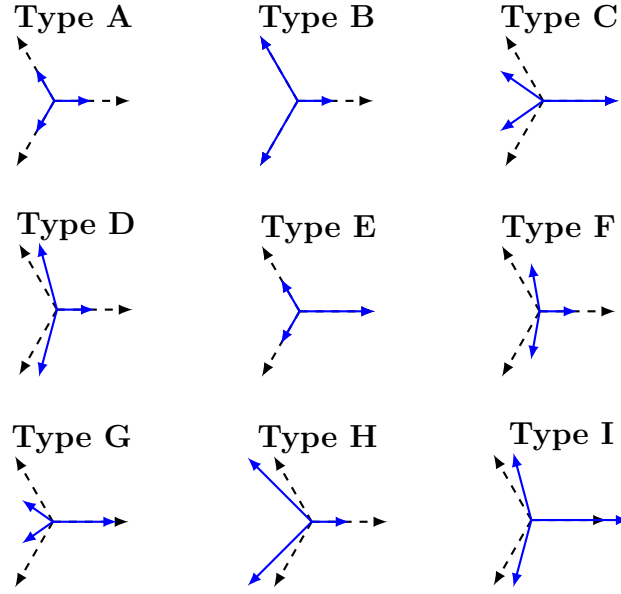


Figure 3.2: Sags and swells signatures illustration [4].

Table 3.2: Link between the proposed technique and sag/swell signatures.

Type	$z_0$	$z_1$	$z_2$	Class
Balanced	0	$E$	0	$\mathcal{C}_1$
A	0	$V$	0	
C	0	$\frac{V+E}{2}$	$\frac{E-V}{2}$	$\mathcal{C}_2$
D	0	$\frac{V+E}{2}$	$\frac{V-E}{2}$	
F	0	$\frac{2V+E}{3}$	$\frac{V-E}{3}$	
G	0	$\frac{2V+E}{3}$	$\frac{E-V}{3}$	
H	$V-E$	$E$	0	$\mathcal{C}_3$
I	$\frac{3(E-V)}{2}$	$E$	0	
B	$\frac{V-E}{3}$	$\frac{V+2E}{3}$	$\frac{V-E}{3}$	$\mathcal{C}_4$
E	$\frac{E-V}{3}$	$\frac{2V+E}{3}$	$\frac{E-V}{3}$	

then, the general form of the signal model can be described as

$$\mathbf{x} = \mathbf{M}_k \mathbf{d}_k + \mathbf{b}, \quad (3.14)$$

where  $k$  refers to the class number and

$$\mathbf{M}_k \triangleq (\mathbf{I}_3 \otimes \mathbf{G}) \mathbf{W}_k. \quad (3.15)$$

The proposed classification technique can be decomposed into two steps: 1) we focus on the determination of the phasor configuration that is the class number  $k$ , from the three-phase signals  $\mathbf{x}$ . 2) Once the phasor configuration is determined, then we can classify the

corresponding signature.

It is important to note that in the following sections, we introduce theoretical methods that are based on stationary assumption. The presented methods can also be performed under non-stationary conditions. For this purpose, short-time analysis can be used as a straightforward solution when the parameters of signal are time-varying. This short-time analysis can be performed using consecutive blocks of signals with a sliding window that has a length of  $N_s$  samples. Moreover, an overlapping parameter can be also considered  $0 \leq q < 1$ . In such conditions, the  $l^{th}$  signal block is given by

$$\mathbf{X}_l = \begin{bmatrix} x_0[N_b] & x_1[N_b] & x_2[N_b] \\ \vdots & \vdots & \vdots \\ x_0[N_e] & x_1[N_e] & x_2[N_e] \end{bmatrix}, \quad (3.16)$$

where  $N_b = lN_s(1 - q)$ ,  $N_e = lN_s(1 - q) + N_s - 1$ . In this context, the  $l^{th}$  vectorized block,  $\mathbf{x}_l = \text{vec}(\mathbf{X}_l)$ , is given by

$$\mathbf{x}_l = \mathbf{M}_k \mathbf{d}_{kl} + \mathbf{b}_l, \quad (3.17)$$

where  $\mathbf{s}_{kl}$  corresponds to the  $l^{th}$  augmented time-varying symmetrical components. By using a small window length  $N_s$ , the signal parameters and the class number  $k$  can be tracked over time.

### 3.3 Proposed Classifier based on Information Theoretic Criteria

This section deals with the description of the decision-tree of the proposed classifier and the decision algorithms that aim to classify the input signal into one of the nine considered classes.

#### 3.3.1 Decision Tree

As shown in Fig. 3.3, the proposed decision tree is decomposed into two stages: 1) the pre-classification of input signal into one of the 4 pre-classes ( $\mathcal{C}_1$ ,  $\mathcal{C}_2$ ,  $\mathcal{C}_3$ , and  $\mathcal{C}_4$ ), one should note that the 4 pre-classes are nested<sup>1</sup>. 2) Then, the classification of the corresponding class from the nine sag/swell signatures.

Regarding the pre-classification stage, it can be reformulated as a pure *model order selection* problem. *Model selection* is defined as a task that allows to select a statistical model from given models. In our context, model order refers to the size of the vector

<sup>1</sup>For example, the pre-class  $\mathcal{C}_1$  is a particular case of the pre-class  $\mathcal{C}_3$

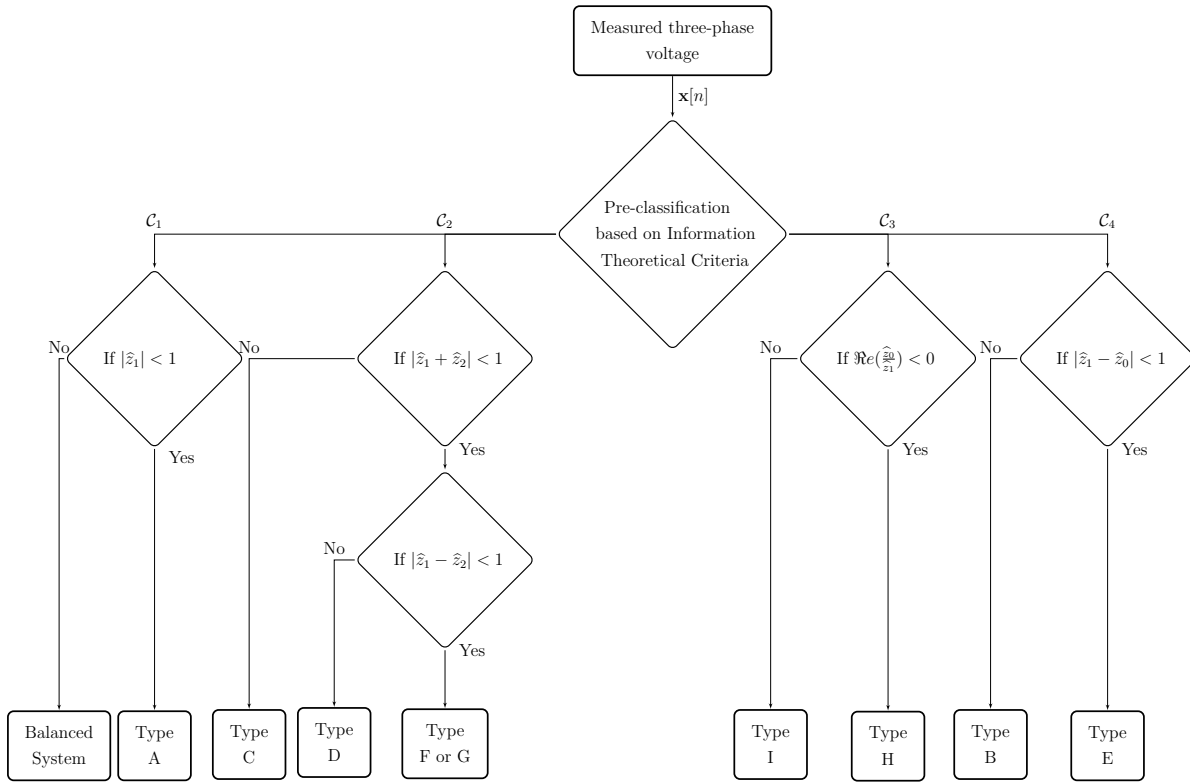


Figure 3.3: Flowchart of the proposed classification algorithm.

$\mathbf{s}_k$ . By identifying the model order, we can select the corresponding pre-class as shown in Table 3.1. It can be noted that the  $\mathbf{s}_k$  size is equal to 2 for the pre-class  $\mathcal{C}_1$ , 4 for the pre-classes  $\mathcal{C}_2$  and  $\mathcal{C}_3$ , and 6 for the pre-class  $\mathcal{C}_4$ . For this end, a detection technique that is based on the application of the Information Theoretic Criterion can be used to determine the model order [169].

For the classification stage, once the pre-class is selected, the corresponding signature class can be obtained using the symmetrical components values. It is important to note that these values are unknown, then we propose to use an estimation technique based on the Maximum Likelihood technique. Maximum likelihood is by far the most used general method of estimation, due to its good statistical performances. Indeed, it has been demonstrated that the Maximum Likelihood Estimator (MLE) is an asymptotically optimal estimator since it minimizes the Root Mean Squared Error (RMSE) [150]. Once the symmetrical components values are estimated, then the corresponding signature class can be selected by analysing these estimated values. For the particular case of signature A, when the pre-class  $\mathcal{C}_1$  is selected, we can discriminate between this signature and that of the balanced power system (BPS), by a simple comparison of  $|\hat{z}_1|$  with the pre-fault value, i.e. 1 pu. However for other pre-classes, the classification process is as follows: if the pre-class  $\mathcal{C}_2$  is selected, two steps are required to discriminate between signatures C, D, F, and G. First, the signature C is obtained if the value of  $|\hat{z}_1 + \hat{z}_2|$  is less than the pre-fault value.

Otherwise, by analyzing the value of  $|\hat{z}_1 - \hat{z}_2|$ , we can discriminate between signatures D, F, and G. If pre-class  $\mathcal{C}_3$  is selected, then the real part of  $(\frac{\hat{z}_0}{\hat{z}_1})$ ,  $\Re e(\frac{\hat{z}_0}{\hat{z}_1})$ , allows identifying the signature I or H. Finally, if the last pre-class ( $\mathcal{C}_4$ ) is selected, a comparison between the value of  $|\hat{z}_1 - \hat{z}_0|$  and pre-fault value can be performed to discriminate between signatures B and E. In this proposed decision tree, it is not possible to discriminate between the signatures F and G.

### 3.3.2 Proposed Classifier Expression

The goal of this subsection is to pre-classify the input signal in one of the four pre-classes. For this purpose, the Information Theoretic Criteria is investigated.

For selecting the corresponding pre-class  $\mathcal{C}_k$ , a pre-classification technique based on Information Theoretical Criteria allows to select  $\mathcal{C}_k$  by minimizing the following penalized likelihood function [156]

$$\hat{k} = \arg \min_{k=1,2,3,4} -2\ln p(\mathbf{x}, \hat{\mathbf{d}}_k) + \gamma_k, \quad (3.18)$$

where  $\ln p(\mathbf{x}, \hat{\mathbf{d}}_k)$  refers to the log-likelihood function of  $\mathbf{x}$  for the pre-class  $k$ .  $\hat{\mathbf{d}}_k$  is the ML estimator of  $\mathbf{d}_k$ . The penalty function,  $\gamma_k$ , relies on two parameters that are the number of free parameters and total number of samples.

#### 3.3.2.1 Expression of the log-likelihood function

We note that when the noise is Gaussian with mean zero and variance,  $\sigma^2$ , the log-likelihood function is expressed as [169]

$$-2\ln p(\mathbf{x}, \hat{\mathbf{d}}_k) = \text{constant} + 3N \ln \hat{\sigma}_k^2, \quad (3.19)$$

where  $\hat{\sigma}_k^2$  is the estimate of the noise variance using the Maximum Likelihood technique under the assumption that the signal comes from class  $\mathcal{C}_k$ . One should note that the noise variance estimator,  $\hat{\sigma}^2$ , allows to provide a measure of the fit goodness. This later competes models with the same model order such as  $\mathcal{C}_2$  and  $\mathcal{C}_3$ . The estimator of noise variance is mathematically given by

$$\hat{\sigma}_k^2 = \frac{1}{3N} \|\mathbf{x} - \mathbf{M}_k \hat{\mathbf{d}}_k\|^2, \quad (3.20)$$

where  $\hat{\mathbf{d}}_k$  is the estimate of the vector  $\mathbf{d}_k$  using Maximum Likelihood technique. As  $\hat{\mathbf{d}}_k = (\mathbf{M}_k^T \mathbf{M}_k)^{-1} \mathbf{M}_k^T \mathbf{x}$ , it follows that

$$\hat{\sigma}_k^2 = \mathbf{x}^T \mathbf{P}_k^\perp \mathbf{x}, \quad (3.21)$$



where  $\mathbf{P}_k^\perp$  denotes the orthogonal projector onto the null space of  $\mathbf{M}_k$  that is given by [170]

$$\mathbf{P}_k^\perp \triangleq \mathbf{I}_{3N} - \mathbf{M}_k(\mathbf{M}_k^T \mathbf{M}_k)^{-1} \mathbf{M}_k^T. \quad (3.22)$$

We note that the computation of  $\mathbf{P}_k^\perp$  requires matrix inversion of  $\mathbf{M}_k^T \mathbf{M}_k$ . This matrix inverse is generally difficult to obtain analytically. Nevertheless, it should be mentioned that an approximate form expression of this matrix inverse can be obtained in particular cases. In the case when the samples number is multiple of a half-cycle ( $N = k\pi/\omega_0$ ) or when it is sufficiently large ( $N \gg 1$ ), it is proved that  $\mathbf{G}^T \mathbf{G} = \frac{N}{2} \mathbf{I}$ . Moreover, as  $\mathbf{W}_k^T \mathbf{W}_k = 3\mathbf{I}$ , we obtain that  $\mathbf{M}_k^T \mathbf{M}_k \approx \frac{3N}{2} \mathbf{I}$ . Therefore, the orthogonal projector,  $\mathbf{P}_k^\perp$ , is approximated as

$$\mathbf{P}_k^\perp \approx \mathbf{I}_{3N} - \frac{2}{3N} \mathbf{M}_k \mathbf{M}_k^T. \quad (3.23)$$

Based on the exact and approximate values of  $\mathbf{P}_k^\perp$ , two pre-classifiers are proposed for selecting the appropriate pre-class. The first pre-classifier is called the Maximum Likelihood (ML) pre-classifier and is obtained by using the exact orthogonal projector  $\mathbf{P}_k^\perp$  (3.22) in (3.21), (3.19), and (3.18). The second one is called the Approximate (App) pre-classifier and is computed from the approximated projector (3.23) in (3.21), (3.19), and (3.18). Compared to the ML pre-classifier, the App pre-classifier has a lower computational complexity since it does not require any matrix inversion and involves a smaller matrix multiplications number. To summary, the estimated classes for the ML and App pre-classifiers are respectively expressed as

$$\hat{k}^{ML} = \arg \min_{k=1,2,3,4} 3N \ln (\mathbf{x}^T \mathbf{P}_k^\perp \mathbf{x}) + \gamma_k \quad (3.24)$$

$$\hat{k}^{App} = \arg \min_{k=1,2,3,4} 3N \ln \left( \|\mathbf{x}\|^2 - \frac{2}{3N} \|\mathbf{M}_k^T \mathbf{x}\|^2 \right) + \gamma_k, \quad (3.25)$$

where  $\|\mathbf{x}\|^2 \triangleq \mathbf{x}^T \mathbf{x}$  is the squared norm of  $\mathbf{x}$ .

### 3.3.2.2 Expression of $\gamma_k$

The objective of the penalty term  $\gamma_k$  is to encourage simplicity over complexity. Mathematically, the log-likelihood function is penalized with respect to  $3N$ , samples number, and  $n_k$ , and estimated parameters. In the literature, several penalty terms have been proposed based on different motivations [169, 171–173]. In this study, we evaluate the performance of the two commonly used penalty terms: the Akaike Information Criterion (AIC)  $\gamma_k^{AIC} = 2n_k$ , and the Bayesian Information Criterion (BIC)  $\gamma_k^{BIC} = n_k \ln(3N)$ .

Let assume that  $l_k$  denotes the size of  $\hat{\mathbf{S}}_k$ . The number of estimated parameters is equal to  $n_k = l_k + 1$  for the pre-class  $k$ . Knowing that the number 1 is due to the noise variance estimation. For pre-classes  $\mathcal{C}_1$ ,  $\mathcal{C}_2$ ,  $\mathcal{C}_3$ , and  $\mathcal{C}_4$ , The AIC and BIC criteria values

are summed up in Table 3.3.

Regarding the classification stage, the estimates of the symmetrical components allow to determine the corresponding signature. Statistically, we can obtain the Maximum Likelihood Estimator of  $\hat{z}_0$ ,  $\hat{z}_1$ , and  $\hat{z}_2$  from the MLE of  $\mathbf{d}_k$ . Then, we propose two estimators of  $\mathbf{d}_k$  that are respectively called the exact and approximate estimators. These estimators are respectively given by [156]

$$\hat{\mathbf{d}}_k^{ML} = (\mathbf{M}_k^T \mathbf{M}_k)^{-1} \mathbf{M}_k^T \mathbf{x} \quad (3.26)$$

$$\hat{\mathbf{d}}_k^{App} = \frac{2}{3N} \mathbf{M}_k^T \mathbf{x}. \quad (3.27)$$

Then, the expression of the  $v^{th}$  symmetrical component, denoted  $\hat{z}_v$ , can be obtained from  $\hat{\mathbf{d}}_k^{ML}$ , or  $\hat{\mathbf{d}}_k^{App}$ , by constructing the complex value

$$\hat{z}_v = [\hat{\mathbf{d}}_k]_{2u} + j[\hat{\mathbf{d}}_k]_{2u+1}, \quad (3.28)$$

where  $[\hat{\mathbf{d}}_k]_u$  refers to the  $u^{th}$  element of  $\hat{\mathbf{d}}_k$ . It should be mentioned that the index  $v$  depends on the pre-class  $\mathcal{C}_k$ . By using Table 3.1, it can be proved that  $v = 1$  when  $u = 0$  for class  $\mathcal{C}_1$ ,  $v = u + 1$  for class  $\mathcal{C}_2$ , and  $v = u$  for classes  $\mathcal{C}_3$  and  $\mathcal{C}_4$ .

In the next section, we present the simulation and experimental results of the proposed classifiers.

### 3.4 Simulation and Experimental Results

This section objective is to evaluate the performance of the proposed classifiers through synthetic and real signals. The first classifier uses respectively the exact ML pre-classifier and estimator obtained from (3.24) and (3.26) and it is denoted by the ML classifier. The second classifier uses respectively the approximate pre-classifier and estimator obtained from (3.25) and (3.27) and it is denoted by the App classifier. Moreover, the performance advantages over other classification techniques will be performed in the following subsection.

In the next, we present Monte Carlo simulation that uses repeated sampling to determine the behaviour of the proposed classifiers.

Table 3.3: Penalty function with respect to class  $\mathcal{C}_k$ .

Class	$\mathcal{C}_1$	$\mathcal{C}_2$	$\mathcal{C}_3$	$\mathcal{C}_4$
$n_k$	3	5	5	7
$\gamma_k^{AIC}$	6	10	10	14
$\gamma_k^{BIC}$	$3\ln(3N)$	$5\ln(3N)$	$5\ln(3N)$	$7\ln(3N)$

### 3.4.1 Monte Carlo Simulation Results

The objective of using synthetic signals is to evaluate the classifiers performances under specific conditions since the reference values are known *a priori*. In this study, we evaluate the proposed classifiers performance through the average probability of correct classification using the above-presented penalty terms, AIC and BIC. For each class  $\mathcal{C}_k$ , 1000 Monte Carlo trials,  $N_{mc} = 1000$ , is used to estimate the average probability of correct classification ( $\hat{\mathcal{P}}_a$ ). For each simulation trial, the proposed classifiers are tested with synthetic signal that is generated in concordance with the presented model in (2.1) and the following parameters:  $\omega_0 = 2\pi f_0/F_s$ , where  $f_0 = 50$  Hz and  $F_s = 48 \times f_0 = 2400$  Hz. The amplitudes and initial phases of the three complex phasors for 4-classes and signatures types are given in Tables 3.4 and 3.5.

The average probability of correct classification can be estimated as

$$\hat{\mathcal{P}}_a = \frac{1}{4N_{mc}} \sum_{k=1}^4 \sum_{n=1}^{N_c} \delta(k - \hat{k}_n), \quad (3.29)$$

where  $\hat{k}_n$  refers to the estimated class for the  $n^{th}$  trial, and  $\delta(l)$  corresponds to the Kronecker delta and it is given by

$$\delta(l) = \begin{cases} 1 & \text{if } l = 1. \\ 0 & \text{otherwise.} \end{cases} \quad (3.30)$$

In the following subsections, different signal lengths,  $N$ , and Signal to Noise Ratio ( $SNR$ ), defined in equation (2.56), are used to analyse the the average probability of correct classification.

#### 3.4.1.1 Probability of correct classification versus number of samples

In this subsection, the classifiers performances are evaluated for different number of samples. In Fig. 3.4, we can analysis the influence of the samples number on the the average probability of correct classification ( $\hat{\mathcal{P}}_a$ ) at  $SNR = 15$  dB. On the whole, we observe that the ML pre-classifier outperforms the approximate pre-classifier. In particular, we can observe that both pre-classifiers achieve same results for particular values of  $N$ . As

Table 3.4: 4-Classes: Simulation parameters.

	$\mathcal{C}_1$	$\mathcal{C}_2$	$\mathcal{C}_3$	$\mathcal{C}_4$
$s_0$	$0.5\angle - 20^\circ$	$1\angle - 20^\circ$	$0.5\angle - 20^\circ$	$1\angle - 20^\circ$
$s_1$	$0.5\angle - 140^\circ$	$0.66\angle - 159.10^\circ$	$1.32\angle - 159.10^\circ$	$0.5\angle - 140^\circ$
$s_2$	$0.5\angle 100^\circ$	$0.66\angle 119.11^\circ$	$1.32\angle 119.11^\circ$	$0.5\angle 100^\circ$

Table 3.5: Signatures types: simulation parameters.

	$s_0$	$s_1$	$s_2$
A	$0.50\angle -20^\circ$	$0.50\angle -140^\circ$	$0.50\angle 100^\circ$
B	$0.50\angle -20^\circ$	$1\angle -140^\circ$	$1\angle 100^\circ$
C	$1\angle -20^\circ$	$0.66\angle -159.11^\circ$	$0.66\angle 119.11^\circ$
D	$0.50\angle -20^\circ$	$0.90\angle -126.11^\circ$	$0.90\angle 86.10^\circ$
E	$1\angle -20^\circ$	$0.50\angle -140^\circ$	$0.50\angle 100^\circ$
FG	$0.50\angle -20^\circ$	$0.76\angle -129.11^\circ$	$0.76\angle 89.11^\circ$
H	$0.50\angle -20^\circ$	$1.32\angle -159.11^\circ$	$1.32\angle 119.11^\circ$
I	$1.75\angle -20^\circ$	$0.90\angle -93.90^\circ$	$0.90\angle 53.90^\circ$

demonstrated previously, the exact pre-classifier is equal to the approximate pre-classifier when  $N$  is a multiple of a half cycle i.e.  $N = 24k$  samples or when it is sufficiently large ( $N \gg 1$ ). In this regard, it should be mentioned that the phasor measurement units (PMUs) record 50/60 Hz signals (voltages or currents) at a rate of a multiple of a cycle i.e.  $N = 48$  samples per cycle.

Regarding the penalty factors, it can be observed that the ML pre-classifier or App pre-classifier using BIC penalty term outperforms respectively the ML pre-classifier or App pre-classifier using AIC penalty term regardless the number of samples. In the case when  $N$  is sufficiently large, the pre-classifier using BIC penalty term leads to an average probability of correct classification equal to 1. On the other hand, the pre-classifier using AIC penalty term leads to an average probability less than 1. Finally, we can observe that the pre-classifier using BIC penalty term has a faster response time than the pre-classifier using AIC penalty term.

#### 3.4.1.2 Probability of correct classification versus noise variance

A high level noise with a signal to noise ratio between 0 to 5 dB is used to evaluate the noise immunity and capabilities of the proposed pre-classifiers. Figure 3.5 shows the  $SNR$ 's effect on the average probability of correct classification for two values of  $N$  i.e.  $N = 72$  and 480 samples (multiple of a half-cycle). In such conditions, both ML and App pre-classifiers lead to the same average probability. Regarding the values of  $N$ , when  $N = 72$  samples, the ML pre-classifier using BIC penalty term leads to an average probability of 1 when  $SNR > 3$  dB. In the case when  $N = 480$  samples, the ML pre-classifier using BIC penalty term leads to an average probability of 1 when  $SNR > 0.5$  dB. These results prove that the proposed pre-classifier is not sensitive under highly noisy environment. The  $\hat{P}_a$  of the pre-classifier using AIC penalty term is less than 1 whatever samples number and  $SNR$  are. This limitation is deeply investigated by the pre-classifiers confusion matrices presented in Tables 3.6 and 3.7 when  $N = 480$  samples and at  $SNR = 5$  dB.

For the BIC ML pre-classifier, it can be observed that the confusion matrix only contains

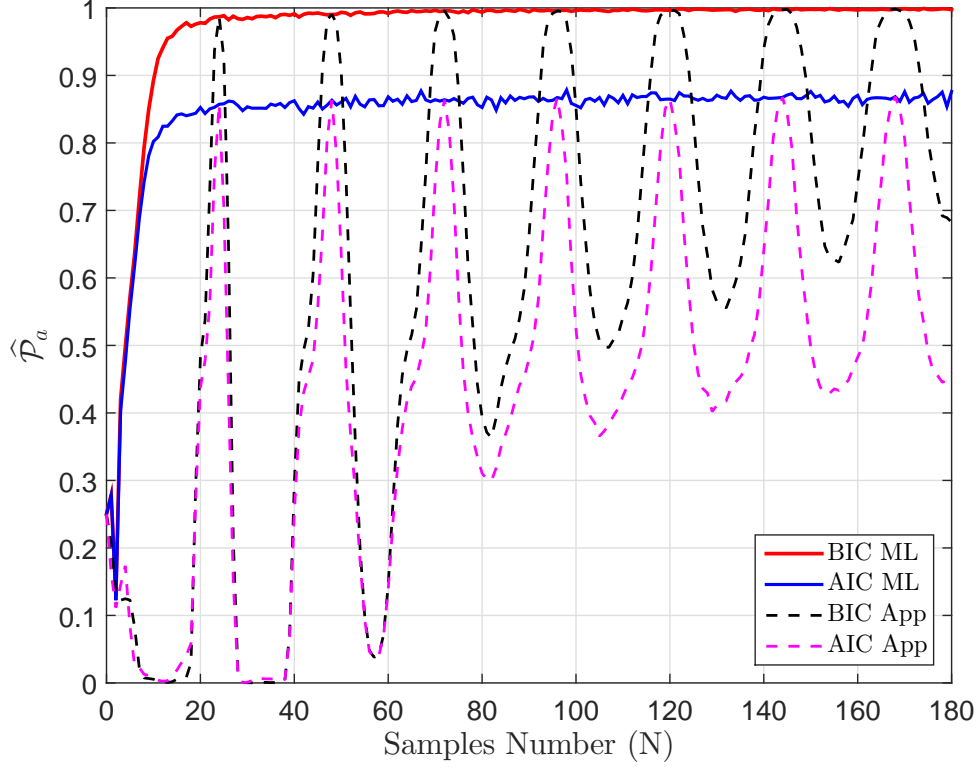


Figure 3.4: Average probability of correct classification versus samples number for  $SNR = 15$  dB.

Table 3.6: AIC criterion: ML pre-classifier confusion matrix.

	$\mathcal{C}_1$	$\mathcal{C}_2$	$\mathcal{C}_3$	$\mathcal{C}_4$
$\mathcal{C}_1$	741	135	124	0
$\mathcal{C}_2$	0	874	0	126
$\mathcal{C}_3$	0	0	861	147
$\mathcal{C}_4$	0	0	0	1000

diagonal elements, which shows that each trial is correctly classified. For the AIC ML pre-classifier, it can be observed that the confusion matrix is upper triangular and contains non-diagonal elements. This structure of upper triangular highlights that the AIC penalty term seems leading to the model order overestimation.

On the other hand, tables 3.8 to 3.11 present the classifiers confusion matrices when  $N = 105$  samples and  $SNR = 15$  dB. For the ML classifier using BIC penalty term, we observe that each trial is correctly classified since confusion matrices contain only diagonal elements. The ML classifier uses the AIC penalty term and the App classifier uses BIC and AIC penalty terms, we observe that the confusion matrices contain non-diagonal elements. Finally, it can be observed that the App classifier seems overestimating the model order when the number of samples is not a multiple of the half of period. The AIC penalty term seems overestimating the model order whatever the number of samples is.

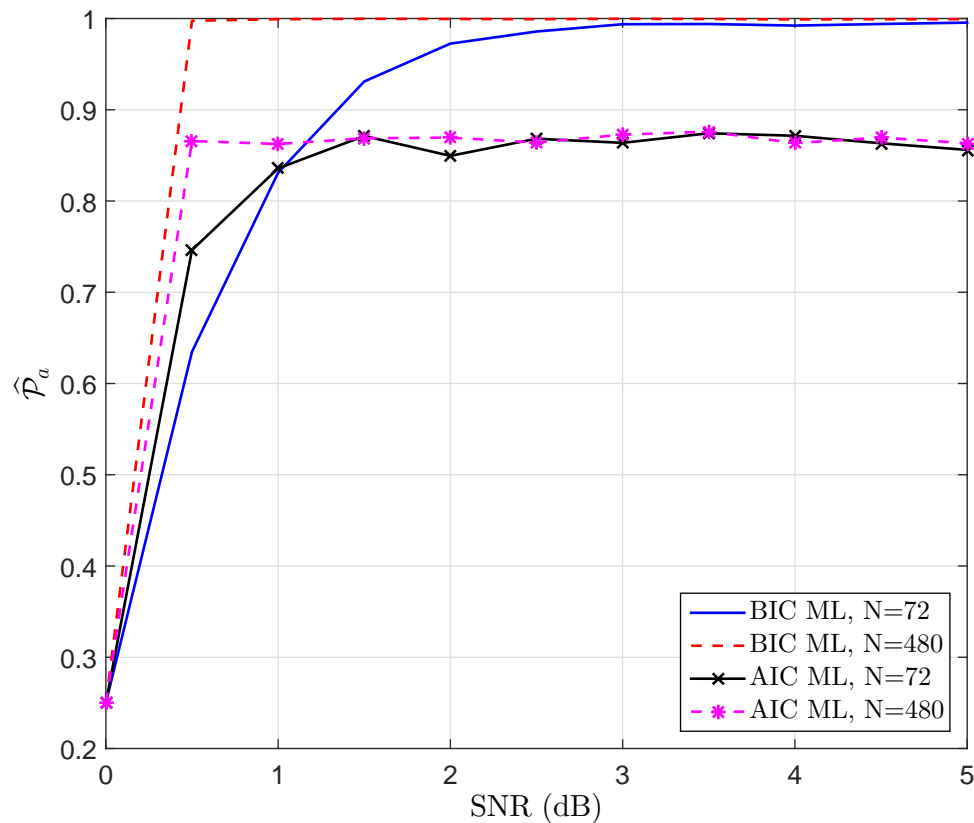


Figure 3.5: Average probability of correct classification versus  $SNR$  for  $N = 72$  and  $N = 480$ .

Table 3.7: BIC criterion: ML pre-classifier confusion matrix.

	$\mathcal{C}_1$	$\mathcal{C}_2$	$\mathcal{C}_3$	$\mathcal{C}_4$
$\mathcal{C}_1$	999	0	1	0
$\mathcal{C}_2$	0	1000	0	0
$\mathcal{C}_3$	0	0	1000	0
$\mathcal{C}_4$	0	0	0	1000

### 3.4.1.3 Robustness of the proposed classifier

In this subsection, the classifier performances are evaluated under harmonic environments. For this purpose, harmonic components are introduced in the signal model in (2.1). The signal model under harmonic environment is given by

$$\begin{aligned}
 x_m[n] &= a_m \cos(nw_0 + \phi_m) \\
 &+ \sum_{h=3,5,7\dots} \alpha (a_{mh} \cos(hnw_0 + \phi_{mh})) + b_m[n],
 \end{aligned} \tag{3.31}$$

where  $a_{mh}$  and  $\phi_{mh}$  are respectively the amplitude and initial phase of the  $h^{th}$  order harmonic. The quantity  $\alpha > 0$  refers to the harmonic parameter. The amplitudes of

Table 3.8: AIC criterion: ML classifier confusion matrix.

	A	B	C	D	E	FG	H	I
A	742	0	0	0	18	129	0	111
B	0	1000	0	0	0	0	0	121
C	0	0	860	0	140	0	0	0
D	0	0	0	861	139	0	0	0
E	0	0	0	0	1000	0	0	0
FG	0	0	0	0	159	841	0	0
H	0	141	0	0	0	0	859	0
I	0	0	0	0	150	0	0	850

Table 3.9: BIC criterion: ML classifier confusion matrix.

	A	B	C	D	E	FG	H	I
A	997	0	0	0	0	2	0	1
B	0	1000	0	0	0	0	0	0
C	0	0	997	0	3	0	0	0
D	0	0	0	998	2	0	0	0
E	0	0	0	0	1000	0	0	0
FG	0	0	0	0	1	999	0	0
H	0	0	0	0	0	0	1000	0
I	0	0	0	0	6	0	0	994

harmonic are set to  $a_{m5} = 0.06$  pu,  $a_{m7} = 0.05$  pu,  $a_{m11} = 0.015$  pu,  $a_{m11} = 0.03$  pu, and  $a_{m13} = 0.03$  pu.

In Fig. 3.6, the  $\hat{\mathcal{P}}_a$  of pre-classifiers is shown versus the Total Harmonic Distortion (THD) when  $N = 144$  samples and at  $SNR = 5$  dB. By varying the amplitudes of harmonics through the scalar  $\alpha$ , we can control the value of Total Harmonic Distortion. For a high THD value, it can be observed that the pre-classifiers performances decrease. For a THD value less than 50%, the pre-classifier using BIC penalty term can lead to a constant  $\hat{\mathcal{P}}_a = 1$ . In contrast, performance of the pre-classifier using AIC penalty term increases when the THD increases. Furthermore, both pre-classifiers  $\hat{\mathcal{P}}_a$  decreases when the THD increases due to the model mismatch.

#### 3.4.1.4 Computation complexity

The goal of this subsection is to give the results that have been achieved by studying the computation complexity of the proposed classifiers. In Fig. 3.7, a comparison of the computation complexity (in second) is performed between the ML and App classifiers.

Table 3.10: AIC criterion: approximate classifier confusion matrix.

	A	B	C	D	E	FG	H	I
A	2	0	0	0	146	852	0	0
B	0	1000	0	0	0	0	0	0
C	0	0	491	0	509	0	0	0
D	0	0	0	952	48	0	0	0
E	0	0	0	0	1000	0	0	0
FG	0	0	0	0	75	925	0	0
H	0	996	0	0	0	0	4	0
I	0	0	0	0	985	0	0	15

Table 3.11: BIC criterion: approximate classifier confusion matrix.

	A	B	C	D	E	FG	H	I
A	63	0	0	0	0	936	0	0
B	0	1000	0	0	0	0	0	0
C	0	0	853	0	147	0	0	0
D	0	0	0	1000	0	0	0	0
E	0	0	0	0	1000	0	0	0
FG	0	0	0	0	0	1000	0	0
H	0	892	0	0	0	0	108	0
I	0	0	0	0	879	0	0	121

In this test, the computation times of the proposed classifiers are evaluated by averaging the execution time through 1000 Monte Carlo trials. The obtained results show that the computation time of both classifiers are increasing proportionally to samples number. However, the App classifier has a lower computation complexity than the ML classifier since this later slope is bigger than that of the approximate classifier. In the case when the signal length  $N$  is a multiple of a half-cycle, the approximate classifier leads to the same statistical performance as the ML classifier and has a lower computation cost. In such conditions, the approximate classifier can be considered as an attractive choice for the pre-classification applications.

#### 3.4.1.5 Comparative study

In this section, we propose a comparison between the ML classifier using the BIC penalty term (BIC-ML) and two others techniques, namely the symmetrical components (SCA) and the three-phases three-angles algorithms (TP-TAA).



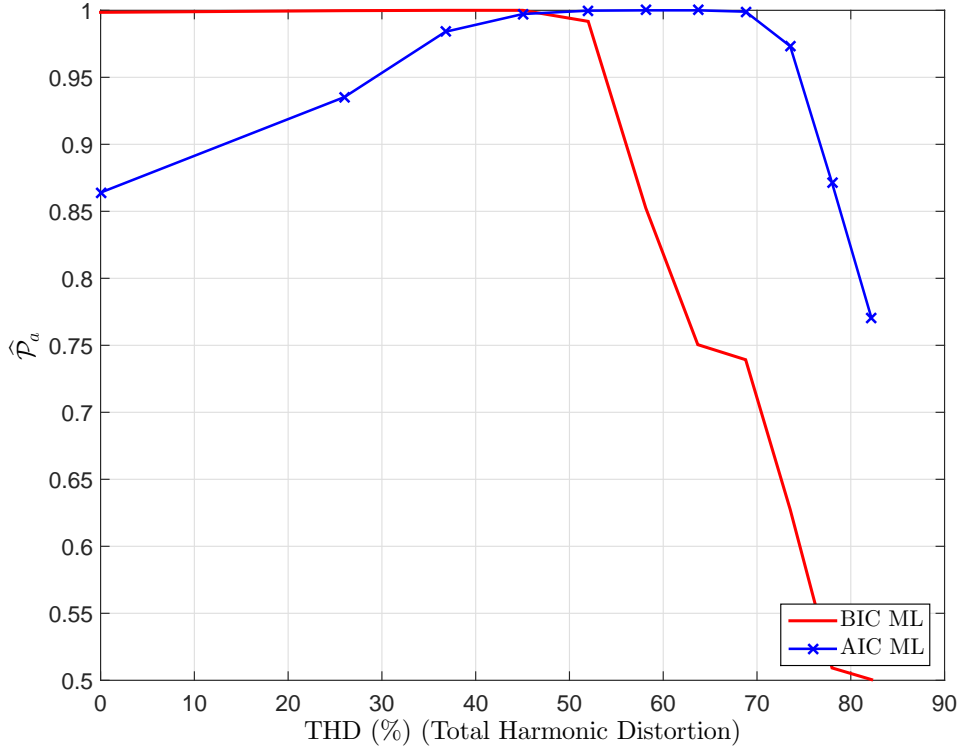


Figure 3.6: Harmonic effect on the proposed classifier. Comparison between ML classifiers using BIC and AIC penalty terms.

### 3.4.1.5.1 Symmetrical component algorithm (SCA)

The symmetrical component algorithm allows to identify the six sags sub-types among the C and D types [100]. Regarding sags sub-types, an illustration of the six sag sub-types among C and D types are illustrated in Fig. 1.17. In this case, we use the angle between the drop in positive- and negative-sequence voltages to classify the corresponding sag sub-type. This angle is defined as

$$T = \frac{1}{60^\circ} \arg \left( \frac{V_2}{1 - V_1} \right), \quad (3.32)$$

where  $T$  is rounded to the nearest integer value and used to identify the voltage sag as follows

$$T = \begin{cases} 0 \rightarrow \text{sag type } C_a \\ 1 \rightarrow \text{sag type } D_c \\ 2 \rightarrow \text{sag type } C_b \\ 3 \rightarrow \text{sag type } D_a \\ 4 \rightarrow \text{sag type } C_c \\ 5 \rightarrow \text{sag type } D_b. \end{cases} \quad (3.33)$$

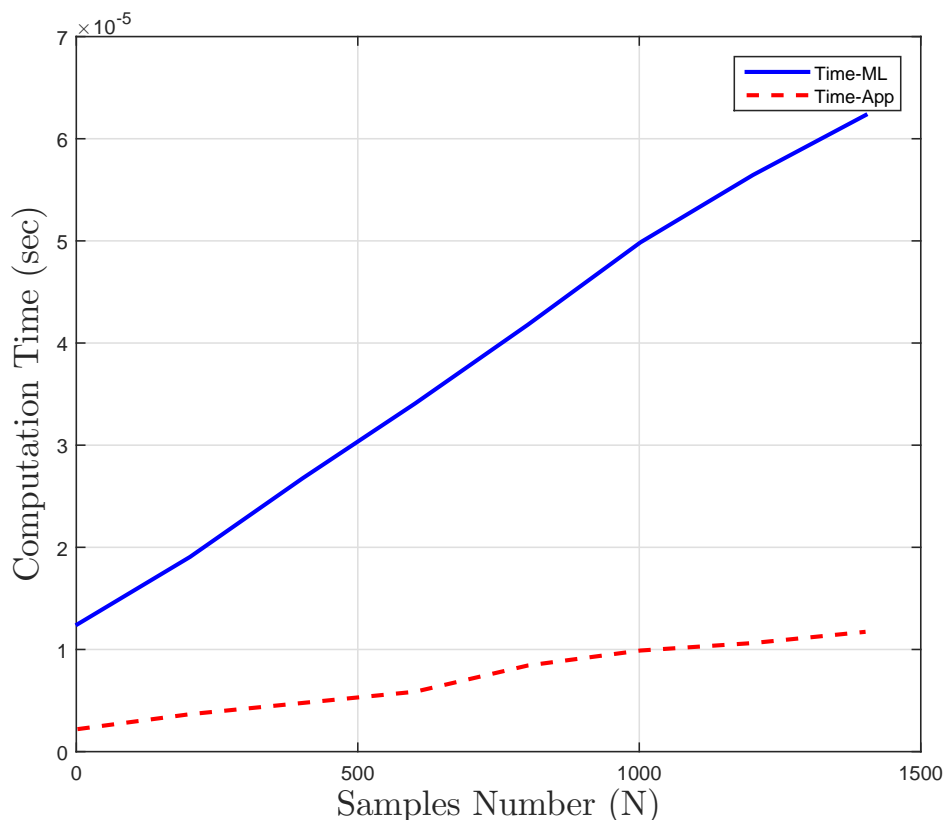


Figure 3.7: Computation time versus  $N$ : Comparison between ML and approximate classifiers.

#### 3.4.1.5.2 Three-phases three-angles algorithm (TP-TAA)

This classifier allows also to identify the above-mentioned C and D voltage sag sub-types [174]. This classifier uses the following parameters for classifying the corresponding sag sub-type: the inverse remains voltage (IRV), the remains root means square voltage (RV), the delta inverse remains voltage ( $\Delta$ IRV), and the three angles  $\alpha$ ,  $\beta$ , and  $\gamma$ . These parameters are given by the below-detailed equations.

The three angles are given by

$$\begin{cases} \alpha = \angle V_a - \angle V_b \\ \beta = \angle V_b - \angle V_c \\ \gamma = \angle V_c - \angle V_a. \end{cases} \quad (3.34)$$

The RV voltage is the voltage drop amplitude given in pu by

$$RV_m = |1 - V_m|. \quad (3.35)$$

The IRV voltage is the ratio of the RV in each phase compared to the lowest value of the

Table 3.12: Voltage sags type C: comparison of the proposed classifier with SC and TP-TA algorithms.

Case	<b>C</b>	<b>C</b>	<b>C</b>
$\widehat{V}_a$	$0.85\angle -20^\circ$	$0.85\angle -20^\circ$	$0.85\angle -20^\circ$
$\widehat{V}_b$	$0.56\angle -118^\circ$	$0.46\angle -110^\circ$	$0.65\angle -168^\circ$
$\widehat{V}_c$	$0.56\angle 160^\circ$	$0.65\angle 168^\circ$	$0.46\angle 110^\circ$
<b>SCA</b>	<b>D<sub>c</sub></b>	<b>D<sub>c</sub></b>	<b>C<sub>a</sub></b>
<b>TP-TAA</b>	<b>C<sub>a</sub></b>	<b>C<sub>a</sub></b>	<b>D<sub>c</sub></b>
<b>BIC ML</b>	<b>C</b>	<b>C</b>	<b>C</b>

RV voltages ( $RV_{min}$ )

$$IRV_m = \frac{RV_m}{RV_{min}}. \quad (3.36)$$

The two higher values of the IRV voltage ( $IRV_{max1}$  and  $IRV_{max2}$ ) are used to compute the ( $\Delta IRV$ )

$$\Delta IRV = IRV_{max1} - IRV_{max2}. \quad (3.37)$$

The TPTA algorithm uses the voltage  $\Delta IRV$  and the angles to identify the voltage sag type as follows

$$\begin{cases} RV_{min} = 0 \rightarrow \text{sag type } D_m \\ \Delta IRV \geq 3 \text{ and } \theta \geq 120^\circ \rightarrow \text{sag type } D_m \\ \Delta IRV < 3 \text{ and } \theta < 120^\circ \rightarrow \text{sag type } C_b, \end{cases} \quad (3.38)$$

where  $\theta$  is the angle opposed to the  $RV_{max}$ , when the voltage sag is type D, and it is opposed to  $RV_{min}$ , when the voltage sag is type C.  $m$  corresponds to the same phase of  $RV_{min}$ , when  $\Delta IRV < 3$  and  $RV_{min} = 0$ . It corresponds to  $RV_{max}$  phase, when  $\Delta IRV \geq 3$ .

### 3.4.1.5.3 Numerical examples

The classification algorithms performances are evaluated using the phasor configurations presented in [174]. For each technique, we use the ML estimator-based half-cycle window length in (3.26) for estimating the phasors.

It can be observed from Tables 3.12, 3.13, 3.14, and 3.15 that the proposed classifier (BIC ML) shows good classification accuracy in all cases, while the two other algorithms (SCA and TP-TAA) exhibit erroneous results. Indeed, this is due to large-phase angle jump and amplitude. The obtained results show that the BIC ML algorithm leads to higher classification accuracy.

Table 3.13: Voltage sags type C: comparison of the proposed classifier with SC and TP-TA algorithms.

Case	<b>C</b>	<b>C</b>	<b>C</b>
$\widehat{V}_a$	$0.85\angle -20^\circ$	$0.85\angle -20^\circ$	$0.92\angle 0^\circ$
$\widehat{V}_b$	$0.78\angle -177^\circ$	$0.65\angle -168^\circ$	$0.80\angle -122^\circ$
$\widehat{V}_c$	$0.34\angle 104^\circ$	$0.46\angle 110^\circ$	$0.80\angle 123^\circ$
<b>SCA</b>	<b>C<sub>a</sub></b>	<b>D<sub>c</sub></b>	<b>C<sub>a</sub></b>
<b>TP-TAA</b>	<b>C<sub>a</sub></b>	<b>C<sub>a</sub></b>	<b>C<sub>a</sub></b>
<b>BIC ML</b>	<b>C</b>	<b>C</b>	<b>C</b>

Table 3.14: Voltage sags type D: comparison of the proposed classifier with SC and TP-TA algorithms.

Case	<b>D</b>	<b>D</b>	<b>D</b>
$\widehat{V}_a$	$0.87\angle -20^\circ$	$0.10\angle 84.29^\circ$	$0.70\angle 0^\circ$
$\widehat{V}_b$	$0.40\angle -131^\circ$	$0.81\angle -90.71^\circ$	$0.92\angle -114^\circ$
$\widehat{V}_c$	$0.82\angle 133^\circ$	$0.91\angle 90.63^\circ$	$0.92\angle 110^\circ$
<b>SCA</b>	<b>D<sub>b</sub></b>	<b>D<sub>a</sub></b>	<b>D<sub>a</sub></b>
<b>TP-TAA</b>	<b>D<sub>b</sub></b>	<b>D<sub>a</sub></b>	<b>C<sub>b</sub></b>
<b>BIC ML</b>	<b>D</b>	<b>D</b>	<b>D</b>

### 3.4.2 Experimental Tests

This section objective is to evaluate the performances of the proposed ML classifiers using BIC and AIC penalty terms using real data. The used real data are obtained from the DOE/EPRI National Database of Power System Events [3]. In this study, five recorded events are used, which correspond to the following event-code: 2825, 2827, 2802, 2786, and 2911. Indeed, each recorded event corresponds to voltage sag or/and swell. For the classifier setting, we set the length of window and overlap to a half-cycle i.e. 64 samples.

Table 3.15: Voltage sags type C and D: comparison of the proposed classifier with SC and TP-TA algorithms.

Case	<b>C</b>	<b>D</b>	<b>D</b>
$\widehat{V}_a$	$1\angle 0.6^\circ$	$0.92\angle 06^\circ$	$0.70\angle 0^\circ$
$\widehat{V}_b$	$0.81\angle -152^\circ$	$0.92\angle -130^\circ$	$0.92\angle -114^\circ$
$\widehat{V}_c$	$0.47\angle 126^\circ$	$0.70\angle 120^\circ$	$0.92\angle 110^\circ$
<b>SCA</b>	<b>C<sub>a</sub></b>	<b>D<sub>c</sub></b>	<b>D<sub>a</sub></b>
<b>TP-TAA</b>	<b>C<sub>a</sub></b>	<b>C<sub>a</sub></b>	<b>C<sub>b</sub></b>
<b>BIC ML</b>	<b>C</b>	<b>D</b>	<b>D</b>

The event signals, estimated phasors amplitudes, the classified pre-class and signatures for the above-presented events are showed by Figs. 3.8 to 3.12.

Regarding the first event presented by Fig. 3.8, it can be observed that the BIC and AIC pre-classifiers lead to the same result under balanced and unbalanced conditions. More precisely, under balanced conditions, null zero- and negative-sequences ( $\mathcal{C}_1$ ) are selected by both pre-classifiers. Under unbalanced conditions, they select a non-null symmetrical sequence ( $\mathcal{C}_4$ ). Both pre-classifiers seem leading to good classification accuracy under balanced and unbalanced conditions. For the second event (Fig. 3.9), a null zero- and negative-sequences ( $\mathcal{C}_1$ ) are selected under balanced conditions by both pre-classifiers. Under unbalanced conditions, we observe that different classification result are obtained. The pre-classifier using AIC penalty term achieves a non-null symmetrical-sequence ( $\mathcal{C}_4$ ), while the pre-classifier using BIC penalty term achieves a null zero-sequence ( $\mathcal{C}_2$ ). The BIC pre-classifier seems achieving good results of classification after 0.12 s, while the

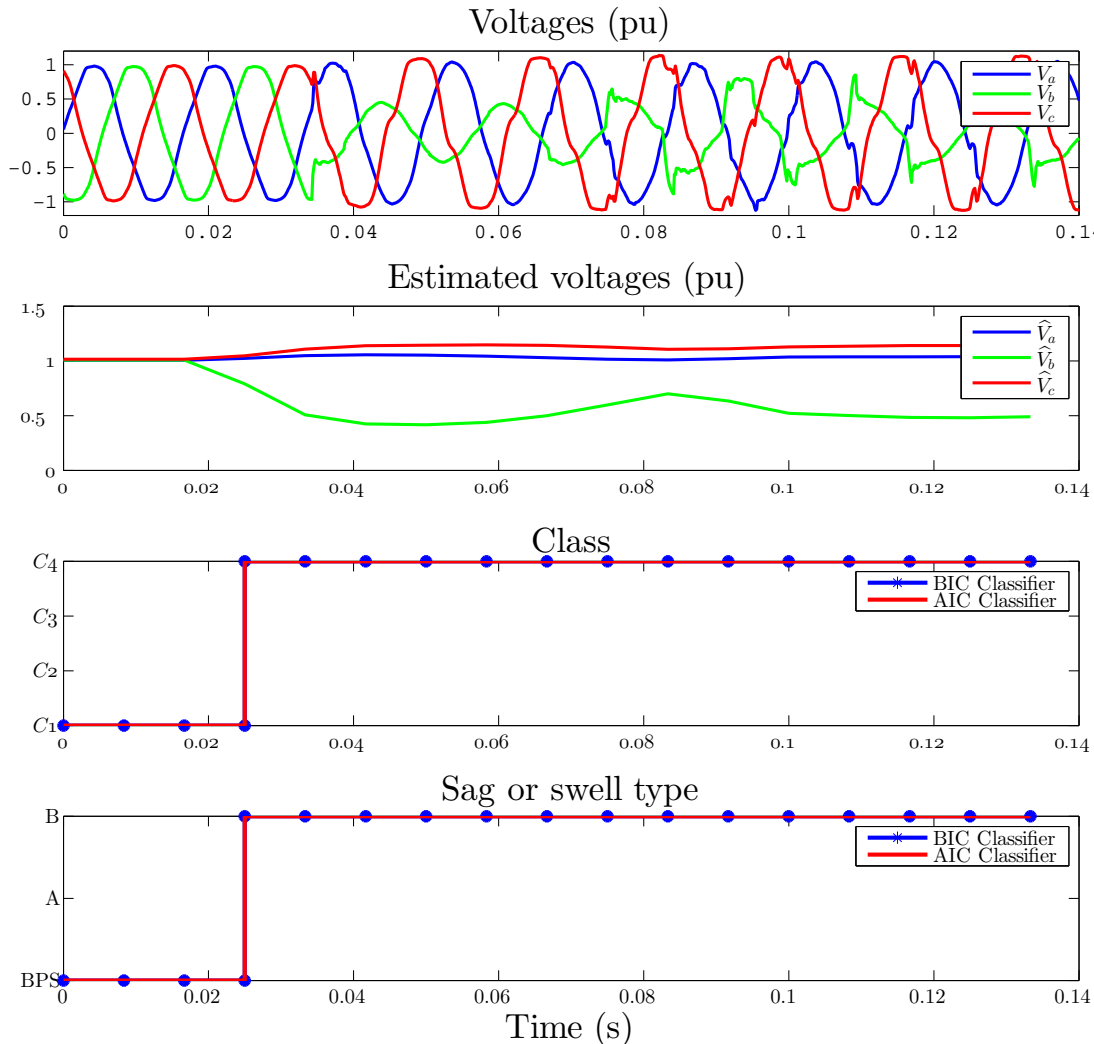


Figure 3.8: Event 1 (2827): Voltage sag and swell classification. Comparison between ML classifiers using BIC and AIC penalty terms.

AIC penalty term seems leading to erroneous classification results. Indeed, the AIC pre-classifier gives a type FG instead of type A. Concerning the third event (Fig. 3.10), different results of classification are obtained by these two pre-classifiers. Under balanced conditions, null zero- and negative-sequences ( $\mathcal{C}_1$ ) are selected by the BIC pre-classifier, while null zero-sequence ( $\mathcal{C}_2$ ) is selected by the other one. Under unbalanced conditions, a null zero-sequence ( $\mathcal{C}_2$ ) is obtained by the BIC pre-classifier, while the AIC pre-classifier gives non-null symmetrical-sequences ( $\mathcal{C}_4$ ). Moreover, both pre-classifiers give the same result after 0.10 s. For the fifth event (Fig. 3.11), different classification results are obtained under balanced conditions ( $\mathcal{C}_1$  and  $\mathcal{C}_3$ ), while they lead to the same results after 0.03 s. For the fifth event (Fig. 3.12), same result is obtained except between 0.03 s and 0.04 s.

Finally, It can be observed that the classifier using BIC penalty term seems achieving

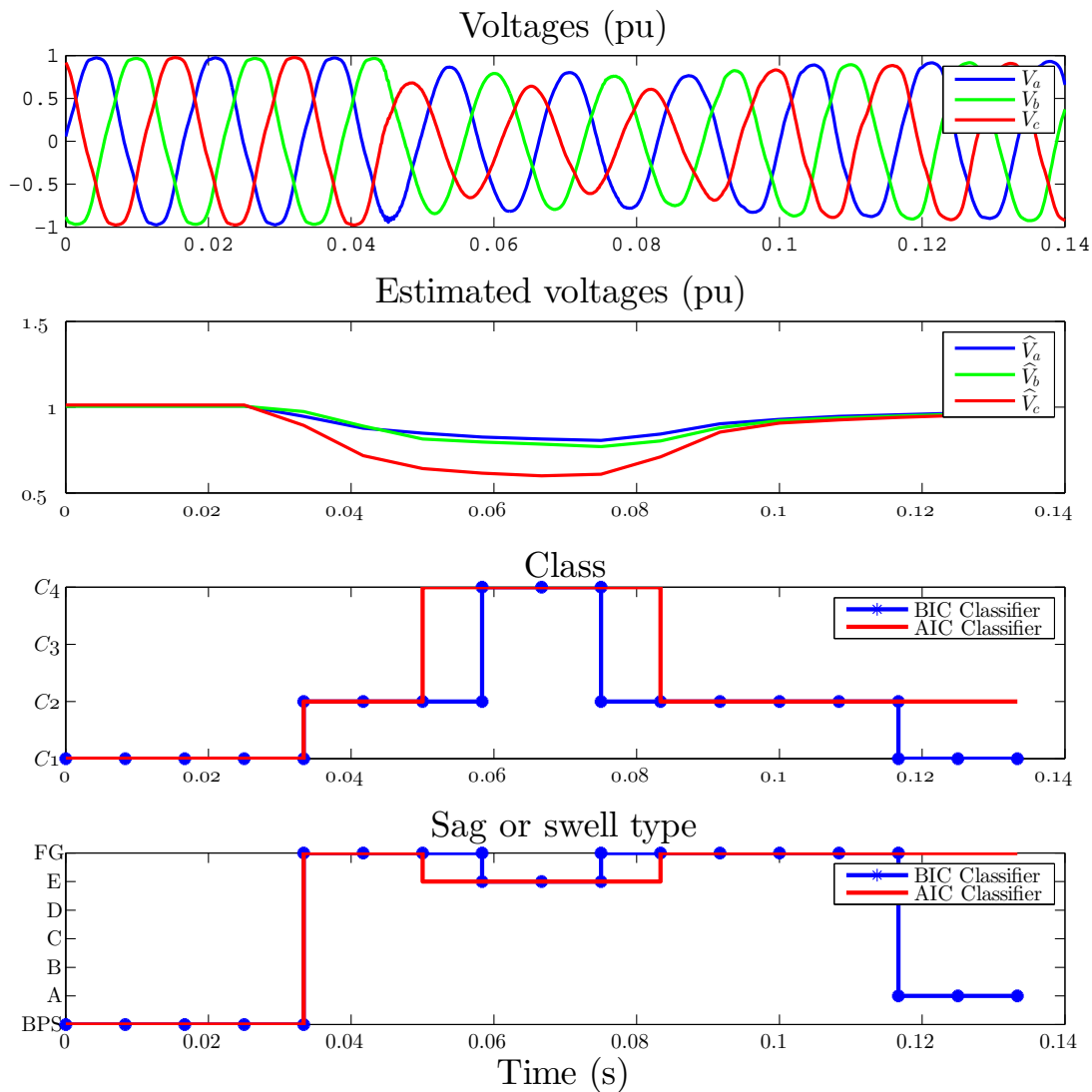


Figure 3.9: Event 2 (2825): Voltage sag and swell classification. Comparison between ML classifiers using BIC and AIC penalty terms.

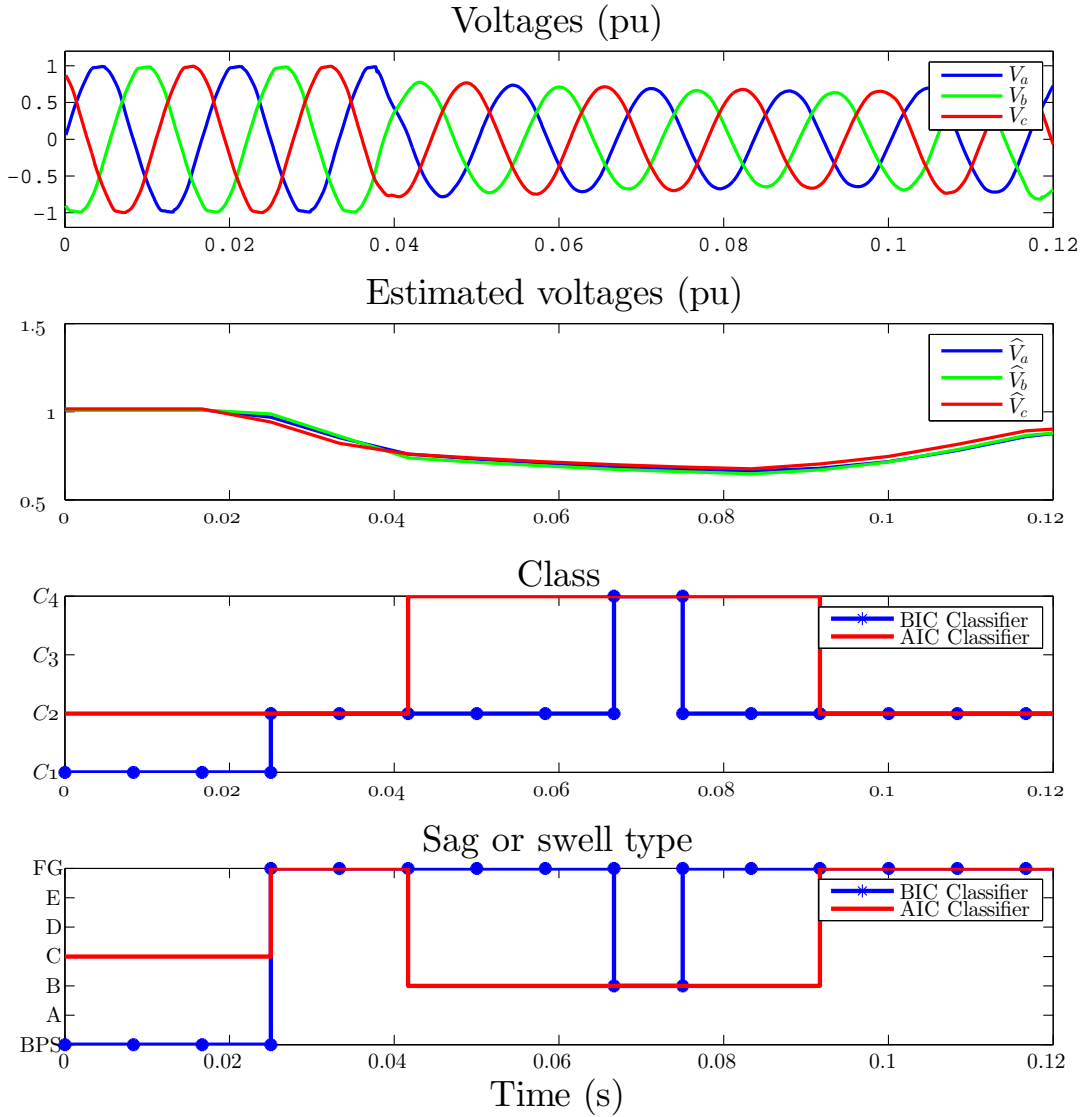


Figure 3.10: Event 3 (2802): Voltage sag and swell classification. Comparison between ML classifiers using BIC and AIC penalty terms.

good classifications under balanced and unbalanced conditions compared to those of the classifier using AIC penalty term. According to the Monte Carlo results, the ML classifier using BIC penalty term provides accurate results than other classifier even for a small number of samples.

### 3.4.3 Discussion

In the previous sections, the performances of the ML and App classifiers using BIC and AIC penalty terms were assessed under the influence of the following parameters on the performance: signal length, noise level, harmonics, and window length (overlap). The achieved simulation results have clearly shown that higher classification performance is reached by the proposed ML classifier using BIC penalty term regardless the signal length,

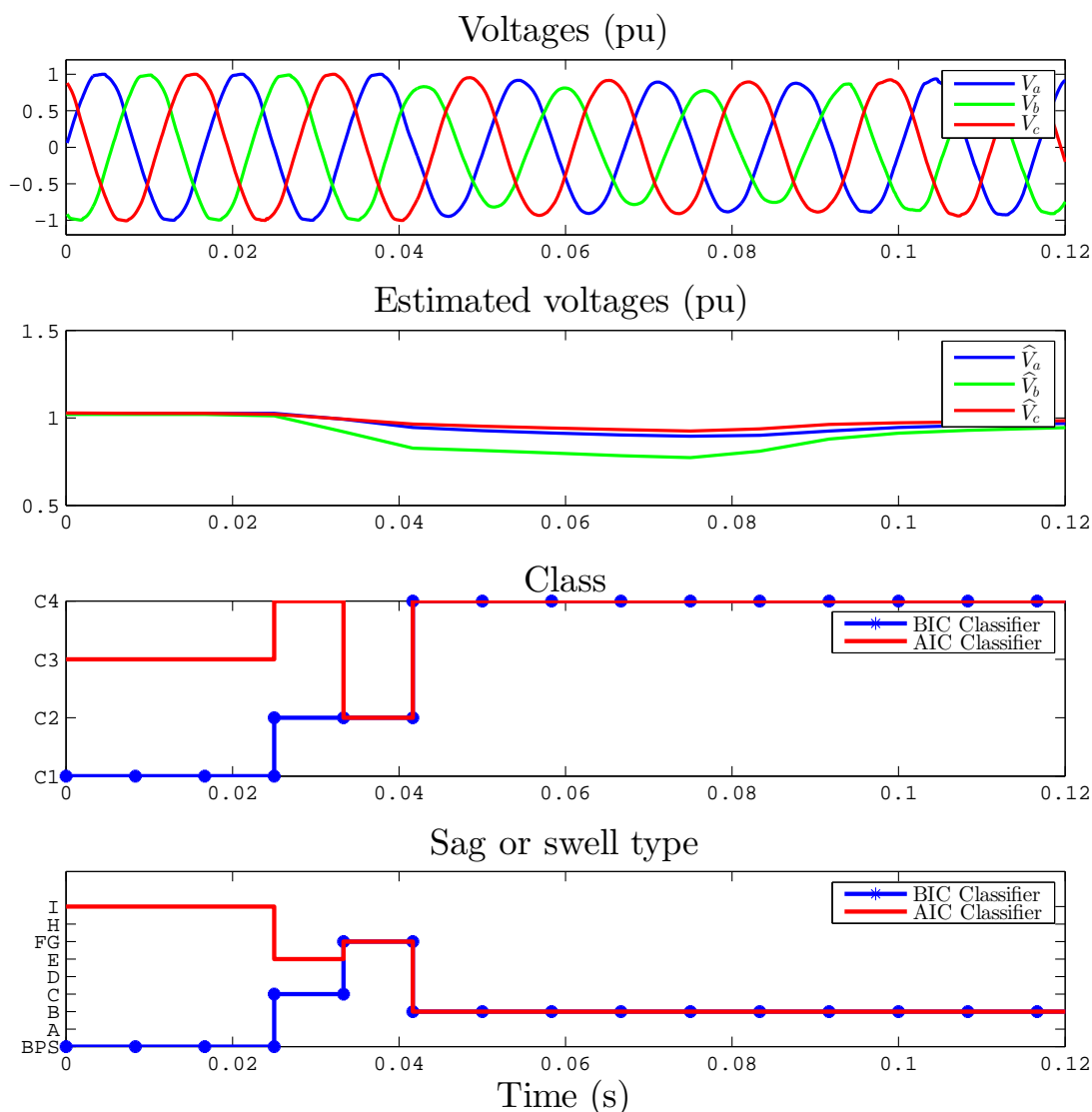


Figure 3.11: Event 4 (2786): Voltage sag and swell classification. Comparison between ML classifiers using BIC and AIC penalty terms.

$N$ , and  $SNR$ .

The statistical performances of the ML and App classifiers depend on the signal length and on the  $SNR$ . Particularly, the ML classifier performances can be increased by increasing the signal length and  $SNR$ . Furthermore, a comparison was performed between both ML and App classifiers. Based on simulation results, the best classification performance generally can be obtained by the ML classifier. However, the performance of the ML classifier can be reached by the App classifier for particular values of  $N$ . Especially, in the case when the signal length is a multiple of a half-cycle. We have also compared the ML and App classifiers using two different penalty terms BIC and AIC. Most simulation results have clearly shown that the ML classifier using the BIC penalty term achieves a higher classification performance compared to those of the ML classifier using the AIC penalty term. Indeed, the AIC penalty term seems overestimating the true values of



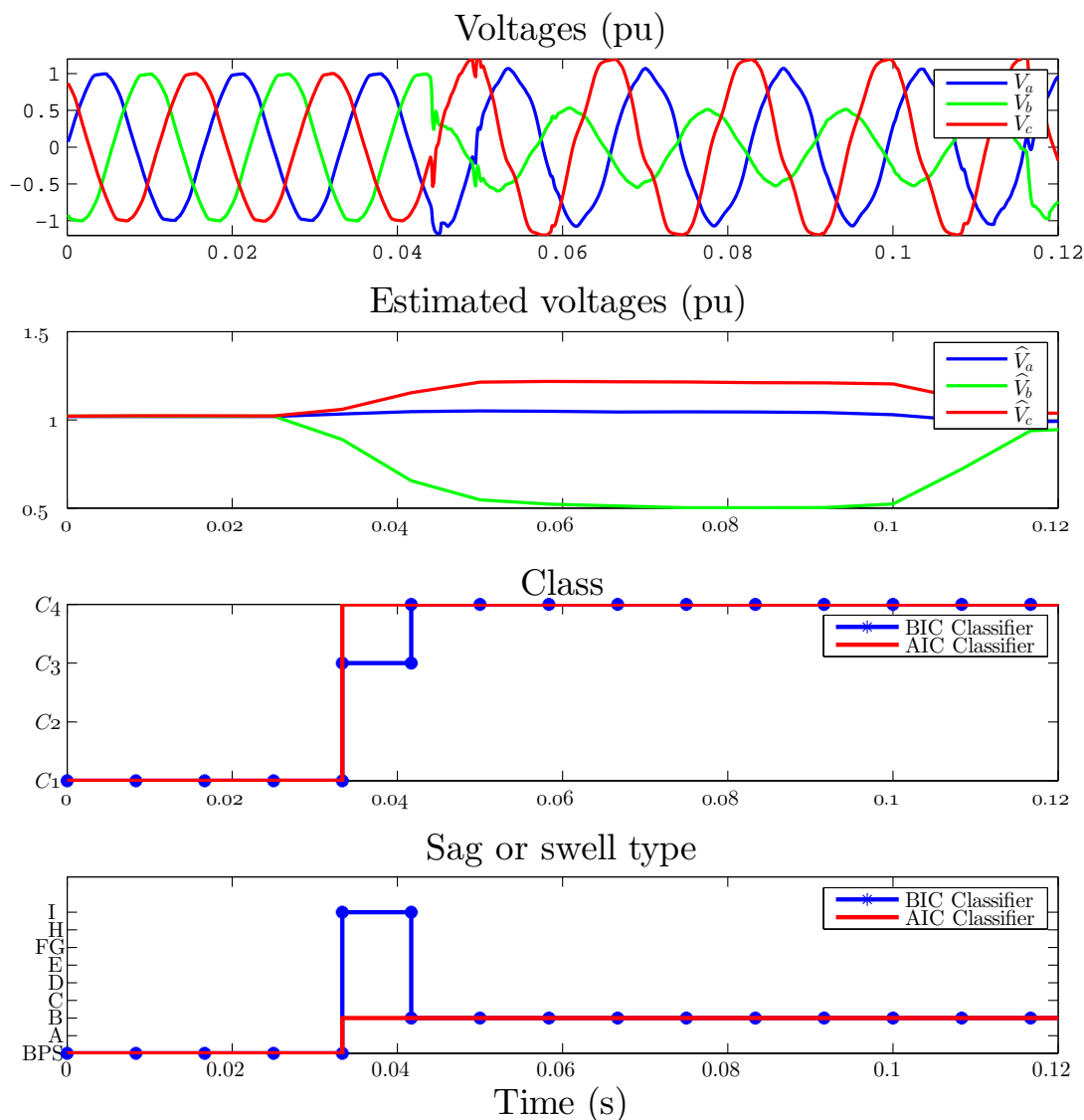


Figure 3.12: Event 5 (2911): Voltage sag and swell classification. Comparison between ML classifiers using BIC and AIC penalty terms.

non-zero symmetrical components.

Concerning the computation complexity, the performed test has shown that the App classifier has a lower computation time compared to the ML classifier. Indeed, the ML classifier involves more matrix multiplications and matrix inversion than the approximate classifier. Nevertheless, the App classifier performance critically relies on the signal length. In the case when the signal length is not a multiple of a half-cycle, the performance of the App classifier is rapidly degrading.

Regarding the case when the parameters of signal are time-varying (quasi-stationary conditions), small length of sample window is required for tracking the corresponding sag/swell signature. Indeed, there is a natural trade-off between the statistical performance and tracking. For meeting the minimum duration of sag/swell defined in the standard IEEE std. 1159, a half-cycle window must be chosen. According to Monte

Carlo simulation, the approximate classifier leads to a higher classification performance for a half-cycle window and it has a lower computation complexity. To easily meet this criterion, it is advised to set the sampling frequency to  $F_s = Nf_0$ , where  $N \gg 2$  and  $f_0$  corresponds to the fundamental frequency ( $f_0 = 50$  Hz or  $f_0 = 60$  Hz).

### 3.5 Conclusion

This chapter has described a new technique for power quality disturbances classification applied to voltage sags and swells. The proposed technique is based on Information Theoretical Criteria and it is mainly decomposed into two steps: 1) The pre-classification of input signal into one of the four pre-classes that depend on the number of non-zero symmetrical components. Various types of sag and swell can be found in each class. 2) The classification of the corresponding sag/swell signature using the ML estimate of the symmetrical components.

Afterwards, the use of two Information Theoretical Criteria, i.e. the AIC and BIC, have been investigated. In terms of average probability of correct classification, the achieved simulation results have clearly shown that the ML and App classifiers using BIC penalty term outperform respectively the ML and App classifiers using AIC penalty term whatever the signal length and  $SNR$  are. Specifically, a confusion matrix analysis has shown that the AIC seems slightly overestimating the true number of non-zero symmetrical component even for a large signal length or  $SNR$ . Under harmonic environment, the classifier using the BIC penalty term has shown a good robustness for a moderate Total Harmonic Distortion (THD < 50%).

The proposed approximate classifier can be considered as an attractive choice for classification application requiring lower computation complexity since small number of matrix multiplications is needed. Based on the achieved simulation and experimental results, the ML classifier allows having better statistical performances compared to those of the approximate classifier in most of the cases. However, in case when the signal length is a multiple of a half-cycle, the approximate classifier has a lower computation complexity and can reach the ML classifier performances.



# Conclusions and Perspectives

## Conclusions

Power quality monitoring applied to the electric grid becomes of high interest for the electrical power system community. Indeed, PQ monitoring is considered as the most efficient strategy used to ensure availability, reliability, and safety of the electric grids. In essence, the future power system needs to provide the utility companies with full visibility and pervasive control. Moreover, it is expected to be self-healing, performing energy transactions across the system, and resilient to system anomalies and disturbances. For this purpose, it becomes imperative to integrate advanced algorithms to characterize PQ disturbances. These characterization algorithms should allow an accurate and effective event detection and classification at an early stage. As previously reported in chapter 1, several techniques have been proposed for PQ characterization. However, feature extraction of these techniques lead to poor estimation under high noisy environment and require long data to achieve good resolution. Moreover, their performances critically degrade under off-nominal conditions. Regarding classification, classical techniques are very sensitive to large variations in amplitude, phase angle, or frequency. Moreover, they can not provide a complete sag and swell classification. For pattern-recognition-based techniques, the performances critically depend on the learning stage, that requires a training database, and on feature extraction process.

In this context, this thesis has proposed parametric spectral-based approaches for PQ disturbances estimation and classification.

For the estimation approach, frequency and phasor estimator based on the Maximum Likelihood (ML) method has been proposed. As opposed to most of the previous works, the proposed estimator fully exploits the multidimensional nature of electrical signals. Regarding frequency estimation, we have presented ML and discrete time Fourier transform (DTFT) techniques. Both techniques require the maximization of a 1-dimensional cost-function. For this purpose, an optimization algorithm based on the Newton-Raphson method has been proposed. As illustrated by the simulation and experimental results in chapter 2, this optimization algorithm allows to improve frequency and phasor estimations accuracy and has lower computational complexity than the downhill simplex algorithm.

Furthermore, the proposed ML-based Newton-Raphson estimator achieves good performances even under off-nominal conditions compared to the DTFT approach, when the signal length is not equal to a multiple of the fundamental half-period. Indeed, it has been demonstrated that the proposed estimator can be implemented using the DTFT when the signal length is equal to a multiple of the fundamental half-period. Simulation results have also shown that the proposed estimator meets, on the average, the M-class requirements of the IEEE standard in terms of TVE and FE under steady-state conditions.

Concerning the classification approach, we have proposed a PQ disturbances classification approach with a particular focus on voltage sags and swells signatures. The proposed algorithm was able to provide a complete sag and swell classification. Specifically, it is based on Maximum Likelihood and Information Theoretic Criteria methods, where we have investigated the use of AIC and BIC criteria. As illustrated in the simulation and experimental results in chapter 3, the BIC criterion outperforms the AIC one in terms of average probability of correct classification. As compared to pattern recognition-based classifiers, the proposed classifier does not require any training database and no parameter to be set. Furthermore, the proposed classifier fully exploits three-phase information that allow better classification performances as compared to most of the PQ disturbance classification techniques. The achieved results have clearly shown that the proposed algorithm has higher classification performances as compared to classical classifiers i.e. the symmetrical components and three-phases three-angles algorithms. For applications requiring a low computational complexity, we have also proposed an approximate classifier that involves fewer matrix multiplications and no matrix inversion. However, this approximate classifier damages the classification performance when the number of samples is not a multiple of a half-cycle.

The proposed approaches have been tested, compared, and validated with simulation under different faulty environments and using real power system data obtained from DOE/EPRI National Database of Power System Events. The achieved simulations and experimental results have clearly illustrated the effectiveness of the proposed estimator as compared to the DTFT approach, regardless of the window length. Furthermore, these results have shown that the proposed classifier has higher classification performance than the symmetrical components and three-phases three-angles algorithms for voltage sags and swells.

## Perspectives

In this thesis, the performances of the proposed estimator were evaluated in steady-state testing conditions recommended by the IEEE Std. C37.118.2011. The proposed estimator performances should however be evaluated under dynamic conditions reported

by this standard. In this regard, its performances should be evaluated according to the requirement of PMU standard through the Rate of Change of Frequency Error (RFE).

Further investigations should focus on the reliability and robustness of the proposed classifier under other critical disturbances. In particular, the impact of frequent fault caused by renewable energy on the proposed algorithms should be highlighted. Moreover, we should deal with the evaluation of the proposed classifier performances for the classification of other critical PQ disturbances, such as the transient and the flicker (Table A.1).

Fault location becomes of great interest among intelligent monitoring that could lead to the realization of self-healing networks, which is an important feature of smart grids. Therefore, forthcoming studies should deal with intelligent algorithms of fault location for transmission and distribution power systems.



# Appendices





# Appendix A

## Power Quality Variations and Events Characterization and Methods

Table A.1 lists various PQ variations and events, their characterization methods, and possible causes.

Table A.1: Classification of the power quality disturbances and their causes.

Broad Categories	Specific Categories	Characterization methods	Typical causes
Transients	Impulsive	Peak magnitude, rise time and duration	Lightning strike, transformer energization, capacitor switching
	Oscillatory	Peak magnitude, frequency components	Line or capacitor or load switching
Short duration voltage variation	Sag	Magnitude, duration	Ferroresonant transformers, single line-to-ground faults
	Swell	Magnitude, duration	Ferroresonant transformers, single line-to-ground faults
	Interruption	Duration	Temporary (self-clearing) faults
Long duration voltage variation	Undervoltage	Magnitude, duration	Switching on loads, capacitor de-energization
	Oversvoltage	Magnitude, duration	Switching off loads, capacitor de-energization
	Sustained interruption	Duration	Faults
Voltage imbalance		Symmetrical components	Single-phase loads, single-phasing condition
Waveform distortion	Harmonics	THD, Harmonic spectrum	Adjustable speed drives and other nonlinear loads
	Notching	THD, Harmonic spectrum	Power electronic converters
	DC offset	Volts, Amps	Geo-magnetic disturbance, half-wave rectification
Voltage flicker		Frequency of occurrence, modulating frequency	Arc furnace, arc lamps

# Appendix B

## Major Components of Phasor Measurement Unit

Major components of a phasor measurement unit are shown in Fig. B.1. The analog-to-digital (A/D) converter allows converting the analog inputs into digital data. First, each cycle of the input signal (voltage or current) is sampled and then the fundamental frequency is estimated using the discrete Fourier transform, which is one of the most common frequency and phasor estimation algorithm used by PMUs measurements. The voltage or current phasor is obtained by converting the sampled data to a complex number. A combination of the three-phase phasors allows providing the zero-, positive-, and negative-sequences. This figure shows also an anti-aliasing low-pass filter (LPF) and an analog-to-digital (A/D) converter [175]. Data obtained from several phasor measurement units at same time-tags are collected by a phasor data concentrator (PDC). Hierarchy of the phasor measurement systems and levels of phasor data concentrators (PDC) is given by Fig. B.2.

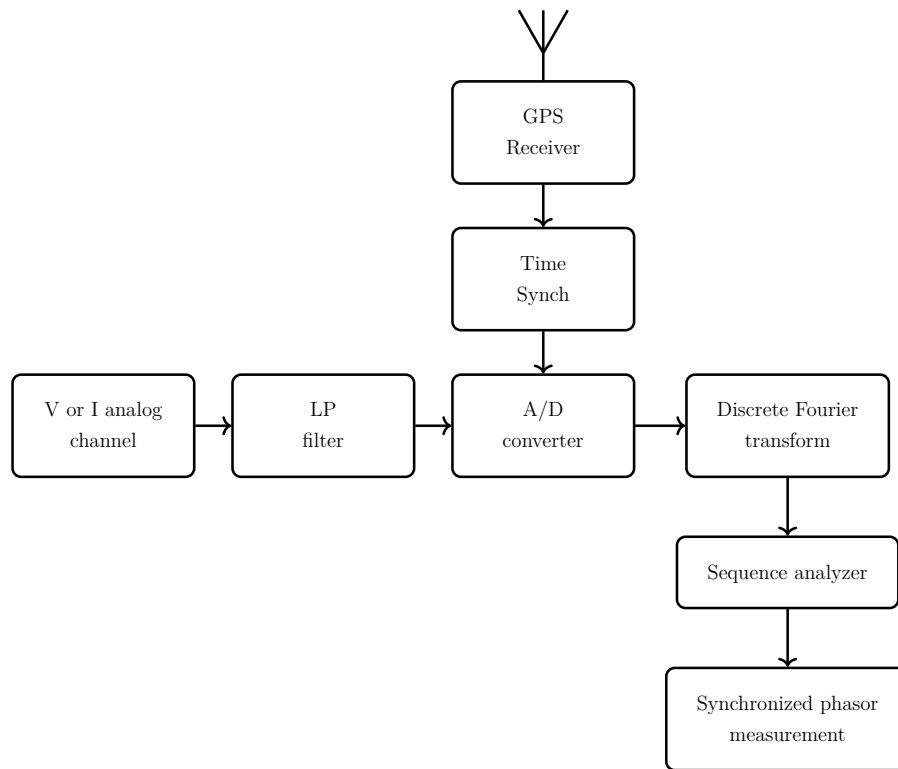


Figure B.1: Flowchart of a phasor measurement unit.

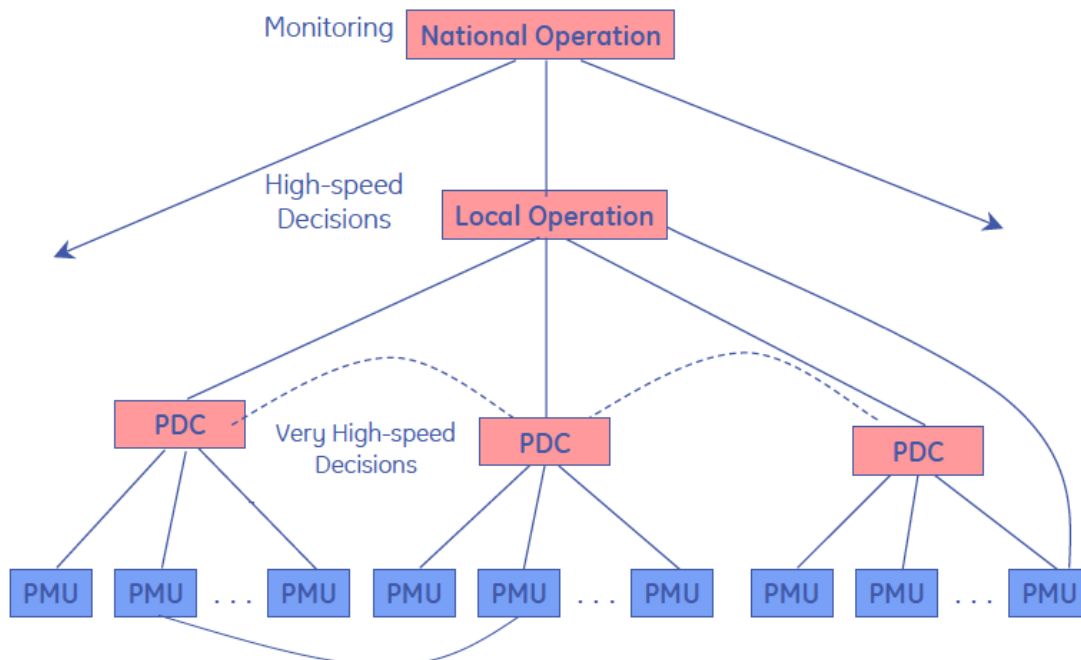


Figure B.2: Phasor measurement systems hierarchy and phasor data concentrators (PDC) levels.

# Appendix C

## TVE Expression for Off-Nominal Frequency

By neglecting the influence of the noise in (2.1), the signal model can be approximated by

$$x_m[k] = a_m \cos(w_0 k + \phi_m), \quad (\text{C.1})$$

where  $w_0 = (w_n + \delta)$ ,  $w_n$  corresponds to the nominal angular frequency and  $\delta$  refers to the angular deviation. Using matrix notations,  $\mathbf{X} = \mathbf{G}(w_0)\mathbf{S}$  and the ML estimator of  $\hat{\mathbf{S}}$  can be expressed as

$$\hat{\mathbf{S}} = \left( \mathbf{G}^T(w_n)\mathbf{G}(w_n) \right)^{-1} \mathbf{G}^T(w_n)\mathbf{X} \quad (\text{C.2})$$

$$= \left( \mathbf{G}^T(w_n)\mathbf{G}(w_n) \right)^{-1} \mathbf{G}^T(w_n)\mathbf{G}(w_n + \delta)\mathbf{S}. \quad (\text{C.3})$$

Let us introduce the following decompositions  $\mathbf{S} = [\mathbf{s}_a, \mathbf{s}_b, \mathbf{s}_c]$  and  $\hat{\mathbf{S}} = [\hat{\mathbf{s}}_a, \hat{\mathbf{s}}_b, \hat{\mathbf{s}}_c]$ . For phase  $m$ , the estimation error can be expressed as

$$\mathbf{s}_m - \hat{\mathbf{s}}_m = \mathbf{M}(w_n, \delta)\mathbf{s}_m. \quad (\text{C.4})$$

where  $\mathbf{M}(w_n, \delta)$  is a  $2 \times 2$  matrix, which is defined as

$$\mathbf{M}(w_n, \delta) \triangleq \mathbf{I}_{22} - \left( \mathbf{G}^T(w_n)\mathbf{G}(w_n) \right)^{-1} \mathbf{G}^T(w_n)\mathbf{G}(w_n + \delta) \quad (\text{C.5})$$

Finally, the TVE for the phasor  $m$  can be expressed as

$$TVE_m = \frac{\|\mathbf{s}_m - \hat{\mathbf{s}}_m\|}{a_m} = \frac{\|\mathbf{M}(w_n, \delta)\mathbf{s}_m\|}{a_m} \quad (\text{C.6})$$

where  $\mathbf{s}_m = [a_m \cos(\phi_m), -a_m \sin(\phi_m)]^T$ . If the fundamental frequency is equal to the nominal frequency ( $f_0 = f_n = 60$  Hz), then the matrix  $\mathbf{M}(w_n, \delta) = \mathbf{0}$  and so  $TVE_m = 0$ . When  $\delta \neq 0$ , one can note that  $TVE_m > 0$ .

For the DTFT estimator ( $\hat{\mathbf{S}} = \frac{2}{N}\mathbf{G}^T(w_n)\mathbf{X}$ ), the expression of the TVE is simply obtained by replacing  $\mathbf{M}(w_n, \delta)$  with  $\mathbf{M}^{DTFT}(w_n, \delta) \triangleq \mathbf{I}_{22} - \frac{2}{N}\mathbf{G}^T(w_n)\mathbf{G}(w_n + \delta)$  in (C.6).



# References

- [1] M. H. J. Bollen and F. Hassan, *Integration of distributed generation in the power system*, vol. 80. John Wiley & Sons, 2011.
- [2] M. H. J. Bollen and I. Gu, *Signal processing of power quality disturbances*, vol. 30. John Wiley & Sons, 2006.
- [3] DOE/EPRI National Database Repository of Power System Events: Online; available at: [http://pqmon.epri.com/disturbance\\_library/](http://pqmon.epri.com/disturbance_library/) (last accessed: May 2016).
- [4] V. Ignatova, P. Granjon, and S. Bacha, "Space vector method for voltage dips and swells analysis," *IEEE Transactions on Power Delivery*, vol. 24, pp. 2054–2061, October 2009.
- [5] J. Hu, J. Zhu, and G. Platt, "Smart grid the next generation electricity grid with power flow optimization and high power quality," in *Proceedings of the 2011 IEEE ICEMS, Beijing (China)*, pp. 1–6, August 2011.
- [6] H. Farhangi, "The path of the smart grid," *IEEE Power and Energy Magazine*, vol. 8, no. 1, pp. 18–28, February 2010.
- [7] R. C. Dugan, M. F. McGranaghan, and H. W. Beaty, "Electrical power systems quality," *New York, NY: McGraw-Hill*, 1996.
- [8] X. Fang, S. Misra, G. Xue, and D. Yang, "Smart grid the new and improved power grid: A survey," *IEEE Communications Surveys & Tutorials*, vol. 14, no. 4, pp. 944–980, October 2012.
- [9] P. W. Sauer, M. A. Pai, and J. H. Chow, *Power System Dynamics and Stability: With Synchrophasor Measurement and Power System Toolbox*. John Wiley & Sons, 2017.
- [10] A. Kusko and M. T. Thompson, *Power quality in electrical systems*. McGraw-Hill, 2007.

- [11] H. Chung, S. Hui, and K. Tse, "Reduction of power converter emi emission using soft-switching technique," *IEEE Transactions on Electromagnetic Compatibility*, vol. 40, pp. 282–287, August 1998.
- [12] M. H. J. Bollen, I. Y. H. Gu, S. Santoso, M. F. Mcgranaghan, P. A. Crossley, M. V. Ribeiro, and P. F. Ribeiro, "Bridging the gap between signal and power," *IEEE Signal Processing Magazine*, vol. 26, no. 4, pp. 12–31, July 2009.
- [13] P. F. Ribeiro, C. A. Duque, P. M. Ribeiro, and A. S. Cerqueira, *Power systems signal processing for smart grids*. John Wiley & Sons, 2013.
- [14] M. Bollen, "What is power quality?," *Electric Power Systems Research*, vol. 66, no. 1, pp. 5–14, 2003.
- [15] E. Fuchs and M. A. Masoum, *Power quality in power systems and electrical machines*. Academic press, 2011.
- [16] H. Farhangi, "The path of the smart grid," *IEEE Power and Energy Magazine*, vol. 8, February 2010.
- [17] G. T. Heydt, *Electric power quality*. Stars in a circle publications, 1991.
- [18] M. Liserre, T. Sauter, and J. Y. Hung, "Future energy systems: Integrating renewable energy sources into the smart power grid through industrial electronics," *IEEE industrial electronics magazine*, vol. 4, no. 1, pp. 18–37, 2010.
- [19] R. Banos, F. Manzano-Agugliaro, F. Montoya, C. Gil, A. Alcayde, and J. Gómez, "Optimization methods applied to renewable and sustainable energy: A review," *Renewable and Sustainable Energy Reviews*, vol. 15, no. 4, pp. 1753–1766, 2011.
- [20] F. Manzano-Agugliaro, A. Alcayde, F. Montoya, A. Zapata-Sierra, and C. Gil, "Scientific production of renewable energies worldwide: an overview," *Renewable and Sustainable Energy Reviews*, vol. 18, pp. 134–143, 2013.
- [21] J. M. Carrasco, L. G. Franquelo, J. T. Bialasiewicz, E. Galván, R. C. PortilloGuisado, M. M. Prats, J. I. León, and N. Moreno-Alfonso, "Power-electronic systems for the grid integration of renewable energy sources: A survey," *IEEE Transactions on Industrial Electronics*, vol. 53, no. 4, pp. 1002–1016, 2006.
- [22] A. Mohd, E. Ortjohann, A. Schmelter, N. Hamsic, and D. Morton, "Challenges in integrating distributed energy storage systems into future smart grid," in *Proceeding of IEEE 2008 International Symposium on Industrial Electronics, Cambridge (United Kingdom)*, pp. 1627–1632, IEEE, 2008.



- 
- [23] A. R. Bergen, *Power Systems Analysis*. Pearson Education India, July 2000.
- [24] K. D. McBee and M. G. Simoes, “Utilizing a smart grid monitoring system to improve voltage quality of customers,” *IEEE Transactions on Smart Grid*, vol. 3, pp. 738–743, June 2012.
- [25] IEEE, “IEEE approved draft guide for the interoperability of energy storage systems integrated with the electric power infrastructure,” *IEEE P2030.2/D9.0*, pp. 1–136, June 2015.
- [26] S. Amin and B. Wollenberg, “Toward a smart grid: power delivery for the 21st century,” *IEEE Power and Energy Magazine*, vol. 3, no. 5, pp. 34–41, September 2005.
- [27] V. C. Gungor, B. Lu, and G. P. Hancke, “Opportunities and challenges of wireless sensor networks in smart grid,” *IEEE Transactions on Industrial Electronics*, vol. 57, no. 10, pp. 3557–3564, September 2010.
- [28] A. Baghini, *Handbook of power quality*. John Wiley & Sons, 2008.
- [29] A. Kusko and M. T. Thompson, *Power quality in electrical systems*. McGraw-Hill, 2007.
- [30] W. G. Morsi and M. El-Hawary, “Power quality evaluation in smart grids considering modern distortion in electric power systems,” *Electric Power Systems Research*, vol. 81, no. 5, pp. 1117–1123, 2011.
- [31] M. H. J. Bollen, *Understanding Power Quality Problems*, vol. 3. IEEE Press New York, October 1999.
- [32] S. H. Jaramillo, G. Heydt, and E. O’Neill-Carrillo, “Power quality indices for aperiodic voltages and currents,” *IEEE Transactions on Power Delivery*, vol. 15, no. 2, pp. 784–790, 2000.
- [33] M. Laughton, “Analysis of Unbalanced Polyphase Networks by the Method of Phase Co-ordinates. Part 2: Fault Analysis,” in *Proceedings of the Institution of Electrical Engineers*, vol. 116, pp. 857–865, May 1969.
- [34] IEEE, “IEEE recommended practice for monitoring electric power quality,” *IEEE Std 1159-2009 (Revision of IEEE Std 1159-1995)*, pp. c1–81, June 2009.
- [35] IEC, “Testing and measurement techniques—power quality measurement methods,” *International Electrotechnical Commission Standard 61000-4-30*, January 2015.
-

- [36] Std, EN and others, “Voltage characteristics of electricity supplied by public distribution systems,” in *EN Std. 50160*, 2002.
- [37] Y. H. Gu and M. H. J. Bollen, “Time-frequency and time-scale domain analysis of voltage disturbances,” *IEEE Transactions on Power Delivery*, vol. 15, pp. 1279–1284, October 2000.
- [38] A. G. Phadke and J. S. Thorp, *Synchronized phasor measurements and their applications*. Springer Science & Business Media, 2008.
- [39] J. Arrillaga and N. R. Watson, *Power system harmonics*. John Wiley & Sons, 2004.
- [40] J. Arrillaga, *Power system harmonic analysis*. John Wiley & Sons, 1997.
- [41] V. Wagner, J. C. Balda, D. Griffith, A. McEachern, T. Barnes, D. Hartmann, D. Phileggi, A. Emmanuel, W. F. Horton, W. E. Reid, *et al.*, “Effects of harmonics on equipment,” *IEEE Transactions on Power Delivery*, vol. 8, no. 2, pp. 672–680, 1993.
- [42] IEC, “Electromagnetic compatibility (EMC) part 4–7: Testing and measurement techniques—general guide on harmonics and interharmonics measurements and instrumentation, for power supply systems and equipment connected thereto,” *IEC Std. 61000-4-7*, 2002.
- [43] Z. Zeng, H. Yang, R. Zhao, and C. Cheng, “Topologies and control strategies of multi-functional grid-connected inverters for power quality enhancement: A comprehensive review,” *Renewable and Sustainable Energy Reviews*, vol. 24, pp. 223–270, 2013.
- [44] A. Ipakchi and F. Albuyeh, “Grid of the future,” *IEEE Power and Energy Magazine*, vol. 7, no. 2, pp. 52–62, 2009.
- [45] M. H. J. Bollen, P. Ribeiro, I. Y. Gu, and C. A. Duque, “Trends, challenges and opportunities in power quality research,” *European Transactions on Electrical Power*, vol. 20, no. 1, pp. 3–18, 2010.
- [46] S. Chattopadhyay, M. Mitra, and S. Sengupta, *Electric Power Quality*. Springer, March 2011.
- [47] P. Granjon and G. S. L. Phua, “Estimation of geometric properties of three-component signals for system monitoring,” *Mechanical Systems and Signal Processing*, vol. 97, pp. 95–111, 2017.

- 
- [48] G. Cablea, P. Granjon, and C. Bérenguer, “Three-phase electrical signals analysis for mechanical faults monitoring in rotating machine systems,” *Mechanical Systems and Signal Processing*, vol. 92, pp. 278–292, 2017.
- [49] IEC, “Electromagnetic compatibility (EMC), part 1: General, section 1: Application and interpretation of fundamental definitions and terms,” *International Electrotechnical Commission Standard 61000-1-1.1*.
- [50] IEEE, “IEEE standard 519, recommended practices and requirements for harmonic control in electrical power systems,,” *ANSI/IEEE Std. 519-/992, IEEE, New York*, 1993.
- [51] K. Narendra, D. R. Gurusinghe, and A. D. Rajapakse, “Dynamic performance evaluation and testing of phasor measurement unit (PMU) as per ieeec37.118.1 standard,” in *Doble Client Committee Meetings Int. Protect. Testing Users Group*, 2012.
- [52] IEEE, “IEEE standard for synchrophasor measurements for power systems, IEEE standard C37.118.1-2011 (revision of IEEE standard C37.118-2005),” December 2011.
- [53] Q. Zhang, Y. Chakhchoukh, V. Vittal, G. T. Heydt, N. Logic, and S. Sturgill, “Impact of PMU measurement buffer length on state estimation and its optimization,” *IEEE Transactions on Power Systems*, vol. 28, pp. 1657–1665, May 2013.
- [54] IEEE, “IEEE standard for synchrophasor measurements for power systems, IEEE standard C37.118.2005(revision of IEEE std. 1344–1995),” 2005.
- [55] J. Depablos, V. Centeno, A. G. Phadke, and M. Ingram, “Comparative testing of synchronized phasor measurement units,” in *Power Engineering Society General Meeting, IEEE*, pp. 948–954, June.
- [56] IEEE, “IEEE standard for synchrophasor measurements for power systems amendment 1: Modification of selected performance requirements, IEEE standard C37.118.1a-2014 (amendment to IEEE standard C37.118.1-2011),” April 2014.
- [57] A. Papoulis and A. Maradudin, “The fourier integral and its applications,” 1963.
- [58] E. O. Brigham and R. Morrow, “The fast Fourier transform,” *IEEE Spectrum*, vol. 4, no. 12, pp. 63–70, 1967.
- [59] D. C. Robertson, O. I. Camps, J. S. Mayer, and W. B. Gish, “Wavelets and electromagnetic power system transients,” *IEEE Transactions on Power Delivery*, vol. 11, no. 2, pp. 1050–1058, 1996.

- [60] G. Barchi, D. Macii, and D. Petri, "Accuracy of one-cycle dft-based synchrophasor estimators in steady-state and dynamic conditions," in *Instrumentation and Measurement Technology Conference (I2MTC), 2012 IEEE International*, pp. 1529–1534, IEEE, July 2012.
- [61] P. Stoica and R. L. Moses, *Introduction to spectral analysis*, vol. 1. Prentice Hall Upper Saddle River, 1997.
- [62] S. M. Kay and S. L. Marple, "Spectrum analysis—a modern perspective," *Proceedings of the IEEE*, vol. 69, no. 11, pp. 1380–1419, 1981.
- [63] P. Flandrin, *Time-frequency/time-scale analysis*, vol. 10. Academic press, 1998.
- [64] D. C. Robertson, O. I. Camps, J. S. Mayer, and W. B. Gish, "Wavelets and electromagnetic power system transients," *IEEE Transactions on Power Delivery*, vol. 11, no. 2, pp. 1050–1058, 1996.
- [65] S. M. Kay, *Modern spectral estimation*. Pearson Education India, 1988.
- [66] W. A. Ibrahim and M. M. Morcos, "Artificial intelligence and advanced mathematical tools for power quality applications: A survey," *IEEE Transactions on Power Delivery*, vol. 17, no. 2, pp. 668–673, 2002.
- [67] S. Nath, P. Sinha, and S. K. Goswami, "A wavelet based novel method for the detection of harmonic sources in power systems," *International Journal of Electrical Power & Energy Systems*, vol. 40, no. 1, pp. 54–61, 2012.
- [68] S. Santoso, E. J. Powers, W. M. Grady, and P. Hofmann, "Power quality assessment via wavelet transform analysis," *IEEE transactions on Power Delivery*, vol. 11, no. 2, pp. 924–930, 1996.
- [69] P. Pillay and A. Bhattacharjee, "Application of wavelets to model short-term power system disturbances," *IEEE Transactions on Power Systems*, vol. 11, no. 4, pp. 2031–2037, 1996.
- [70] B. Biswal, M. Biswal, S. Mishra, and R. Jalaja, "Automatic classification of power quality events using balanced neural tree," *IEEE Transactions on Industrial Electronics*, vol. 61, pp. 521–530, January 2014.
- [71] N. E. Huang, Z. Shen, S. R. Long, M. C. Wu, H. H. Shih, Q. Zheng, N.-C. Yen, C. C. Tung, and H. H. Liu, "The empirical mode decomposition and the hilbert spectrum for nonlinear and non-stationary time series analysis," in *Proceedings of the Royal Society of London A: Mathematical, Physical and Engineering Sciences*, vol. 454, pp. 903–995, The Royal Society, 1998.

- 
- [72] S. Shukla, S. Mishra, and B. Singh, "Empirical-mode decomposition with hilbert transform for power-quality assessment," *IEEE Transactions on Power Delivery*, vol. 24, no. 4, pp. 2159–2165, 2009.
- [73] R. Kumar, B. Singh, and D. T. Shahani, "Recognition of single-stage and multiple power quality events using hilbert–huang transform and probabilistic neural network," *Electric Power Components and Systems*, vol. 43, no. 6, pp. 607–619, 2015.
- [74] M. Manjula, S. Mishra, and A. Sarma, "Empirical mode decomposition with hilbert transform for classification of voltage sag causes using probabilistic neural network," *International Journal of Electrical Power & Energy Systems*, vol. 44, no. 1, pp. 597–603, 2013.
- [75] O. Ozgonenel, T. Yalcin, I. Guney, and U. Kurt, "A new classification for power quality events in distribution systems," *Electric Power Systems Research*, vol. 95, pp. 192–199, 2013.
- [76] D. Saxena, S. Singh, K. Verma, and S. K. Singh, "HHT-based classification of composite power quality events," *International Journal of Energy Sector Management*, vol. 8, no. 2, pp. 146–159, 2014.
- [77] V. M. Saiz and J. B. Guadalupe, "Application of kalman filtering for continuous real-time tracking of power system harmonics," *IEE Proceedings-Generation, Transmission and Distribution*, vol. 144, no. 1, pp. 13–20, 1997.
- [78] I. Kamwa, R. Grondin, and D. McNabb, "On-line tracking of changing harmonics in stressed power systems: application to hydro-quebec network," *IEEE Transactions on Power Delivery*, vol. 11, no. 4, pp. 2020–2027, 1996.
- [79] S. S. Haykin *et al.*, *Kalman filtering and neural networks*. Wiley Online Library, 2001.
- [80] T. K. Moon and W. C. Stirling, *Mathematical methods and algorithms for signal processing*. Prentice Hall, 2000.
- [81] P. Dash and M. Chilukuri, "Hybrid s-transform and kalman filtering approach for detection and measurement of short duration disturbances in power networks," *IEEE Transactions on Instrumentation and Measurement*, vol. 53, no. 2, pp. 588–596, 2004.
- [82] J. Reddy, P. K. Dash, R. Samantaray, and A. K. Moharana, "Fast tracking of power quality disturbance signals using an optimized unscented filter," *IEEE Transactions on Instrumentation and Measurement*, vol. 58, no. 12, pp. 3943–3952, 2009.
-

- [83] A. A. Abdelsalam, A. A. Eldesouky, and A. A. Sallam, "Classification of power system disturbances using linear kalman filter and fuzzy-expert system," *International Journal of Electrical Power & Energy Systems*, vol. 43, no. 1, pp. 688–695, 2012.
- [84] Y. Amirat, Z. Oubrahim, and M. E. H. Benbouzid, "On phasor estimation for voltage sags detection in a smart grid context," in *Proceedings of the 2015 IEEE ISIE, Buzios-Rio de Janeiro (Brazil)*, pp. 1351–1356, June 2015.
- [85] Z. Oubrahim, V. Choqueuse, Y. Amirat, and M. E. H. Benbouzid, "Maximum likelihood frequency and phasor estimations for electric power grid monitoring," *IEEE Transactions on Industrial Informatics*, vol. PP, pp. 1–1, July 2017.
- [86] Z. Oubrahim, V. Choqueuse, Y. Amirat, and M. E. H. Benbouzid, "An improved algorithm for power system fault type classification based on least square phasor estimation," in *Proceedings of the 2015 IEEE IECON, Yokohama (Japan)*, pp. 2735–2740, November 2015.
- [87] S. Khokhar, A. A. B. M. Zin, A. S. B. Mokhtar, and M. Pesaran, "A comprehensive overview on signal processing and artificial intelligence techniques applications in classification of power quality disturbances," *Renewable and Sustainable Energy Reviews*, vol. 51, pp. 1650–1663, November 2015.
- [88] M. K. Saini and R. Kapoor, "Classification of power quality events—a review," *International Journal of Electrical Power & Energy Systems*, vol. 43, no. 1, pp. 11–19, 2012.
- [89] R. O. Duda, P. E. Hart, D. G. Stork, *et al.*, *Pattern classification*, vol. 2. Wiley New York, 1973.
- [90] L. Devroye, L. Györfi, and G. Lugosi, *A probabilistic theory of pattern recognition*, vol. 31. Springer Science & Business Media, 2013.
- [91] J. Huang, M. Negnevitsky, and D. T. Nguyen, "A neural-fuzzy classifier for recognition of power quality disturbances," *IEEE Transactions on Power Delivery*, vol. 17, no. 2, pp. 609–616, 2002.
- [92] L. V. Fausett, *Fundamentals of neural networks*. Prentice-Hall, 1994.
- [93] P. Jackson, "Introduction to expert systems," *Addison-Wesley Pub. Co., Reading, MA*, 1986.
- [94] B. Biswal, P. K. Dash, and B. K. Panigrahi, "Non-stationary power signal processing for pattern recognition using hs-transform," *Applied Soft Computing*, vol. 9, no. 1, pp. 107–117, 2009.

- 
- [95] B. Biswal, P. K. Dash, B. K. Panigrahi, and J. Reddy, "Power signal classification using dynamic wavelet network," *Applied Soft Computing*, vol. 9, no. 1, pp. 118–125, 2009.
- [96] W. G. Morsi and M. El-Hawary, "Novel power quality indices based on wavelet packet transform for non-stationary sinusoidal and non-sinusoidal disturbances," *Electric Power Systems Research*, vol. 80, no. 7, pp. 753–759, 2010.
- [97] Z. Oubrahim, V. Choqueuse, Y. Amirat, and M. E. H. Benbouzid, "Classification of three-phase power disturbances based on model order selection in smart grid applications," in *Proceedings of the 2016 IEEE IECON*, Florence (Italy), pp. 5143–5148, December 2016.
- [98] Z. Oubrahim, V. Choqueuse, Y. Amirat, and M. E. H. Benbouzid, "Disturbances classification based on a model order selection method for power quality monitoring," *IEEE Transactions on Industrial Electronics*, vol. 64, no. 12, pp. 9421–9432, April 2017.
- [99] M. H. J. Bollen and L. Zhang, "Different methods for classification of three-phase unbalanced voltage dips due to faults," *Electric Power Systems Research*, vol. 66, no. 1, pp. 59–69, July 2003.
- [100] M. H. J. Bollen, "Algorithms for characterizing measured three-phase unbalanced voltage dips," *IEEE Transactions on Power Delivery*, vol. 18, pp. 937–944, July 2003.
- [101] C. M. Bishop, *Pattern recognition and machine learning*. springer, 2006.
- [102] K. Fukunaga, *Introduction to statistical pattern recognition*. Academic press, 2013.
- [103] I. Kamwa, R. Grondin, V. Sood, C. Gagnon, J. Mereb, *et al.*, "Recurrent neural networks for phasor detection and adaptive identification in power system control and protection," *IEEE Transactions on Instrumentation and Measurement*, vol. 45, no. 2, pp. 657–664, 1996.
- [104] A. S. Cerqueira, D. D. Ferreira, M. V. Ribeiro, and C. A. Duque, "Power quality events recognition using a svm-based method," *Electric Power Systems Research*, vol. 78, no. 9, pp. 1546–1552, 2008.
- [105] L. Ma and K. Y. Lee, "Fuzzy neural network approach for fault diagnosis of power plant thermal system under different operating points," in *Proceedings of the 2008 IEEE Power and Energy Society General Meeting, Pennsylvania (USA)*, pp. 1–7, IEEE, 2008.
-

- [106] S. S. Haykin, S. S. Haykin, S. S. Haykin, and S. S. Haykin, *Neural networks and learning machines*, vol. 3. Pearson Upper Saddle River, NJ, USA:, 2009.
- [107] C. Lee and S. Nam, "Efficient feature vector extraction for automatic classification of power quality disturbances," *Electronics Letters*, vol. 34, no. 11, pp. 1059–1061, 1998.
- [108] I. Monedero, C. Leon, J. Roperro, A. Garcia, J. M. Elena, and J. C. Montano, "Classification of electrical disturbances in real time using neural networks," *IEEE Transactions on Power Delivery*, vol. 22, no. 3, pp. 1288–1296, 2007.
- [109] M. Valtierra-Rodriguez, R. de Jesus Romero-Troncoso, R. A. Osornio-Rios, and A. Garcia-Perez, "Detection and classification of single and combined power quality disturbances using neural networks," *IEEE Transactions on Industrial Electronics*, vol. 61, pp. 2473–2482, May 2014.
- [110] C. Bhende, S. Mishra, and B. Panigrahi, "Detection and classification of power quality disturbances using s-transform and modular neural network," *Electric Power Systems Research*, vol. 78, pp. 122–128, December 2008.
- [111] M. Uyar, S. Yildirim, and M. T. Gencoglu, "An effective wavelet-based feature extraction method for classification of power quality disturbance signals," *Electric Power Systems Research*, vol. 78, pp. 1747–1755, October 2008.
- [112] M. Negnevitsky, V. Faybisovich, S. Santoso, E. Powers, W. Grady, and A. Parsons, "Discussion of "power quality disturbance waveform recognition using wavelet-based neural classifier-part 1: Theoretical foundation" [closure to discussion]," *IEEE Transactions on Power Delivery*, vol. 15, no. 4, pp. 1347–1348, October 2000.
- [113] W. Kanitpanyacharoean and S. Premrudeepreechacharn, "Power quality problem classification using wavelet transformation and artificial neural networks," in *Proceedings of the 2004 PES General Meeting*, New York (USA), pp. 1496–1501, October 2004.
- [114] V. N. Vapnik and S. Kotz, *Estimation of dependences based on empirical data*, vol. 40. Springer-Verlag New York, 1982.
- [115] V. N. Vapnik and V. Vapnik, *Statistical learning theory*, vol. 1. Wiley New York, 1998.
- [116] S. Ekici, "Classification of power system disturbances using support vector machines," *Expert Systems with Applications*, vol. 36, no. 6, pp. 9859–9868, 2009.



- 
- [117] P. Janik and T. Lobos, “Automated classification of power-quality disturbances using svm and rbf networks,” *IEEE Transactions on Power Delivery*, vol. 21, no. 3, pp. 1663–1669, 2006.
- [118] W.-M. Lin, C.-H. Wu, C.-H. Lin, and F.-S. Cheng, “Detection and classification of multiple power-quality disturbances with wavelet multiclass svm,” *IEEE Transactions on Power Delivery*, vol. 23, no. 4, pp. 2575–2582, 2008.
- [119] Z. Liu, Y. Cui, and W. Li, “A classification method for complex power quality disturbances using EEMD and rank wavelet SVM,” *IEEE Transactions on Smart Grid*, vol. 6, no. 4, pp. 1678–1685, January 2015.
- [120] P. G. Axelberg, I. Y.-H. Gu, and M. H. J. Bollen, “Support vector machine for classification of voltage disturbances,” *IEEE Transactions on Power Delivery*, vol. 22, no. 3, pp. 1297–1303, July 2007.
- [121] H. Erişti, A. Uçar, and Y. Demir, “Wavelet-based feature extraction and selection for classification of power system disturbances using support vector machines,” *Electric Power Systems Research*, vol. 80, pp. 743–752, July 2010.
- [122] Y. Zhan, H. Z. CHENG, Y. F. DING, G. Y. Lü, and Y.-b. SUN, “S-transform-based classification of power quality disturbance signals by support vector machines,” *Proceedings of the CSEE*, vol. 4, p. 009, 2005.
- [123] G.-S. Hu, J. Xie, and F.-F. Zhu, “Classification of power quality disturbances using wavelet and fuzzy support vector machines,” in *Proceedings of 2005 International Conference on Machine Learning and Cybernetics, Guangzhou (China)*, vol. 7, pp. 3981–3984, 2005.
- [124] G.-S. Hu, F.-F. Zhu, and Z. Ren, “Power quality disturbance identification using wavelet packet energy entropy and weighted support vector machines,” *Expert Systems with Applications*, vol. 35, no. 1, pp. 143–149, 2008.
- [125] D. De Yong, S. Bhowmik, and F. Magnago, “An effective power quality classifier using wavelet transform and support vector machines,” *Expert Systems with Applications*, vol. 42, no. 15, pp. 6075–6081, 2015.
- [126] P. Dash, S. Mishra, M. Salama, and A. Liew, “Classification of power system disturbances using a fuzzy expert system and a fourier linear combiner,” *IEEE Transactions on Power Delivery*, vol. 15, no. 2, pp. 472–477, 2000.
- [127] V. F. Pires, T. G. Amaral, and J. Martins, “Power quality disturbances classification using the 3-d space representation and pca based neuro-fuzzy approach,” *Expert Systems with Applications*, vol. 38, no. 9, pp. 11911–11917, 2011.
-

- [128] C.-C. Liao and H.-T. Yang, "Recognizing noise-influenced power quality events with integrated feature extraction and neuro-fuzzy network," *IEEE Transactions on Power Delivery*, vol. 24, no. 4, pp. 2132–2141, 2009.
- [129] M. Biswal and P. K. Dash, "Measurement and classification of simultaneous power signal patterns with an s-transform variant and fuzzy decision tree," *IEEE Transactions on Industrial Informatics*, vol. 9, no. 4, pp. 1819–1827, 2013.
- [130] A. A. Abdelsalam, A. A. Eldesouky, and A. A. Sallam, "Classification of power system disturbances using linear kalman filter and fuzzy-expert system," *International Journal of Electrical Power & Energy Systems*, vol. 43, no. 1, pp. 688–695, 2012.
- [131] L. Saikia, S. Borah, and S. Pait, "Detection and classification of power quality disturbances using wavelet transform, fuzzy logic and neural network," in *Proceedings of the 2006 IEEE INDICON*, Kolkata (India), pp. 1–5, December 2010.
- [132] B. Biswal, P. K. Dash, and B. K. Panigrahi, "Power quality disturbance classification using fuzzy c-means algorithm and adaptive particle swarm optimization," *IEEE Transactions on Industrial Electronics*, vol. 56, pp. 212–220, January 2009.
- [133] S. K. Meher and A. K. Pradhan, "Fuzzy classifiers for power quality events analysis," *Electric Power Systems Research*, vol. 80, pp. 71–76, September 2010.
- [134] J. G. Decanini, M. S. Tonelli-Neto, F. C. Malange, and C. R. Minussi, "Detection and classification of voltage disturbances using a fuzzy-artmap-wavelet network," *Electric Power Systems Research*, vol. 81, pp. 2057–2065, December 2011.
- [135] J. Huang, M. Negnevitsky, and T. D. Nguyen, "A neural-fuzzy classifier for recognition of power quality disturbances," *IEEE Transactions on Power Delivery*, vol. 17, no. 2, pp. 609–616, April 2002.
- [136] B. Bizjak and P. Planinšič, "Classification of power disturbances using fuzzy logic," in *Proceedings of the 2006 IEEE EPE-PEMC*, Portoroz (Slovenia), pp. 1356–1360, September 2006.
- [137] H. Erişti and Y. Demir, "A new algorithm for automatic classification of power quality events based on wavelet transform and SVM," *Expert Systems with Applications*, vol. 37, no. 6, pp. 4094–4102, 2010.
- [138] M. Chilukuri and P. Dash, "Multiresolution s-transform-based fuzzy recognition system for power quality events," *IEEE Transactions on Power Delivery*, vol. 19, no. 1, pp. 323–330, 2004.

- 
- [139] T. Back, *Evolutionary algorithms in theory and practice: evolution strategies, evolutionary programming, genetic algorithms*. Oxford university press, 1996.
- [140] A. G. Bakirtzis, P. N. Biskas, C. E. Zoumas, and V. Petridis, “Optimal power flow by enhanced genetic algorithm,” *IEEE Transactions on Power Systems*, vol. 17, no. 2, pp. 229–236, 2002.
- [141] W. A. Ibrahim and M. M. Morcos, “Artificial intelligence and advanced mathematical tools for power quality applications: a survey,” *IEEE Transactions on Power Delivery*, vol. 17, no. 2, pp. 668–673, 2002.
- [142] G. Celli, E. Ghiani, S. Mocci, and F. Pilo, “A multiobjective evolutionary algorithm for the sizing and siting of distributed generation,” *IEEE Transactions on Power Systems*, vol. 20, no. 2, pp. 750–757, 2005.
- [143] O. Sen, S. Zhengxiang, W. Jianhua, and C. Degui, “Application of lvq neural networks combined with genetic algorithm in power quality signals classification,” in *Proceedings of the 2002 IEEE International Conference on Power System Technology, Kunming (China)*, vol. 1, pp. 491–495, IEEE, 2002.
- [144] W. M. Al-Hasawi and K. M. El-Naggar, “A genetic based algorithm for voltage flicker measurement,” *International Journal of Electrical Power & Energy Systems*, vol. 26, no. 8, pp. 593–596, 2004.
- [145] S. Gunal, O. N. Gerek, D. G. Ece, and R. Edizkan, “The search for optimal feature set in power quality event classification,” *Expert Systems with Applications*, vol. 36, no. 7, pp. 10266–10273, 2009.
- [146] C.-F. Juang, “A hybrid of genetic algorithm and particle swarm optimization for recurrent network design,” *IEEE Transactions on Systems, Man, and Cybernetics, Part B (Cybernetics)*, vol. 34, no. 2, pp. 997–1006, 2004.
- [147] B. Panigrahi and V. R. Pandi, “Optimal feature selection for classification of power quality disturbances using wavelet packet-based fuzzy k-nearest neighbour algorithm,” *Transmission and Distribution*, vol. 3, no. 3, pp. 296–306, 2009.
- [148] K. Manimala, K. Selvi, and R. Ahila, “Hybrid soft computing techniques for feature selection and parameter optimization in power quality data mining,” *Applied Soft Computing*, vol. 11, no. 8, pp. 5485–5497, 2011.
- [149] M.-H. Wang and Y.-F. Tseng, “A novel analytic method of power quality using extension genetic algorithm and wavelet transform,” *Expert Systems with Applications*, vol. 38, no. 10, pp. 12491–12496, 2011.

- [150] S. M. Kay, “Fundamentals of statistical signal processing, volume i: Estimation theory,” *Prentice Hall*, April 1993.
- [151] A. Phadke, “Synchronized phasor measurements a historical overview,” in *Proceedings of the 2002 IEEE TDCE, Yokohama (Japan)*, vol. 1, pp. 476–479, October 2002.
- [152] IEEE, “IEEE standard definitions for the measurement of electric power quantities under sinusoidal, nonsinusoidal, balanced, or unbalanced conditions,” *IEEE Std 1459-2010 (Revision of IEEE Std 1459-2000)*, pp. 1–50, March 2010.
- [153] K. B. Petersen, M. S. Pedersen, *et al.*, “The matrix cookbook,” *Technical University of Denmark*, vol. 7, p. 15, November 2008.
- [154] G. H. Golub and V. Pereyra, “The differentiation of pseudo-inverses and nonlinear least squares problems whose variables separate,” *SIAM Journal on Numerical Analysis*, vol. 10, pp. 413–432, April 1972.
- [155] I. S. Gradshteyn and I. M. Ryzhik, *Table of Integrals, Series, and Products*. Academic press, May 2014.
- [156] P. Stoica and R. L. Moses, *Introduction to Spectral Analysis*, vol. 1. Prentice Hall Upper Saddle River, February 1997.
- [157] J. C. Lagarias, J. A. Reeds, M. H. Wright, and P. E. Wright, “Convergence properties of the nelder–mead simplex method in low dimensions,” *SIAM Journal on optimization*, vol. 9, no.1, pp. 112–147, December 1998.
- [158] R. P. Brent, *Algorithms for minimization without derivatives*. Courier Corporation, 2013.
- [159] G. E. Forsythe, C. B. Moler, and M. A. Malcolm, “Computer methods for mathematical computations,” *Prentice-Hall*, 1977.
- [160] M. J. Powell, “On search directions for minimization algorithms,” *Mathematical Programming*, vol. 4, no. 1, pp. 193–201, 1973.
- [161] K. I. McKinnon, “Convergence of the nelder–mead simplex method to a nonstationary point,” *SIAM Journal on Optimization*, vol. 9, no. 1, pp. 148–158, 1998.
- [162] S. M. Kay, “Fundamentals of Statistical Signal Processing,” *PTR Prentice-Hall, Englewood Cliffs, NJ*, April 1993.

- 
- [163] M. M. Begovic, P. M. Djuric, S. Dunlap, and A. G. Phadke, "Frequency tracking in power networks in the presence of harmonics," *IEEE Transactions on Power Delivery*, vol. 8, no. 2, pp. 480–486, April 1993.
- [164] M. H. J. Bollen, I. Gu, S. Santoso, M. Mcgranaghan, P. Crossley, M. Ribeiro, and P. Ribeiro, "Bridging the gap between signal and power," *IEEE Signal Processing Magazine*, vol. 26, no. 4, pp. 12–31, July 2009.
- [165] T. Routtenberg and L. Tong, "Networked detection of voltage imbalances for three-phase power systems," in *Proceedings of the 2015 IEEE ISIE*, Buzios-Rio de Janeiro (Brazil), pp. 1345–1350, June 2015.
- [166] N. Hadjsaid and J.-C. Sabonnadière, *Power Systems and Restructuring*. 2013.
- [167] J. L. Blackburn, *Symmetrical Components for Power Systems Engineering*. CRC Press, June 1993.
- [168] T. Andersson, "Test and Evaluation of Voltage Dip Immunity," *Master Thesis, University of Gothenburg*, 2002.
- [169] P. Stoica, H. Li, and J. Li, "Amplitude estimation of sinusoidal signals: Survey, new results, and an application," *IEEE Transactions on Signal Processing*, vol. 48, no. 2, pp. 338–352, February 2000.
- [170] G. H. Golub and V. Pereyra, "The differentiation of pseudo-inverses and nonlinear least squares problems whose variables separate," *SIAM Journal on numerical analysis*, vol. 10, pp. 413–432, April 1973.
- [171] H. Akaike, "Information theory and an extension of the maximum likelihood principle," in *Selected Papers of Hirotugu Akaike*, pp. 199–213, Springer, 1998.
- [172] H. Akaike, "A new look at the statistical model identification," *IEEE Transactions on Automatic Control*, vol. 19, no. 6, pp. 716–723, 1974.
- [173] G. Schwarz *et al.*, "Estimating the dimension of a model," *The annals of statistics*, vol. 6, no. 2, pp. 461–464, 1978.
- [174] M. Madrigal and B. Rocha, "A contribution for characterizing measured three-phase unbalanced voltage sags algorithm," *IEEE Transactions on Power Delivery*, vol. 22, no. 3, pp. 1885–1890, July 2007.
- [175] C.-S. Chen, C.-W. Liu, and J.-A. Jiang, "A new adaptive PMU based protection scheme for transposed/untransposed parallel transmission lines," *IEEE Transactions on Power Delivery*, vol. 17, pp. 395–404, April 2002.



## **Contribution à la Surveillance de la Qualité de l'Énergie du Réseau Electrique à l'aide de Techniques Paramétriques de Traitement du Signal**

**Résumé**—Cette thèse porte sur la surveillance des perturbations de la qualité de l'énergie d'un réseau électrique via des techniques paramétriques de traitement du signal. Pour élaborer nos algorithmes de traitement du signal, nous avons traité les problèmes d'estimation des différentes grandeurs du réseau électrique triphasé et de classification des perturbations de la qualité d'énergie. Pour ce qui est du problème d'estimation, nous avons développé une technique statistique basée sur le maximum de vraisemblance. La technique proposée exploite la nature multidimensionnelle des signaux électriques. Elle utilise un algorithme d'optimisation pour minimiser la fonction de vraisemblance. L'algorithme utilisé permet d'améliorer les performances d'estimation tout en étant d'une faible complexité calculatoire en comparaison aux algorithmes classiques. Une analyse plus poussée de l'estimateur proposé a été effectuée. Plus précisément, ses performances sont évaluées sous un environnement incluant entre autres la pollution harmonique et interharmonique et le bruit. Les performances sont également comparées aux exigences de la norme IEEE C37.118.2011. La problématique de classification dans les réseaux électriques triphasés a plus particulièrement concerné les perturbations que sont les creux de tension et les surtensions. La technique de classification proposée consiste globalement en deux étapes : 1) une pré-classification du signal dans l'une des 4 pré-classes établis et en 2) une classification du type de perturbation à l'aide de l'estimation des composants symétriques. Les performances du classificateur proposés ont été évaluées, entre autres, pour différentes nombre de cycles, de *SNR* et de *THD*. L'estimateur et le classificateur proposés ont été validés en simulation et en utilisant les données d'un réseau électrique réel du DOE/EPRI National Database of Power System Events. Les résultats obtenus illustrent clairement l'efficacité des algorithmes proposés quand à leur utilisation comme outil de surveillance de la qualité d'énergie.

**Mots-Clés**—Réseau électrique, qualité de l'énergie, surveillance, perturbations, creux de tension et surtensions, estimation de la fréquence et du phaseur, Phasor Measurement Units (PMUs), IEEE C37.118.2014, classification, composantes symétriques, système électrique déséquilibré.

## **On Electric Grid Power Quality Monitoring using Parametric Signal Processing Techniques**

**Abstract**—This thesis deals with electric grid monitoring of power quality (PQ) disturbances using parametric signal processing techniques. The first contribution is devoted to the parametric spectral estimation approach for signal parameter extraction. The proposed approach exploits the multidimensional nature of the electrical signals. For spectral estimation, it uses an optimization algorithm to minimize the likelihood function. In particular, this algorithm allows to improve the estimation accuracy and has lower computational complexity than classical algorithms. An in-depth analysis of the proposed estimator has been performed. Specifically, the estimator performances are evaluated under noisy, harmonic, interharmonic, and off-nominal frequency environment. These performances are also compared with the requirements of the IEEE Standard C37.118.2011. The achieved results have shown that the proposed approach is an attractive choice for PQ measurement devices such as phasor measurement units (PMUs). The second contribution deals with the classification of power quality disturbances in three-phase power systems. Specifically, this approach focuses on voltage sag and swell signatures. The proposed classification approach is based on two main steps: 1) the signal pre-classification into one of 4 pre-classes and 2) the signature type classification using the estimate of the symmetrical components. The classifier performances have been evaluated for different data length, signal to noise ratio, interharmonic, and total harmonic distortion. The proposed estimator and classifier are validated using real power system data obtained from the DOE/EPRI National Database of Power System Events. The achieved simulations and experimental results clearly illustrate the effectiveness of the proposed techniques for PQ monitoring purpose.

**Keywords**—Electric grid, power quality, monitoring, disturbances, voltage sags and swells, frequency and phasor estimations, phasor measurement units (PMUs), IEEE C37.118.2014, classification, symmetrical components, unbalanced power system.